Prediction of shoreline–shelf depositional process regime guided by palaeotidal modelling

Daniel S. Collins, Alexandros Avdis, Martin R. Wells, Christopher D. Dean, Andrew J. Mitchell, Peter A. Allison, Howard D. Johnson, Gary J. Hampson, Jon Hill, Matthew D. Piggott

PII: S0012-8252(21)00328-7

DOI: https://doi.org/10.1016/j.earscirev.2021.103827

Reference: EARTH 103827

To appear in: *Earth-Science Reviews*

Received date: 16 July 2020

Revised date: 28 March 2021

Accepted date: 1 October 2021

Please cite this article as: D.S. Collins, A. Avdis, M.R. Wells, et al., Prediction of shoreline–shelf depositional process regime guided by palaeotidal modelling, *Earth-Science Reviews* (2021), https://doi.org/10.1016/j.earscirev.2021.103827

Prediction of shoreline–shelf depositional process regime guided by palaeotidal modelling

Daniel S. Collins[1,2], Alexandros Avdis[2], Martin R. Wells[3], Christopher D. Dean[4], Andrew J. Mitchell[2], Peter A. Allison[2], Howard D. Johnson[2], Gary J. Hampson[2], Jon Hill[5], and Matthew D. Piggott[2]

[1] *Shell International Ltd, London, SE1 7NA, UK*

[2] *Department of Earth Science and Engineering, Imperial College London, South Kensington Campus, London, SW7 2AZ, UK*

[3] *BP plc, Chertsey Road, Sunbury-on-Thames, Middlesex TW16 7LN, UK*

[4] *Department of Earth Science, Natural History Museum, London, SW7 5BD, UK*

[5] *Environment Department, University of York, Heslington, York, YO10 5DD, UK*

ABSTRACT

Ancient shoreline–shelf depositional systems are influenced by an unusually wide array of geological, biological and hydrodynamic processes, with sediment transport and deposition primarily determined by the interaction of river, wave (including storm) and tidal processes, and changes in relative sea level. Understanding the impact of these processes on shoreline–shelf morphodynamics and stratigraphic preservation remains challenging. Numerical modelling integrated with traditional facies analysis provides an increasingly viable approach, with the potential to quantify, and thereby improve understanding of, the impact of these complex coastal sedimentary processes. An integrated approach is presented here that focuses on palaeotidal modelling to investigate the controls on ancient tides and their influence on sedimentary deposition and preservation – one of the three cornerstones of the ternary process classification scheme of shoreline-shelf systems. Numerical tidal modelling methodology is reviewed and illustrated in three palaeotidal model case studies of different scales and focus. The results are synthesised in the context of shoreline–shelf processes, including a critique and modification of the process-based classification scheme.

The emphasis on tidal processes reflects their global importance throughout Earth's history. Ancient palaeotidal models are able to highlight and quantify the following four controls on tidal processes: (1) the physiography (shape and depth) of oceans (1000s km scale) determines the degree of tidal resonance;

(2) the physiography of ocean connections to partly enclosed water bodies (100–1000s km scale) determines the regional-scale flux of tidal energy (inflow versus outflow); (3) the physiography of continental shelves influences shelf tidal resonance potential; and (4) tides in relatively local-scale embayments (typically 1–10s km scale) are influenced by the balance of tidal amplification due to funnelling, shoaling and resonance effects versus frictional damping. In deep time, palaeogeographic and palaeobathymetric uncertainty can be accounted for in palaeotidal models by performing sensitivity analyses to different scenarios, across this range of spatial scales.

These tidal process controls are incorporated into an updated predictive decision tree for determining shoreline–shelf process regime in terms of the relative interaction of wave, fluvial and tidal processes. The predictive decision tree considers the effects of basin physiography, shelf width and shoreline morphology on wave, fluvial and tidal processes separately. Uncertainty and ambiguity in applying the widely used three-tier process classification scheme are reduced by using the decision tree in conjunction with a proposed two-tier classification of process regime that is limited to primary and secondary processes. This two-tier classification scheme is illustrated in the three case studies, showing how integration of numerical modelling with facies analysis of the preserved stratigraphic record improves confidence in prediction of tide-influenced shoreline-shelf process regimes. Wider application of this approach will further improve process-based classifications and predictions of modern and ancient shoreline–shelf systems.

Keywords: Shoreline–Shelf; Wave; Tide; Fluvial; Process regime; Numerical Modelling; Palaeotidal.

1 INTRODUCTION

Shoreline–shelf landscapes at the land-sea interface are some of the most dynamic settings on earth, containing a complex array of sedimentary systems that include deltaic, estuarine, paralic, shallow marine and shelfal environments. The type, morphology, depositional architecture and spatio-temporal evolution of these systems reflect dynamic interactions between three main groups of forcing conditions (Townend, 2012; Zhou et al., 2017). First, hydrodynamic processes operate on a range of spatio-temporal scales and principally include tides, river flow and wave climate (e.g. Galloway, 1975; Boyd et al., 1992; Ainsworth et al., 2011), but also larger magnitude-lower frequency extreme events such as storms. Second, the 'sedimentology' of the system includes both the rate of sediment supply and the range of grain sizes and characteristics of the sediment sources (Orton and Reading, 1993). Third, landscape setting describes the physiographic characteristics of the land-sea interface and receiving sedimentary basin (Zhou et al.,

2014), which depends on various factors, most notably antecedent geology, sea level change, accommodation space (often related to tectonics) and, increasingly, anthropogenic influence (sediment supply, dredging, vegetation change, etc.). Additional processes that mediate interactions between these factors include biological activity (e.g. fauna-sediment reworking) and vegetation cover. Furthermore, feedbacks exist between these controls such that changes, for example, in sea level can influence shoreline morphology (landscape setting) and cause potentially dramatic changes in tide and/or wave influence(e.g. Yoshida et al., 2007; Collins et al., 2018c). In the case of natural shoreline–shelf systems, morphological change is generally related to the intrinsic feedback between hydrodynamics, sediment transport and morphology, but this feedback is invariably conditioned and constrained by the various factors governing landscape setting and sediment character of the system (Zhou et al., 2017).

Obtaining a better understanding of shoreline–shelf systems is of increasing importance in the 21st Century. Anthropogenic climate change has the potential to significantly impact shorelines through changes in sea level and rates of sediment weathering, erosion and supply. Anthropogenic influence on shorelines also extends to direct displacement of large volumes of sediment in engineering works and indirectly through, for example, changes in sediment erosion versus deposition related to vegetation clearing (Tomašových and Kidwell, 2017) and modified balances between morphology, hydrodynamics and sediment transport. As such, present-day configurations of shoreline systems are often the result of ongoing and intrinsically coupled natural, social and economic feedbacks, the impacts of which on future long-term shoreline configurations are only just being explored (Zhou et al., 2017). However, ancient stratigraphic records containing an archive of past changes in shoreline–shelf environments can form a useful reference for interpreting the potential future response of shorelines to changes in climatically-driven processes, provided these can be disentangled from other allogenic and autogenic controls (e.g. Reading and Collinson, 1996; Hampson, 2016). Some of these ancient stratigraphic units deposited at or near shorelines have contributed significantly to global conventional and unconventional hydrocarbon production. Characterising, classifying and understanding the difference in facies, architecture and morphology between reservoirs formed in different shoreline–shelf systems has underpinned efforts to interpret and predict reservoir distribution and performance, to ultimately improve hydrocarbon recovery. Similar reservoirs also form vital freshwater aquifers, geothermal reservoirs and current and future reservoirs for CO2 storage in carbon, capture and storage (CCS) projects.

Due to the complexity and evident importance of these settings, a variety of classification systems have evolved for categorising shoreline–shelf depositional systems (see reviews by Elliott, 1986; Boyd et al., 1992; Johnson and Baldwin, 1996; Reading and Collinson, 1996; James and Dalrymple, 2010; Ainsworth

et al., 2011). However, the most widely applied classifications relate shoreline–shelf morphology and idealised sections of preserved stratigraphy to the relative strength of river, wave and tide processes (Coleman and Wright, 1975; Galloway, 1975; Hayes, 1975; Hayes, 1979; Boyd et al., 1992; Ainsworth et al., 2011), conditioned by the overarching controls of relative sea level change versus sediment supply (Curray, 1964; Boyd et al., 1992; Dalrymple, 1992), sediment grain size (Orton and Reading, 1993) and tectono-physiographic setting (Reading and Collinson, 1996).

Whilst the variety and variability of controls on shoreline–shelf systems make it impossible to quantitatively understand and fully model 'real world' systems, numerical modelling has become an increasingly important tool for simplifying and understanding the diverse and complex set of controls on such systems. Numerical models simulate 'virtual world' systems subject to selected processes operating under controlled boundary conditions (Zhou et al., 2017). Models of virtual systems represent a conceptual idealisation of the real world for the processes modelled, producing robust, reliable and realistic simulation results calibrated with real world measurements (Zhou et al., 2017). In the case of shoreline–shelf systems, there is now a wide body of research that investigate long-term morphodynamics and shoreline depositional processes using a process-based modelling approach. Most of these studies have so far investigated the influence of varying tide, river and wave hydrodynamics (de Vriend et al., 1993; Van der Wegen and Roelvink, 2008; Nahon et al., 2012; Leonardi et al., 2014; Zhou et al., 2014; Rossi et al., 2016; Zhou et al., 2017), but other factors such as salinity differences (Olabarrieta et al., 2018; Zhou et al., 2020), sediment sorting processes (Zhou et al., 2015) have also been shown to significantly impact shoreline circulation and morphology.

Improved understanding and recognition of process interactions along modern and ancient shorelines has led to refined process-based classifications and predictive models of shoreline systems (Ainsworth et al., 2008; Ainsworth et al., 2011; Vakarelov and Ainsworth, 2013; Nyberg and Howell, 2016). In the case of ancient systems, an important improvement has been wider application of theoretical relationships between the strength of wave or tide processes and shoreline–shelf physiography, derived from palaeogeographic reconstructions, in order to support facies and stratigraphic interpretations of ancient depositional processes, most notably the impact of shoreline geometry and on tidal resonance or amplification (Godin, 1993; Yoshida et al., 2007; van Cappelle et al., 2018; Zuchuat et al., 2019). Simple theoretical relationships provide a quick method of estimating shoreline–shelf wave and tidal potential but lack the ability to assess or understand spatio-temporal variability and the sensitivity to, and interaction of, potential physiographic controls. Instead, hydrodynamic numerical modelling enables deeper discussion of these factors, ranging from multi-process morphodynamic simulations (Geleynse et al.,

2011; Rossi et al., 2016) to simulations of specific shoreline processes. Of the trivariate controls of tide, river and wave processes, tidal forcing has proven both slightly easier to predict using numerical modelling (given that it relates to well understood planetary motions) and perhaps more relevant to understanding ancient shoreline-shelf processes, given that tides operate globally through the whole Earth system (Stammer et al., 2014), influence sediment transport to some capacity along all shorelines globally and have operated throughout the vast majority of Earth's history (Green et al., 2017). In comparison, river processes only operate directly along a small portion of global shorelines, waves depend on wind patterns, fetch and basin physiography, and both river and wave processes depend on complicated atmospheric and climatic processes. As such, numerical tidal simulations (e.g. Slingerland, 1986; Ericksen and Slingerland, 1990; Martel et al., 1994; Wells et al., 2005a; Mitchell et al., 2010; Collins et al., 2018a; Collins et al., 2018b; Dean et al., 2019) have been extensively validated against modern sedimentary environments and, through integration with sedimentological and stratigraphic datasets, have provided unique information on the physiographic controls on tidal processes and sedimentary preservation along ancient tide-influenced shorelines. However, the implications of ancient tidal model simulations on the classification, prediction and interpretation of shoreline–shelf depositional process regimes have not yet been fully explored.

This review article aims to assess the implications of palaeotidal model simulations for classification and prediction of shoreline depositional process regime by discussing three main questions: (1) How do we classify and predict shoreline-shelf depositional systems, especially regarding hydrodynamic processes? (2) What do existing present-day and ancient numerical tidal models indicate about the controls on tides? (3) How can we use this understanding to improve predictions of shoreline–shelf process regime?

2 BACKGROUND

2.1 Classification, identification and prediction of clastic depositional shoreline–shelf systems and process regime

2.1.1 Shoreline–shelf classifications

There is no single unifying classification of clastic shorelines and shelves. As with all natural systems, clastic shorelines form in response to multiple controls, and different parameters can be used for the purpose of classification (e.g. Reading and Collinson, 1996). Seminal models for clastic shoreline systems initially focused on modern deltas, particularly the relationship between delta front morphology and the relative influence of wave, tidal and fluvial process (Coleman and Wright, 1975; Galloway, 1975). This

ternary classification scheme was widely adopted and modified to include a wider range of depositional settings by Boyd et al. (1992), notably the bivariate wave versus tide classification of clastic coasts (Hayes, 1975; Hayes, 1979) and variability in grain size (Orton and Reading, 1993). Boyd et al. (1992) and Dalrymple (1992) developed predictive evolutionary relationships between long-term equilibrium depositional environments, where sediment accumulation and erosion are essentially balanced (Zhou et al., 2017). These relationships addressed a wide range of shoreline–shelf depositional systems and recognised the overarching control of rate of sediment supply versus rate of relative sea level change (shoreline transgression versus regression). These seminal models and classifications of shoreline–shelf systems necessarily focused on relative process end-members to establish the full range of depositional system types in the continuous spectrum of potential mixed-energy systems.

The extensive range of models provide a means to classify shoreline–shelf systems at a particular time and in a particular location. However, these models were not intended to predict more detailed process variations either spatially at a given time, temporally at a given location, or both spatially and temporally (Boyd et al., 1992). Such dynamic changes in depositional processes on various spatial and temporal scales may be caused by variations in any of the multitude of controls impacting shoreline–shelf systems. For example, changes in shoreline physiography (morphology and bathymetry), fluctuations in accommodation space creation versus sediment supply rates, and variations in regional basin physiography may all form dominant controls on shoreline-shelf systems.

Within individual shoreline systems, complex arrangements of discrete depositional elements attributed to different combinations of wave, tide and fluvial processes have been recognized in analyses of: (1) modern delta geomorphology and sedimentological data, including the Danube (e.g. Bhattacharya and Giosan, 2003), Ganges-Brahmaputra (e.g. Willis, 2005), Mahakam (e.g. Allen and Chambers, 1998), Mekong (e.g. Nguyen et al., 2000; Ta et al., 2002b), Mitchell (e.g. Nanson et al., 2013) and Changjiang (Yangtze) (e.g. Hori et al., 2002) deltas; and (2) approximately contemporaneous ancient stratigraphic units, including the Permian Kookfontein and Waterford formations in the Karoo Basin (Gomis-Cartesio et al., 2016), Cretaceous Ferron Sandstone, Western Interior Seaway (e.g. Gardner et al., 2004; Bhattacharya and MacEachern, 2009; Li et al., 2011; Li et al., 2015), Cretaceous Sego Sandstone, Western Interior Seaway (Willis and Gabel, 2001; Legler et al., 2014; van Cappelle et al., 2016), Cretaceous Horseshoe Canyon Formation, Western Interior Seaway (Willis and Gabel, 2001; Legler et

al., 2014; Ainsworth et al., 2015; Ainsworth et al., 2016; van Cappelle et al., 2016) and Miocene Belait Formation, NW Borneo (Lambiase et al., 2003; Collins et al., 2017b; Collins et al., 2018c). Consequently, these and many other depositional systems frequently indicate mixed-process regimes, with variable wave, tide and fluvial interactions in both space (e.g. along and/or perpendicular to depositional strike) and time (on various timescales e.g. daily, seasonal, annual or longer). These mixed-energy systems cannot be fully resolved in the early process classification models (Coleman and Wright, 1975; Galloway, 1975; Boyd et al., 1992). Therefore, Ainsworth et al. (2011) developed a new semi-quantitative, process-based classification scheme based on the relative importance of primary, secondary and tertiary processes: represented by 'dominated', 'influenced' or 'affected' descriptors, respectively. This higher-resolution process-based approach enhances comparison of modern and ancient shoreline deposits (Fig. 1A). However, a quantitative process analysis of modern shorelines by Nyberg and Howell (2016) suggests the thresholds separating primary, secondary and tertiary processes are ambiguous, resulting in these authors favouring a two-tier classification (Fig. 1B). Furthermore, the additional ambiguity in the process interpretation of several common sedimentary structures means that most studies of ancient, mixed-process shoreline deposits have adopted a two-tier process classification (e.g. Bhattacharya and Giosan, 2003; Lambiase et al., 2003; Coates and MacEachern, 2007; Gani and Bhattacharya, 2007; Hansen et al., 2007; Buatois et al., 2012; Vakarelov et al., 2012; Amir Hassan et al., 2013; Legler et al., 2013; Chen et al., 2014; Legler et al., 2014; Ainsworth et al., 2015; Gugliotta et al., 2015; Li et al., 2015; Ainsworth et al., 2016; Amir Hassan et al., 2016; Gomis-Cartesio et al., 2016; Gugliotta et al., 2016a; Rossi and Steel, 2016; Vaucher et al., 2016; Collins et al., 2017b; Collins et al., 2018c).

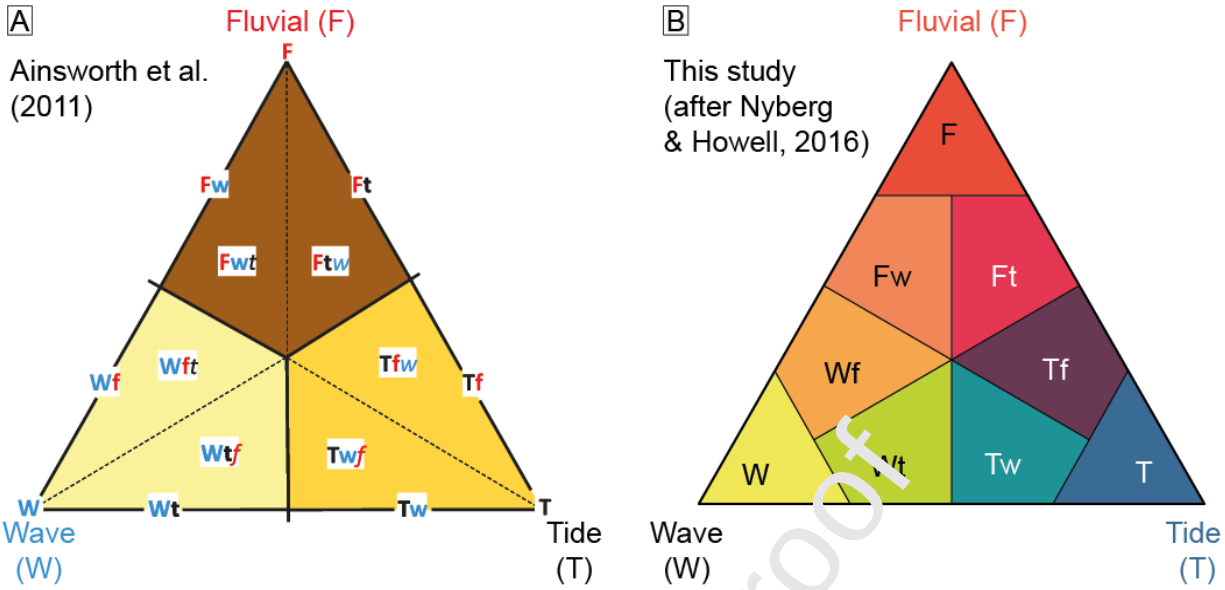

Fig. 1. Two contrasting ternary process classifications for shoreline depositional systems. (A) The three-tier classification of Ainsworth et al. (2011) utilizes primary, secondary, and tertiary processes, which are referenced as 'dominated' (capitalized and bold), 'influenced' (lower case and bold) and 'affected' (lower case italics and not bold), respectively. For example, wave dominated, tide influenced and fluvial affected is written **Wt*f***. (B) The two-tier classification of Nyberg and Howell (2016) recognizes the primary and secondary processes, and is favored in this study (see text for discussion).

2.1.2 Process classification of present-day global shorelines

Nyberg and Howell (2016) developed the first, systematic, semi-automated classification of global shoreline process regime (Fig. 2) by combining several datasets and methodologies: (1) proxies for wave, tide and fluvial processes, including wave height, tidal amplitude and river discharge; (2) depositional versus erosional shorelines, determined by combining global lithology maps and digital elevation models; and (3) algorithms for determining the 'tidal coefficient' for modifying tidal amplitude using shoreline rugosity or 'roughness index'. This integrated approach predicts shoreline classification with an 85% success rate compared to manual interpretation based principally on shoreline morphology (e.g. Ainsworth et al., 2011), and is consistent with earlier comparisons of shoreline morphology with quantitative metrics of wave, tide and river power along large, but non-global, stretches of siliciclastic coastlines (e.g. Harris et al., 2002). By subdividing the global shoreline into 5 km segments, this methodology classifies 28% of global shorelines as depositional, of which 62% are wave-dominated, 35% tide-dominated and 3% fluvial-dominated (Fig. 2A) (Nyberg and Howell, 2016). On a global scale, over 90% of shorelines on narrow shelves (≤25 km) are wave-dominated and <5% tide-dominated, whereas

over 30% of shorelines on wide shelves (>75 km) are tide-dominated (Fig. 2B). Along depositional shorelines, tide dominance increases from <20% on narrow shelves to >50% on wide shelves (Fig. 2C). Fluvial-dominated systems are prone to more wave modification on narrow shelves and to more tide modification on wide shelves (Fig. 2B and C).

Tide-dominated deltas are widely distributed (Figs 2A and 4A), including: (1) at low and high latitudes; (2) along open-ocean shorelines and in partly enclosed oceans and seas; and (3) along straight and highly embayed shorelines. Their locations encompass a range of tectonic settings, including strike-slip transtensional rift (e.g. Colorado delta), forearc (e.g. Cooper delta), foreland (e.g. Mahakam and Fly deltas) and passive margin settings (Ganges Brahmaputra delta) (Nyberg and Howell, 2016). Tide-dominated deltas preferentially occur along macrotidal shorelines (Fig. 4A), but they also occur along mesotidal shorelines (e.g. Mekong and Mahakam deltas). However, tide-dominated deltas exclusively occur along shorelines with elevated tidal bed shear stresses, where tidal currents at their maximum strength are capable of transporting at least coarse sand (Fig. 4D).

Although the Nyberg and Howell (2015) classification provides a consistent, reproducible approach for identifying process distribution along global shorelines, it has some limitations. As is observed in modern systems, more rugose and funnel-shaped shorelines are strongly correlated with tide dominance, but not all present-day embayments are tide dominated. Likewise, smoother shorelines are correlated with wave dominance. None of the tidal coefficients consider theoretical and quantifiable relationships between shoreline physiography and the tidal prism (D'Alpaos et al., 2010). Lastly, wave height and tidal range are inadequate proxies for differentiating wave- and tide-dominance in mixed-energy systems (e.g. Anthony and Orford, 2002; Dalrymple, 2010b; Mulhern et al., 2017) because these parameters are not directly related to sediment entrainment (unlike bed shear stress).

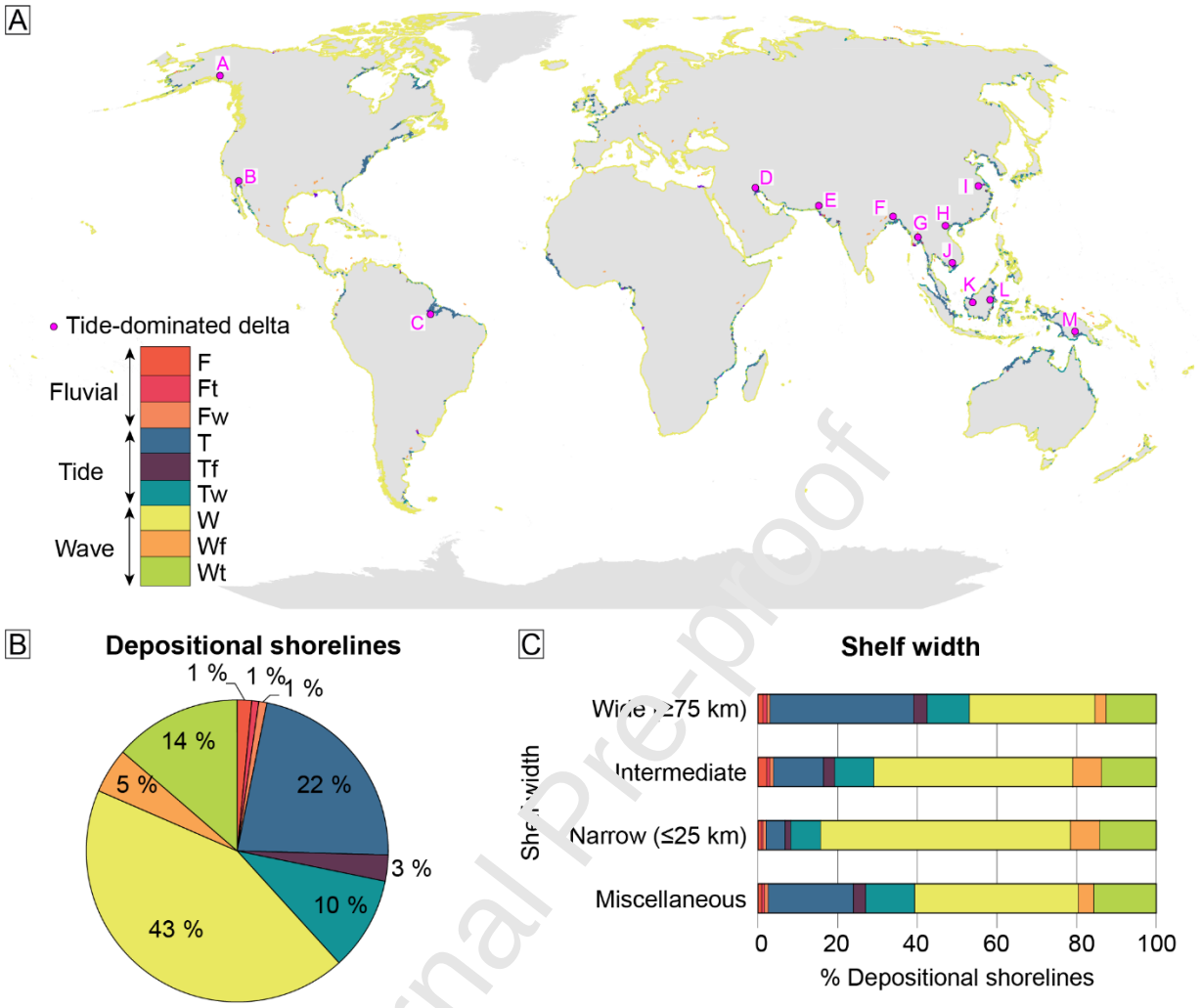

Fig. 2. Quantification of modern global shoreline process regimes (from Nyberg and Howell, 2016). (A) Two-tier ternary process classification of modern shorelines (see Fig. 1B) showing the locations (pink dots) of tide-dominated deltas (Goodbred and Saito, 2012): A) Copper; B) Colorado; C) Amazon; D) Shatt-al-Arab; E) Indus; F) Ganges-Brahmaputra; G) Irrawaddy; H) Red River; I) Yangtze; J) Mekong; K) Rajang; L) Mahakam; and M) Fly. Figures 4A and D show the same delta locations on a global map of tidal range and tidal bed shear stress, respectively. (B) Proportion of the two-tier process classifications along depositional shorelines. (C) Relationship between binned shelf width and proportion of the two-tier process classification along depositional shorelines. The miscellaneous class is for shallow seas and seaways (e.g. Baltic Sea).

2.1.3 Identification of ancient shoreline–shelf processes

The study and interpretation of ancient physical processes from sedimentary rocks has required a rigorous, multi-scale approach that has developed over the last 60–70 years (see reviews by Walker and Plint, 1992; Reading, 1996). This methodology is underpinned by rigorous facies analysis, which relies on detailed, qualitative descriptions of distinctive combinations of sedimentary and biological structures (e.g. Reading, 1978; Reading, 1996). However, small-scale (*c.* 1–100s cm) facies are typically based on subtle differences that are non-unique in terms of depositional processes and environment (Walker and James, 1992). Hence, sedimentological and stratigraphic descriptions and interpretations are required across the range of scales and dimensions spanning facies, facies associations, facies successions and architectural elements to characterise and interpret ancient processes and environments (Elliott, 1986; Walker and James, 1992; Dalrymple, 2010a; Colombera and Mountney, 2020b). Understanding the relationship between process, sedimentation, sedimentary structures and stratigraphic architecture also requires comparison to the modern, where these aspects may be observed and measured directly in different environments (Middleton, 1965; Allen, 1968; Allen, 1982b; Yang et al., 2008; Collinson and Mountney, 2019; Dalrymple, 2021).

In shoreline–shelf systems, the process-based sedimentological approach centres upon unravelling the relative influence of river, wave and tide processes based on different groups of physical processes, principally unidirectional and bidirectional traction currents and gravitational, oscillatory and suspension flow processes. The confidence level of ancient ternary process interpretations depends on several factors, most notably: (1) the availability and quality of the rock data; (2) the formation and preservation potential of sedimentary facies that can be assigned to specific flow processes; (3) the uncertainty in the process interpretation of sedimentological, stratigraphic and biological features; and (4) the level of existing knowledge of the depositional system under investigation. Recently, a statistical method for classifying shoreline–shelf deposits has been proposed that involves assigning a percentage likelihood that a bed or stratal unit was formed by wave, tide or fluvial processes ('process percentage') and quantifying the relative proportion of each bed or stratal unit (Rossi et al., 2017b; Peng et al., 2018). The 'process percentage' is determined based on the proportion of preserved sedimentary structures, and also the proportion of wave-, tide- or fluvial-dominated interpretations of each sedimentary structure in an extensive literature database (Rossi et al., 2017b; Peng et al., 2018). However, this approach has limitations. First, the volumetric proportion of deposits formed by different processes may not reflect process dominance in the environment of deposition, as highlighted by Dalrymple et al. (2015). Second,

end-member process interpretations of various sedimentary structures are commonly ambiguous. Third, it is difficult to assign percentage values to sedimentary structures formed by combined processes.

Nonetheless, recent advances over the last 10–15 years in process-based sedimentological analysis of end-member and mixed-energy shoreline–shelf systems has increased confidence in palaeoenvironmental and related process interpretations. This is illustrated with a few specific examples, while a more comprehensive analysis of tidal facies is presented later (Section 2.2.3.1). It is now recognized that muddy and sandy heterolithics with a predominance of unidirectional ripple cross-lamination are not limited to tidal settings as was originally emphasized (e.g. Reineck and Wunderlich, 1968) and occasionally uncritically adopted by some sedimentologists. Instead these facies can form in a wide range of environments and under a spectrum of processes, especially those with mixed fluvial and tidal influence (e.g. Dalrymple et al., 2015; Gugliotta et al., 2016b; Kurcinka et al., 2018; Collins et al., 2020; Van Yperen et al., 2020) (Thomas et al., 1987; Martinius et al., 2015; Jablonski and Dalrymple, 2016). Likewise, subtle difference in the interpretation of tidal influence (secondary process) versus tidal modulation (tertiary processes) in cross-stratification have been proposed (Martinius and Gowland, 2011; Gugliotta et al., 2016a) (Martinius et al., 2015). Hummocky and swaley cross-stratification with mudstone drapes have recently been interpreted to record mixed storm and tidal processes (Vakarelov et al., 2012; Wei et al., 2016) or inherent flow variability during storm flows (e.g. Collins et al., 2017b). Lastly, the range of oscillatory to unidirectional flow and the influence of hyperpycnal flow in the origin of hummocky and swaley cross-stratification and related structures (e.g. combined-flow ripples and planar lamination) is now more widely appreciated (Dott and Bourgeois, 1982; Arnott and Southard, 1990; Myrow and Southard, 1996, Myrow et al., 2002; Dumas and Arnott, 2006; Lamb et al., 2008; Tinterri, 2011; Basilici et al., 2012, Perillo et al., 2014).

2.1.4 Prediction of ancient shoreline–shelf depositional process regime

Understanding the physiographic and hydrodynamic controls on the process regime of present-day shorelines (section 2.1.2), and consideration of such controls in ancient case studies, has enabled development of predictive models for ancient shoreline–shelf depositional process regime. Ainsworth et al. (2011) extended previous process-based models of shoreline–shelf systems by including the following aspects: (1) basin physiography (100–1000 km scale), (2) shelf width (10–100 km scale), (3) fluvial versus wave effectiveness, (4) accommodation versus sediment supply (A/S ratio), and (5) shoreline

morphology (1–10 km scale). These were incorporated into a decision tree (Fig. 7A) and two predictive matrices (Fig. 7B and C) for low and high tidal resonance, respectively.

First, basin physiography and shelf width are combined to determine the 'tidal resonance potential of the basin' (Fig. 7A). Tidal resonance occurs when the natural period of oscillation within an ocean, water body, on the shelf or within a shoreline embayment, is coincident with the tidal period (Slingerland, 1986; Allen, 1997; Collins et al., 2018c). The interpretation of tidal resonance potential is calibrated empirically to shelf width (cf. Howarth, 1982). Present-day shorelines suggest that tide-dominated systems are more likely adjacent to shelves greater than 75 km in width (Heap et al., 2004; Ainsworth et al., 2011). Hence, shelf width is used as an approximate empirical cut-off to distinguish modern and ancient shorelines with lower (<75 km shelf width) and higher tidal potential (>75 km shelf width), respectively.

The second decision in the tree (Fig. 3) focuses on fluvial versus wave effectiveness, which is also partly related to ancient shoreline palaeogeography. Shorelines facing large open water bodies are likely to be strongly influenced by wind-driven waves, with a large fetch resulting in a relatively high wave effectiveness. In contrast, shorelines that are more sheltered from direct oceanic waves and/or face smaller water bodies experience lower wave effectiveness. Fluvial effectiveness is controlled by a range of continental processes, including climate, weathering, river hydrology, drainage basin area, slope of the alluvial plain, and hinterland relief and gradient. Predictions of higher fluvial effectiveness must be supported by palaeogeographic, palaeodrainage and palaeohydrological reconstructions, especially where these indicate proximity to the outlets of large fluvial drainages. Consequently, wave and fluvial effectiveness are determined by very different factors, requiring independent facies analysis of preserved stratigraphy.

The third decision, the rate of accommodation space creation versus sediment supply (A/S ratio), is a useful theoretical concept (Muto and Steel, 1997) but difficult to apply practically, even for extensive datasets (Ainsworth et al., 2008; Ainsworth et al., 2011) and for predictions based on parasequence characteristics (Colombera and Mountney, 2020a). The A/S ratio does not directly affect shoreline depositional processes but may modify their relative interaction through changes in physiography. For embayed shorelines, which favour tidal amplification, the degree of wave protection will be: (1) reduced

under low A/S conditions because higher progradation rates cause shorelines to straighten more quickly; and (2) increased under high A/S conditions, when accommodation exceeds sediment supply, because the embayed shoreline geometry will more likely persist (Fig. 3) (Ainsworth et al., 2011). Furthermore, the A/S ratio impacts preservation potential, with more complete preservation of all sub-environments in high A/S settings (van Vliet and Schwander, 1987; Collins et al., 2018c).

Shoreline morphology (c. 1–10 km scale) is the final decision on the tree (Fig. 3), and can have a significant impact on the relative balance of tide, wave and fluvial processes (Fig. 1) (Boyd et al., 1992; Dalrymple et al., 1992; Ainsworth et al., 2008; Ainsworth et al., 2011). Highly-embayed, more rugose shoreline morphologies may promote: (1) amplification of the tidal wave by funnelling and/or resonance effects (Slingerland, 1986; Allen, 1997); and (2) protection from direct wave approach from the open ocean or sea. Therefore, Ainsworth et al. (2011) use shoreline rugosity as a direct proxy for tidal influence, with increasing rugosity corresponding to increased potential for tidal influence (Fig. 3). Their model predicts that all interpreted highly embayed shorelines, and half of interpreted moderately embayed shorelines, are tide-dominated, whereas only a quarter of interpreted straight to lobate shorelines are tide-dominated (Fig. 3A). However, this simplified differentiation is inconsistent with observations of Holocene to present-day embayed shorelines, most notably estuaries (e.g. Dalrymple, 1992; Roy et al., 2001; Boyd et al., 2006; Dalrymple, 2006; Dalrymple, 2010b), which may be wave-dominated (e.g. Roy et al., 1980; Honig and Boyd, 1992; Cooper, 2001; Anthony et al., 2002), tide-dominated (e.g. Hori et al., 2001; Dalrymple et al., 2012), river dominated (e.g. Cooper, 1993; Sondi et al., 1995), and mixed process (d'Anglejan and Brisebois, 1978; Jouanneau and Latouche, 1981; Clifton, 1983; Allen and Posamentier, 1993; Roy et al., 2001). Furthermore, amplifying of tides due to funnelling and resonance effects in embayments may be counteracted by frictional effects (e.g. Dalrymple et al., 1992; Allen, 1997; Mitchell et al., 2010; Collins et al., 2018a; Collins et al., 2018b). Consequently, the variability in predicted processes for ancient embayed shorelines may be higher than that proposed by Ainsworth et al. (2011) (Fig. 3).

Prediction of shoreline processes in ancient successions is enhanced by access to the following: (1) reliable chronostratigraphic information with an appropriate resolution; and (2) overlapping age ranges ('temporal resolution'). The temporal resolution of data and interpretations relating to the inferred controls varies significantly. For example, the temporal resolution of interpreted system tracts relating to

3rd-order (c. 0.5–3.0 Myr) or 4th-order (few 10s ka to c. 0.5 Myr) sea-level cycles (Haq, 2014; Sames et al., 2016) will likely fall within the temporal resolution of regional-scale palaeogeographic maps, which are typically driven by plate tectonics and used for interpreting basin physiography and fluvial versus wave effectiveness (Markwick and Valdes, 2004). In contrast, the physiography of shoreline embayments and the continental shelf may be driven by relative sea level changes or local tectonics, which vary on much smaller timescales (Partington et al., 1993a; Partington et al., 1993b; Egbert et al., 2004; Stammer et al., 2014; Collins et al., 2018a; van Cappelle et al., 2018).

Whilst the predictive framework of Ainsworth et al. (2011) provides an improved methodology for interrogating the process classifications of ancient shoreline-shelf systems, the current decision tree does not sufficiently capture the complex impact of basin physiography on tide and wave processes. For tidal processes, basin physiography complicates: (1) the flux of tidal energy into and out of partly enclosed water bodies (referred to herein as tidal inflow and outflow), and (2) the funnelling, shoaling and resonance effects on continental shelves and within shoreline embayments, which occur on a range of scales (*c.* 1–1000s km width and 1–100s m depth) (Mitchell et al., 2010; Wells et al., 2010b; Collins et al., 2018c). However, basin physiography does not constitute a separate query in the predictive model (Fig. 3) and is treated as a modifying factor to shelf tidal resonance potential (Ainsworth et al., 2011). Open oceans are sufficiently large to allow generation of relatively high *in-situ* tides (Dalrymple, 1992). Therefore, basins that have restricted access to the open oceans generally have a lower potential for producing amplified tidal currents by resonance effects, whereas basins with less restricted access to open oceans have a higher tidal resonance potential. For example, the small tides (typically <1 m tidal range) in the modern Arctic Ocean are primarily due to the restricted access to the Atlantic Ocean preventing northward propagation of the open ocean tidal wave, as well as the basin being too small to have its own tides (Dalrymple and Padman, 2019). However, an exception is that certain restrictive basin physiographies, typically on a smaller-scale (1–10s km), may cause significant amplification of tides by funnelling, shoaling and/or resonance effects (Piper et al., 1990; Martel et al., 1994) (Mitchell et al., 2010; Ainsworth et al., 2011; Mitchell et al., 2011) (Androsov et al., 2002; Leckie and Rumpel, 2003). On the other hand, smaller basins and large areas of wide, shallow shelves may increase frictional dissipation of tides but also waves and may still be tide dominated even at lower tidal ranges. This is illustrated in the White Sea region of the modern Arctic Ocean, where macrotidal ranges occur due to favourable geomorphology for funnelling and shoaling effects, in combination with rotating tides due to the high Coriolis parameter, whilst mean wave height is low to due restricted ocean access (Dalrymple and Padman, 2019). Overall, the generalized treatment of basin physiography in the existing predictive model (Ainsworth et al., 2011) combines two very different effects on tides relating to: (1) basin size (100–1000

km width scale) and bathymetry (100–1000 m depth scale), which has a first order control on the balance of tidal inflow versus outflow; and (2) second-order funnelling and resonance effects relating to basin physiography (10–100s km width scale and 1–100s m depth scale) (Wells et al., 2005a; Wells et al., 2007; Mitchell et al., 2010; Wells et al., 2010b; Collins et al., 2018a; Collins et al., 2018b). Numerical tidal modelling is particularly well-suited to distinguishing between these two basin physiographic controls (Slingerland, 1986; Martel et al., 1994; Wells et al., 2007; Collins et al., 2018a; Collins et al., 2018b) and therefore provides information for shoreline–shelf process prediction.

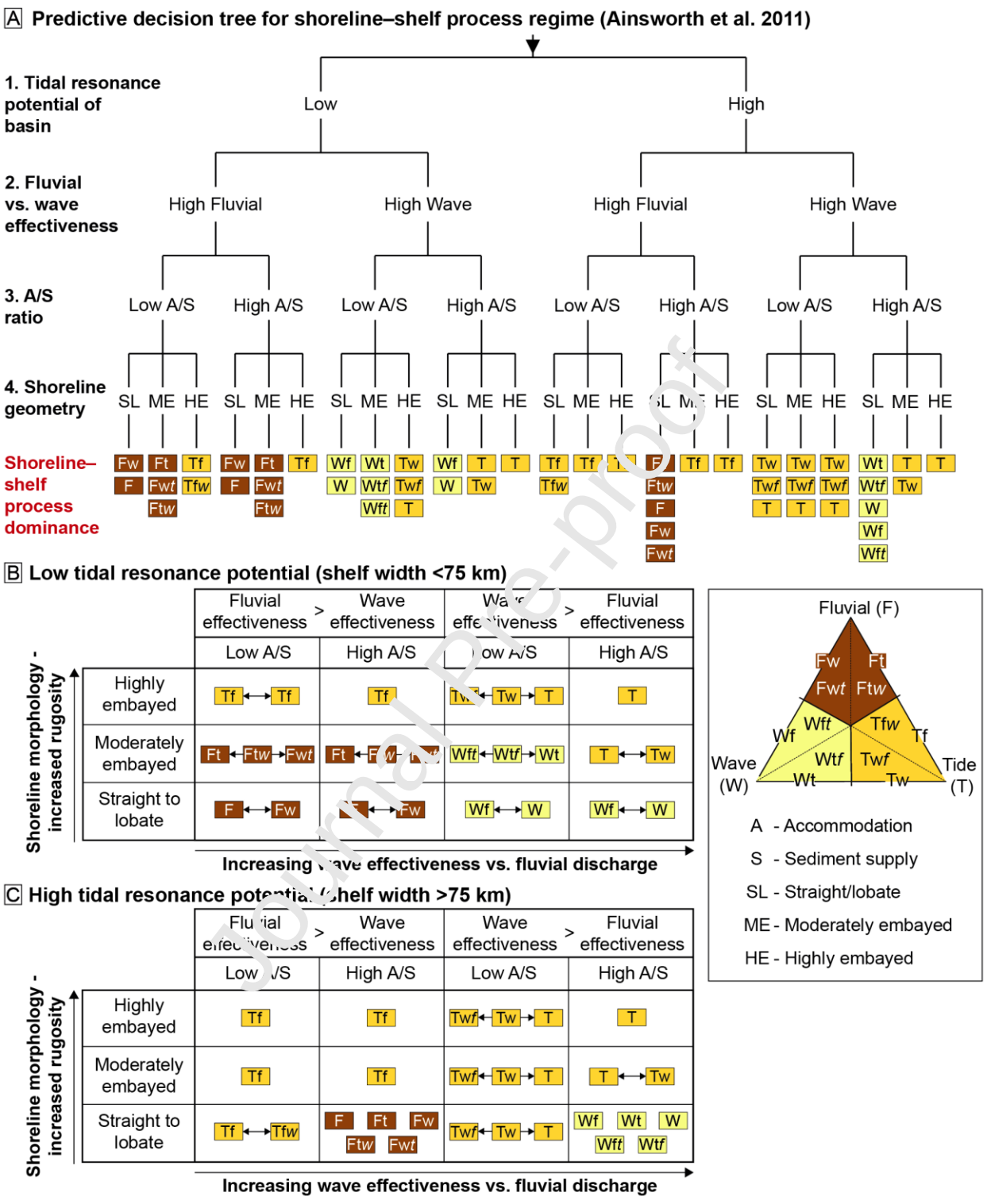

Fig. 3. Predictive model for shoreline process regime (modified from Ainsworth et al. (2011). (A) Decision tree with four main queries predicting shoreline process regime. (B) Predictive matrix for settings with a low tidal potential.

(C) Predictive matrix for settings with a high tidal potential. Abbreviations and color coding are shown in the inset (opposite B).

2.2 Tidal theory, palaeotidal modelling and identification of ancient tidal processes

2.2.1 Tidal theory

Since the mathematical and non-mathematical theory of Earth tides has been reviewed extensively and in detail elsewhere (Defant, 1961; MacMillan, 1966; Pugh, 1987; Dalrymple, 1992; Allen, 1997; Open University Course Team, 1999; Willis, 2005; Kvale, 2006; Kvale, 2012; Longhitano et al., 2012; Reynaud and Dalrymple, 2012; Pugh and Woodworth, 2014; Dalrymple and Padman, 2019), here it will be only briefly discussed in terms of the fundamental concepts and dominant controls impact shallow-water tides (Table 1). Astronomical tides are defined as 'any periodic fluctuation in the water level that is generated by the gravitational attraction of the Moon and Sun' (Dalrymple, 1992) and can be understood by a combination of equilibrium and dynamic theories of tides. In equilibrium tidal theory, the gravitational dynamics of the Earth-Moon-Sun system, combined with the Earth's rotation, results in two oceanic bulges beneath the moon and on the opposite side of the Earth that move clockwise around the Earth to produce twice daily (semidiurnal) high (flood) and low (ebb) tides. Changes in the magnitude of tide-generating forces by the Moon and Sun on varying timescales, in combination with the Earth's tilt, produces various tidal variations and cycles (e.g. diurnal inequality, spring and neap cycles etc.). However, the applicability of equilibrium tidal theory to understanding real-world tides is complicated by several factors, most notably that the Earth's ocean basins are interrupted by significant bathymetric changes and emergent landmasses. Instead, the dynamic tidal theory model tides as the combined effects of many tidal constituents. The 11 most important tidal constituents cause semi-diurnal (M_2, S_2, N_2, K_2), diurnal (K_1, O_1, P_1, Q_1) and long-period (Mf, Mm, Ssa) tides and harmonic convergence and divergence of these constituents result in tidal cycles. The relative importance of diurnal (K_1 and O_1) to semidiurnal (M_2 and S_2) tides is quantified using the ratio *F*, where:

$$F = \left(\frac{K_1 + O_1}{M_2 + S_2}\right)$$

If $F<0.25$, the tide is semi-diurnal, for $0.25<F<1.5$ the tide is mixed semidiurnal dominated, for $1.5<F<3$ the tide is mixed diurnal dominated, and $F>3$ the tide is diurnal (Open University Course Team, 1999).

Name	Description
Astronomical tide	Tide formed by the graviatational and rotational effects of the Moon and Sun on the water in an open ocean or seaway
Bed shear stress	Force per unit area exerted by flow on the sediment surface
Co-oscillating or boundary tide	Tide formed by the propagation of an open-ocean astronomical tide into a connected water body
Coriolis effect and amphidromic cells	The Coriolis effect deflects the tidal wave to the right in the northern hemisphere and left in the southern hemisphere. In the northern hemisphere, this causes the tidal wave to rotate anticlockwise about an amphidromic point of zero tidal range; rotation is clockwise in the southern hemisphere. In enclosed water bodies, the deflected tidal wave (termed a Kelvin wave) pushes against the shoreline, leading to an exponential increase in tidal range from the amphidromic node towards the shoreline. The Coriolis effect also causes asymmetry in the tidal range on either side of elongate water bodies, such as the Yellow Sea, because the incoming tidal wave is larger than the reflected wave.
Diurnal	Once-daily tide where the K_1 and O_1 constituents are more dominant than the M_2 and S_2 constituents
Resonance	Resonance occurs when the tidal period matches a natural mode of oscillation within a water body. Maximum resonance typically occurs when shelf width is approximately a quarter the dominant tidal wavelength, and matches a half-wave oscillator or standing wave in an enclosed basin and quarter-wave oscillator in an open-ended embayment (gulf)
Funnelling	Increase in tidal amplitude caused by progressive narrowing and shallowing of a water body
Semidiurnal	Twice-daily tide where the M_2 and S_2 constituents are more dominant than the K_1 and O_1 constituents
Shoaling	Increase in tidal amplitude caused by progressive shallowing of a water body
Tidal amplitude	Elevation of tidal high water above mean sea level, equal to half the tidal range
Tidal range	Vertical height between consecutive high and low waters over a tidal cycle (twice the tidal amplitude), classified as microtidal (<2 m), mesotidal (2–4 m) and macrotidal (>4 m)

Table 1. Explanations of several tide-related terms used in this paper.

Significant tides, though typically <1 m in tidal range (the difference in sea level between high and low tide), only develop in the open oceans. Open-ocean tides are fundamentally controlled by ocean basin physiography and tides across entire oceans can be 'tuned' to particular tidal constituents. For example, the modern North Atlantic Ocean is close to resonance for the semidiurnal M_2 tide, whereas the modern Pacific Ocean accentuates the diurnal (O_1 and K_1) constituents (Fig. 4). An ocean basin can house resonant tides when the width of the basin, L is equal to a multiple of half wavelengths, $\lambda = \sqrt{gHT}$ (T is the tidal period, g is gravity, and H is water depth) of the tidal wave. Oceanic tides rotate as waves around fixed (amphidromic) points with negligible tidal amplitude (half the tidal range) (Fig. 4). Water on continental shelves and smaller water bodies partly (seas) or fully (lakes) enclosed by land do not develop appreciable *in situ* tides (Dalrymple, 1992). Instead, tides on shelves and in seas rely on the amount of tidal inflow from connected ocean basins which depends on the size, shape and bathymetry of the connection(s) and orientation of connection(s) relative to the oceanic tide (Fig. 4). When oceanic tides

encounter areas of shallower water and constricted physiography, they may undergo amplification due to shoaling, funnelling and resonance (Table 2). Simplified mathematical reviews of these effects are discussed elsewhere (Proudman, 1953; Howarth, 1982; Slingerland, 1986; Allen, 1997; Wells et al., 2007; Kowalik and Luick, 2013). The most relevant points for understanding controls on tides and predicting shoreline–shelf process classification are discussed below.

First, shoaling effects describe the increase in tidal amplitude and current velocity that occurs when water depth decreases, for example, from the deeper ocean onto the continental shelf, and from deeper shelf to shoreline areas. Second, funnelling effects describe the increase in tidal range as a result of physical constriction of the tidal wave, for example, in straits and shoreline embayments. The combination of shoaling and funnelling effects is referred to as convergence effects and these are an important contributing cause of tidal amplification in shoreline – shelf areas. Third, tidal resonance occurs when the natural period of oscillation on the shelf or within a shoreline bathymetric constriction is coincident with the tidal period (Slingerland, 1986; Allen, 1997). On the continental shelf, tidal resonance reaches a maximum when shelf width is one-quarter the tidal wavelength (and for widths 3/4, 5/4, etc.) (e.g. Proudman, 1953; Howarth, 1982). However, this relationship assumes the incident tide is perpendicular to the shelf, friction is inversely proportional to depth and no Coriolis effect, none of which have been widely evaluated. At typical shelf depths (c. 100 m), the quarter wavelength of the dominant semi-diurnal M2 and diurnal K1 tides are c. 350 km and 675 km. As the majority (c. 70%) of modern shelves are <75 km wide (Nyberg and Howell, 2016), tides are closer to resonance as shelf width increases, hence tidal amplitude increases with shelf width (Redfield, 1958; Off, 1963; de Vries Klein, 1977; Cram, 1979; Ainsworth et al., 2011; Reynaud and Dalrymple, 2012). Within an embayment or gulf, tidal resonance occurs when the amount of time taken for the tidal wave to travel for the embayment mouth, to the apex and back to the mouth is the same, or nearly the same, as the time between high and low tides, effectively forming a high amplitude standing wave. The combination of tidal resonance and convergence effects explains the location of the highest tidal ranges globally (O'Reilly et al., 2005). In the Bay of Fundy, eastern Canada, tidal ranges up to 17 m are caused principally by the dominant M_2 tide being very close to resonance, with secondary convergence effects in the landward shallowing and narrowing estuary (e.g. Garrett, 1972; Dalrymple, 2021). In comparison, tides of up to 14m tidal range in the Severn Estuary in the upper reaches of the Bristol Channel, UK, are caused by partial resonance of the dominant M2 tide plus convergence effects in the funnel-shaped and shallowing Severn Estuary (e.g. Gao and Adcock, 2017). Simplified numerical relationships for convergence effects and tidal resonance (e.g. Slingerland, 1986; Allen, 1997; Wells, 2008) can enable first-order interpretations of whether the potentially dominant

semi-diurnal or diurnal tidal constituents may be close to resonance and the potential magnitude of shoaling and funnelling effects in both the modern and ancient.

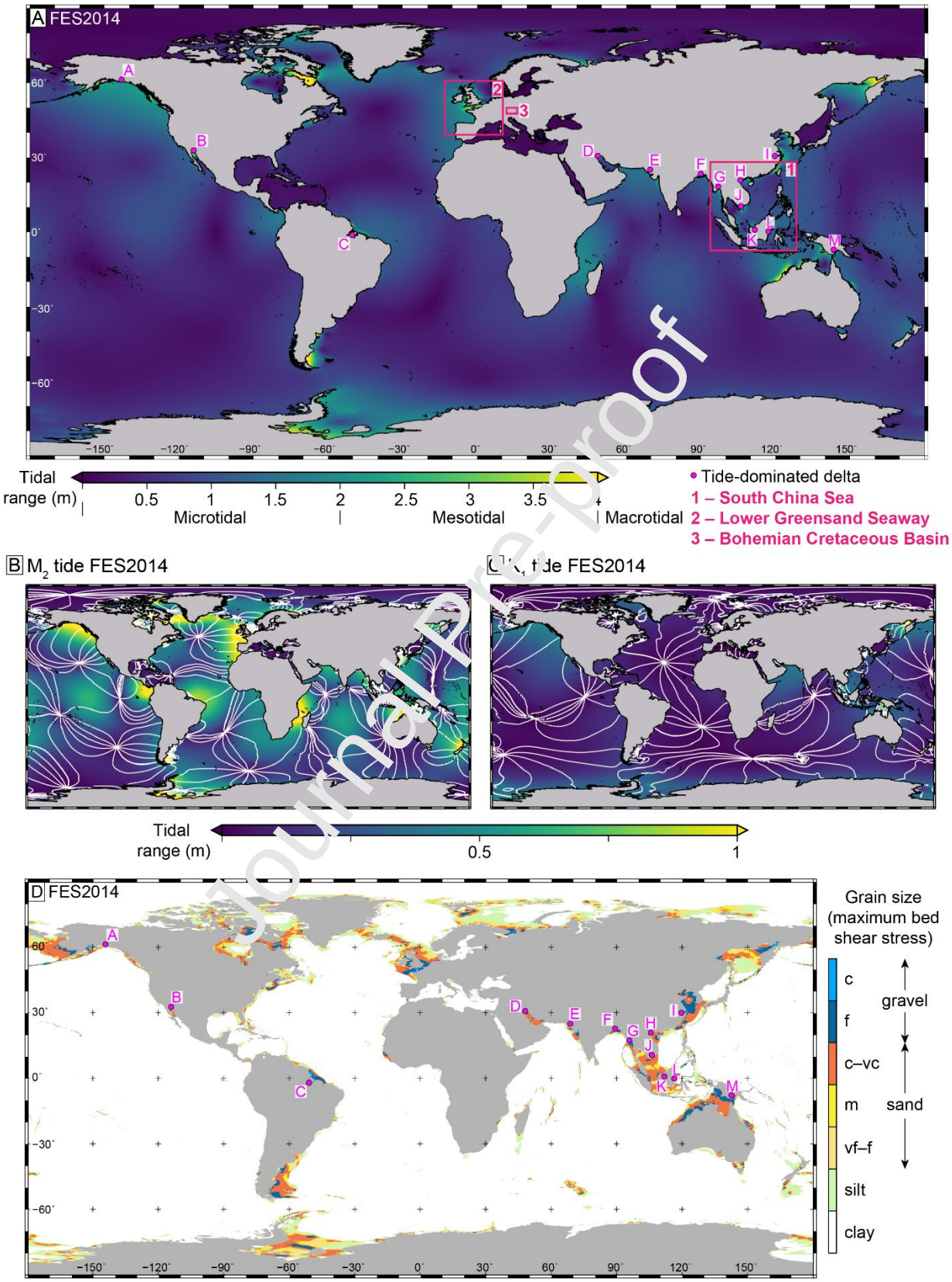

Fig. 4. (A) Present day global tidal range based on the FES 2014 tidal model (Carrère et al., 2015), showing the locations (pink dots) of tide-dominated deltas (Goodbred and Saito, 2012): A) Copper; B) Colorado; C) Amazon; D) Shatt-al-Arab; E) Indus; F) Ganges-Brahmaputra; G) Irrawaddy; H) Red River; I) Yangtze; J) Mekong; K) Rajang; L) Mahakam; and M) Fly. Pink boxes show approximate locations of the palaeotidal modelling case studies. (B, C) Global map of M_2 (B) and K_1 tidal amplitude (C) from FES 2014. Contours join lines of equal phase in 30° intervals and white arrows give the sense of rotation of the major ocean amphidromic systems. (D) Maximum tidal bed shear stress, plotted as the equivalent grain size that could be entrained if available, for FES2014, including the difference in sediment grain size class. Grain size abbreviations: vf = very fine; f = fine; m = medium; c = coarse; vc = very coarse.

2.2.2 Palaeotidal modelling

Palaeotidal numerical modelling can provide quantitative information on ancient shoreline tidal processes and can test their sensitivity to palaeogeographic and palaeobathymetric change and uncertainty (e.g. Martel et al., 1994; Egbert et al., 2004; Wells et al., 2005a; Uehara et al., 2006; Collins et al., 2018a; Collins et al., 2018b). Computational methods for palaeotidal modelling, including tidal forcing boundary conditions and mesh generation, have advanced since early approaches that used structured meshes and open boundary tidal forcing by the M_2 (principal lunar semi-diurnal) tide only, and output tidal amplitude or range (Slater, 1985; Slingerland, 1986; Ericksen and Slingerland, 1990; Martel et al., 1994). More recent simulations have investigated tidal amplitude (Slingerland, 1986; Wells et al., 2005a; Wells et al., 2005b; Wells et al., 2007; Wells et al., 2010a; Wells et al., 2010b) and bed shear stress (Mitchell et al., 2010; Mitchell et al., 2011) in ancient epicontinental seaways, and tidal range and bed shear stress in ancient seas (Collins et al., 2017a; Collins et al., 2018a; Collins et al., 2018b), using models with astronomical tidal forcing and unstructured meshes (Table 2). These diverse case studies illustrate how the sensitivity of shoreline tides to various palaeogeographic and palaeobathymetric changes can improve predictive models of depositional process regimes of ancient shoreline systems.

A multitude of globally applicable numerical tidal models exist (Shum et al., 1997; Stammer et al., 2014), a comprehensive review of which is beyond the aim of this paper. The range of modern ocean tide models can be classified as (1) data-constrained models, those with empirical adjustment to an adopted prior models, (2) barotropic hydrodynamic models that may be constrained by tide information through assimilation, or (3) purely hydrodynamic models with no data constraints (Stammer et al., 2014). Palaeotidal models, where no empirical tidal data are available, must by definition be purely hydrodynamic. The tidal model used in the ancient case studies discussed herein is Fluidity (http://fluidityproject.github.io/), formerly the Imperial College Ocean Model (ICOM), which can be used to simulate both astronomical and co-oscillating boundary tides. Details of the tetrahedral, unstructured meshing and hydrodynamic modelling approach used with Fluidity have been widely documented and will not be repeated herein (Pain et al., 2005; Wells et al., 2005a; Gorman et al., 2007; Gorman et al., 2008; Piggott et al., 2008; Geuzaine and Remacle, 2009; Avdis et al., 2018) (e.g. Wells et al., 2010a) Wells et al., 2007a; Mitchell et al., 2010). Likewise, tidal modelling using Fluidity has been extensively validated against real-world modern tidal amplitude (Wells et al., 2005a; Wells et al., 2005b; Wells et al., 2007; Wells, 2008; Wells et al., 2010a; Wells et al., 2010b; Collins et al., 2017a; Collins et al., 2018a; Collins et al., 2018b) and tidal bed shear stress (Mitchell et al., 2010; Mitchell et al., 2011; Collins et al., 2017a; Collins et al., 2018a; Collins et al., 2018b), which includes global (Wells et al., 2010a; Collins et

al., 2018a; Collins et al., 2018b) and regional comparisons in the Mediterranean Sea (Wells et al., 2005a), North Sea (Wells et al., 2007; Mitchell et al., 2010), Baltic Sea (Wells, 2008) and South China Sea (Collins et al., 2017a; Collins et al., 2018a; Collins et al., 2018b) (see Supplementary Material). As well as Fluidity, other modern hydrodynamic tidal models have been used for palaeotidal modelling, notably the Oregon State University Tidal Inversion Software (OTIS) (Egbert et al., 2004; Green and Huber, 2013; Wilmes and Green, 2014; Green et al., 2017).

Geologic age & reference	Study area	Computational method	Boundary conditions	Key findings
Late Devonian c. 370 Ma (Slingerland, 1986)	Catskill epicontinental sea of North America	Structured grid, finite difference scheme; Navier–Stokes equations; Coriolis parameter (f -plane).	Open boundary tidal forcing, no astronomical tidal forcing; M2 tide only; Variable bathymetry; Chezy approximation for bottom friction.	Microtidal–low mesotidal, locally mesotidal–macrotidal areas due to resonance, funnelling and shoaling effects. Tidal ranges increased by 1) increasing the boundary tidal range; 2) increasing the open boundary width; and 3) increasing the depth of the seaway.
Mid Cretaceous c. 100 Ma (Slater, 1985)	Western Interior Seaway of North America	Structured grid, finite difference scheme; Laplace Tidal Equations; No Coriolis parameter.	Open boundary and astronomical tidal forcing; M2 tide only; Uniform depths; Linear bottom friction with respect to velocity.	Microtidal; Astronomical tidal forcing dominates; Open boundary tide negligible from the Arctic Ocean and possibly significant from the Gulf of Mexico; Tidal range sensitive to water depth (resonance at 200 m water depth).
Mid Cretaceous c. 100 Ma (Ericksen and Slingerland, 1990)	Western Interior Seaway of North America	Structured grid, finite difference scheme; Navier Stokes equations; Coriolis parameter (f -plane).	Open boundary tidal forcing, no astronomical tidal forcing; M2 tide only; Variable bathymetry; Chezy approximation for bottom friction.	Microtidal, locally mesotidal–macrotidal near Gulf of Mexico open boundary; Tidal range increases as seaway depth and Gulf of Mexico connection increases; Open boundary tides argued to be dominant

				contributor to tides, not astronomically forced tides (cf. Slater, 1985).
Miocene c. 22 Ma (Martel et al., 1994)	Alpine foreland basin of France and Switzerland	Structured grid, finite difference scheme; Navier Stokes equations; Coriolis Parameter (f -plane).	Open boundary tidal forcing, no astronomical tidal forcing; M2 tide only; Variable bathymetry; Chezy approximation for bottom friction.	Higher tidal current speeds predicted with wider and deeper open-ocean connections and 2m open boundary tide applied.
Late Carboniferous c. 300 Ma (Wells et al., 2005a,b)	Late Carboniferous sea of NW Europe	Unstructured, tetrahedral mesh, finite element scheme; Navier Stokes equations; No Coriolis parameter; Fluidity tidal model.	Astronomical tidal forcing only; M2 tide only; Variable bathymetry; No treatment of bottom friction.	Extremely microtidal seaway (typically <10 cm tidal range) across NW region across various sensitivity tests; Putative tidal deposits interpreted to be confined to localised estuaries.
Late Carboniferous c. 300 Ma (Wells et al., 2008)	Late Carboniferous sea of NW Europe	Unstructured, tetrahedral mesh, finite element scheme; Navier Stokes equations; Coriolis parameter included; Fluidity tidal model.	Astronomical tidal forcing only; M2, S2, N2, K2, Q1, O1, P1, K1, M_f, M_m and S_{sa} tidal constituents; Variable bathymetry; Bottom drag applied as surface-integral based on quadratic friction law.	Microtidal ranges predicted across the northwest European region (similar to Wells et al., 2005a, b); Extra tidal constituents increase the predicted tidal range to 20–80 cm.

Early Cretaceous, late Aptian, c. 116 Ma (Wells et al., 2010a)	Global	Unstructured, tetrahedral mesh, finite element scheme; Navier Stokes equations; Coriolis parameter included; Fluidity tidal model.	Astronomical tidal forcing only; M2, S2, O1 and K1 tidal constituents modelled independently; Variable bathymetry; Bottom drag applied as surface-integral based on quadratic friction law.	Model results compared to published geologic records; High mesotidal to macrotidal on the Arabian Platform, around India, along the Pacific coast between North and South America, northeast of Australia, and around Southeast Asia; Low microtidal ranges in the proto-South Atlantic Ocean and Weddell Sea.
Early Cretaceous, late Aptian – early Albian, c. 112–107 Ma (Wells et al., 2010b)	Lower Greensand Seaway of NW Europe	Unstructured, tetrahedral mesh, finite element scheme; Navier Stokes equations; Coriolis parameter included; Fluidity tidal model.	Open boundary conditions (from Wells et al., 2010a) and astronomical tidal forcing; M2, S2, O1 and K1 tidal constituents modelled independently; Variable bathymetry; Bottom drag applied as surface-integral based on quadratic friction law.	Overall microtidal increasing to microtidal–macrotidal with increased width and depth of open-ocean connections and more localised funnelling, shoaling and Coriolis effects.
Middle Cretaceous, Early–Middle Turonian, c. 93 Ma (Mitchell et al., 2010)	Bohemian Cretaceous Basin of Central Europe	Unstructured, tetrahedral mesh, finite element scheme; Navier Stokes equations; Coriolis parameter included; Fluidity	Open boundary conditions and astronomical tidal forcing; varying combinations of M2, S2, O1 and K1 tidal constituents; Variable bathymetry; Bottom drag applied as surface-integral	Microtidal–mesotidal across the Bohemian Cretaceous Basin and range of sensitivity tests; Elevated tidal ranges and velocity in local embayments and straits due to funnelling and shoaling effects.

		tidal model.	based on quadratic friction law.	
Early Jurassic, c. 200 Ma (Mitchell et al., 2011)	Laurasian Seaway of NW Europe	Unstructured, tetrahedral mesh, finite element scheme; Navier Stokes equations; Coriolis parameter included; Fluidity tidal model.	Astronomical tidal forcing; M2, S2, O1 and K1 tidal constituents; Variable bathymetry; Bottom drag applied as surface-integral based on quadratic friction law.	Seaway largely microtidal; Flow constriction associated with shallow platforms and straits produced elevated bed shear stresses that were decoupled from tidal range.
Eocene, c. 55 Ma (Green & Huber, 2013)	Global	Finite element grid, 1/4° resolution, Numerical solutions to linearized shallow water equations, including Coriolis parameter; OTIS tidal model.	Includes up to 8 constituents (M2, S2. N2. K2, K1, O1, P1, Q1) and linear bottom drag parameterization (see Egbert et al., 2004); Variable ocean bathymetry and stratification.	Weak M2 tide precited in Eocene ocean except in the Pacific.
Mesozoic–Cenozoic, 5 timeslices from c. 252 Ma to 3 Ma (Green et al., 2017)	Global	Finite element grid, 1/4° resolution, Numerical solutions to linearized shallow water equations, including Coriolis parameter; OTIS tidal model.	M2, S2, K1 and O1 tidal constituents and linear bottom drag parameterization (see Egbert et al., 2004); Variable ocean bathymetry and stratification.	Tidal dissipation during the Cenozoic and Late Cretaceous were weaker than at present, apart from the glacial states over the last 2 Ma.

Oligocene–Miocene, c. 26–5 Ma (Collins et al., 2017a, 2018a)	South China Sea, SE Asia	Unstructured, tetrahedral mesh, finite element scheme; Navier Stokes equations; Coriolis parameter included.	Astronomical tidal forcing; M2, S2, N2, K2, Q1, O1, P1, K1, M_f, M_m and S_{sa} tidal constituents; Variable bathymetry; Bottom drag applied as surface-integral based on quadratic friction law.	Spring tides along South China Sea coastline were largely mesotidal–macrotidal and capable of transporting sand throughout the Late Oligocene to Middle Miocene.
Late Cretaceous middle Campanian, c. 75-77.5 Ma (Dean et al., 2019)	Western Interior Seaway of North America	Unstructured, tetrahedral mesh, finite element scheme; Navier Stokes equations; Coriolis parameter included.	Astronomical tidal forcing; M2, S2, N2, K2, Q1, O1, P1, K1, M_f, M_m and S_{sa} tidal constituents; Variable bathymetry; Bottom drag applied as surface-integral based on quadratic friction law.	Regionally microtidal and mesotidal (2–4 m) along most of the eastern margin of the seaway; increased tidal bed shear stress when seaway center and entrance to Gulf of Mexico are deeper.

Table 2. Summary of previously published palaeotidal models from deep geologic time (excluding the Quaternary).

2.2.3 Identification of ancient tidal processes

2.2.3.1 Tidal facies analysis

Observations across the range of facies- to facies succession scales interpreted as indicating tidal processes have been widely documented from several different shallow-water depositional environments, most notably deltas, estuaries, barrier inlets, embayments, straits and open shelves (Johnson and Baldwin, 1996; Reading and Collinson, 1996; Bhattacharya, 2010; Dalrymple, 2010b; Martinius and van den Berg, 2011; Davis and Dalrymple, 2012; Longhitano et al., 2012). The most significant features are those related to tidal flow reversals, flood–ebb tide versus slack water dynamics and tide-related periodicity, particularly the following: (1) bidirectional cross-bedding and cross-lamination (cm–dm-scale), including the relatively rare variant of 'herringbone' patterns (e.g. Van Straaten, 1953; Reineck, 1963; Boersma, 1969; Klein, 1970a; Klein, 1970b; Klein, 1971; Hayes, 1980; Boersma and Terwindt, 1981; Yoshida et al., 2004); (2) larger-scale (10s m-scale) bidirectionality, such as between separate but closely spaced sand bodies with oppositely-dipping cross-bedding, which have been interpreted to reflect mutually evasive ebb- and flood-tidal channels and bars (Robinson, 1960; Johnson, 1975; Johnson and Levell, 1995; Harris et al., 2004; Sixsmith et al., 2008; Legler et al., 2013; Levell et al., 2020); (3) sigmoidal 'shovel-shaped' cross-bed sets, with extended mud-rich toesets, sometimes with oppositely-dipping current ripples (e.g. Boersma and Terwindt, 1981; Mutti et al., 1984; Mutti et al., 1985; Kreisa and Moila, 1986; Dalrymple and Rhodes, 1995; van den Berg et al., 2007; Tinterri, 2011); (4) multiple reactivation surfaces with an apparent cyclicity or predictable and repeated pattern (e.g. Boersma, 1969; McCabe and Jones, 1977; Reineck and Singh, 1980; Boersma and Terwindt, 1981; Allen, 1982a; Allen and Homewood, 1984); (5) 'paired drapes' or 'double drapes' comprising sandy foresets and associated mudstone and/or carbonaceous (typically finely comminuted 'coffee ground' type) drapes (mm–cm-scale), which are interpreted to form by semi-diurnal to diurnal tidal inequality (e.g. Reineck and Singh, 1980; Visser, 1980; Smith, 1988; De Boer et al., 1989; Nio and Yang, 1991); (6) 'tidal bundles' in the form of lateral and vertical thickness variations of sandy foresets and associated mudstone/carbonaceous drapes (dm–m-scale) , which have been related to spring–neap semi-lunar cycles (e.g.Visser, 1980; Allen, 1981b; Boersma and Terwindt, 1981; Allen and Homewood, 1984; Kreisa and Moila, 1986; Nio and Yang, 1991) (cf. Martinius and Gowland, 2011); (7) heterolithic bedding (cm–m-scale) with apparent, or preferably measured and statistically analysed, cyclicity in the thickness of sandstone–mudstone layers, which are referred to as 'couplets' if other evidence of tidal deposition (e.g. bidirectional current ripples etc.) are observed (Reineck and Wunderlich, 1968; Terwindt, 1971; Terwindt and Breusers, 1972; Reineck and Singh, 1980; Kvale et al., 1989; Archer et al., 1991; Archer, 1995; Greb and Archer, 1995; Kvale, 2006; Kvale, 2012); (8) inclined heterolithic strata (dm–10s m-scale) (Thomas et al., 1987; Smith,

1988; Dalrymple et al., 2003; Choi et al., 2004; Dalrymple and Choi, 2007); (cf. Sisulak and Dashtgard, 2012; Jablonski and Dalrymple, 2016); and (9) ichnofabrics which, in general, show reduced but variable and sporadic bioturbation intensities and predominance of facies-crossing ichnofauna (MacEachern et al., 2005; McIlroy, 2006; McIlroy, 2007; MacEachern and Bann, 2008; Longhitano et al., 2010; Gingras and MacEachern, 2012; Gingras et al., 2012). In terms of micropalaeontological information, the most important potential indicator of tidal processes are palynomorph acmes of coastal biomes whose distribution, abundance and productivity within a depositional system is strongly related to tidal processes, most notably those associated with deposition in mangrove, seagrass and salt marsh settings (e.g. Grindrod, 1988; Wolanski et al., 1992; Woodroffe et al., 2016).

Definitive recognition of tide-influenced sedimentation relies on observing combinations of the features described above because, in isolation, some of these features can form by other processes (e.g. wave, storm and/or fluvial) operating by themselves or, especially, in combination with tides (e.g. Thomas et al., 1987; Hovikoski et al., 2008; Dalrymple, 2010b; Martinius and van den Berg, 2011; Reynaud and Dalrymple, 2012; Dalrymple et al., 2015; Gugliotta et al., 2016a; Gugliotta et al., 2016b; Collins et al., 2020). Mixed-process settings, especially those where fluvial and tidal currents coexist, can exacerbate differences in the strength and sediment transport capacity of ebb- and flood-tidal currents. Strongly skewed palaeocurrent patterns, with one dominant offshore-directed mode, and a weaker oppositely-directed secondary mode, may occur when fluvial, wave and/or storm processes combine with tides, such as in deltaic and estuarine settings (Legler et al., 2013; van Cappelle et al., 2016; Collins et al., 2020; Levell et al., 2020). For example, in the modern microtidal Po Delta, preserved tidal signals in open-water prodelta facies are correlatable to cyclical variations in water-surface steepness and consequent changes in river discharge velocity and sediment transport capacity in distributary channels (Maselli et al., 2020). In modern open-marine shelf settings, storm-induced currents can also contribute to tidal current sediment transport asymmetry (Stride, 1973; Belderson et al., 1982; Stride, 1982). Similarly, storm-enhanced tidal transport systems have been inferred to explain unidirectional palaeocurrent patterns in ancient shallow-marine deposits (Banks, 1973; Johnson, 1975; Anderton, 1976; Levell, 1980) and, in the modern Fly River delta, sediment transport to and across the delta front may be controlled by wave-induced resuspension together with tides, storm surge and barotropic flow (Harris et al., 2004). Autogenic tidal processes responsible for mutually evasive ebb and flood tidal channels can also create skewed palaeocurrent patterns in the stratigraphic record, particularly where: (1) channel preservation is unequal, (2) ebb and flood tidal channels are so effectively shielded from each other that evidence of the secondary

reversing tide is absent, and/or (3) incomplete outcrop or subsurface dataset (Sixsmith et al., 2008; Legler et al., 2014).

Confident identification of tidal influence and its relative importance with respect to other processes (e.g. wave, storm and/or fluvial) requires reconstruction of shoreline palaeo-geomorphology at the scale of the depositional system (c. 1–100s km), based on detailed facies analysis in the context of high-resolution stratigraphic and regional palaeogeographic relationships. Such confidence in interpretation requires data of high quality and density, such as provided by extensive outcrop data (e.g. Willis and Gabel, 2001; Legler et al., 2013; Legler et al., 2014; Ainsworth et al., 2016; Rossi et al., 2016; van Cappelle et al., 2016; Kurcinka et al., 2018; Van Yperen et al., 2020) or subsurface datasets containing 3D seismic data, densely spaced wells and/or extensive cores (e.g. Hubbard et al., 2011; Willis and Fitris, 2012; Holgate et al., 2013). In practice, such datasets and confident interpretations are rare. It is therefore appropriate to focus comparison of 'rock-record' data with tidal model predictions at bedform scale (*c.* mm–10s m), at which interpretations of bed shear stress as a proxy for tidal current velocity (section 3.2.3) can be readily made. Other tidal model outputs, including tidal range (section 3.2.2) and tidal phase, are typically less straightforward to interpret from available 'rock-record' data (Wells et al., 2005a; Mitchell et al., 2010).

2.2.3.2 Palaeotidal range analysis

Analysis of palaeotidal range from the rock record requires observations and interpretation at a range of scales: depositional system morphology (c. 1–100s km), depositional environments (c. 0.1–1 km) and depositional elements and facies (<1 to 10s m) may all preserve an imprint of tidal sedimentary processes but do not permit accurate constraints on tidal range, often not even the ability to differentiate microtidal, mesotidal and macrotidal regimes (Table 3) (Wells et al., 2005a). Alternative methods used to estimate palaeotidal range are: (1) interpretations of water depth from stratigraphic position within interpreted fining-upward channel-fill units (Nio et al., 1983) (Yang and Nio, 1985); (2) stratigraphic thickness estimates of interpreted intertidal deposits in tidal flat units (Klein, 1970a; Klein, 1971), although these units are very similar to interpreted channel-fill units within the fluvial-to-marine transition zone (e.g. Olson, 1972; Dalrymple and Choi, 2007; Amir Hassan et al., 2013; Gugliotta et al., 2016a; Collins et al., 2018c; Collins et al., 2020); and (3) average calculations of characteristic mudstone drape spacings based on groups of sandstone–mudstone couplets from interpreted spring and neap conditions, and various assumptions regarding dune height and speed, dry bulk sediment density, and current velocity for

sediment entrainment (Allen, 1981b). Depositional systems subject to higher tidal ranges are more likely to be tide-dominated, but this relationship is inconsistent (e.g. Hayes, 1979; Mulhern et al., 2017), especially for mixed-process systems (e.g. Davis and Hayes, 1984). Furthermore, higher tidal ranges may not always correspond to stronger tidal currents (Dalrymple, 2010b), as shown in both modern macrotidal environments (e.g. Yang et al., 2008) and palaeotidal models (Mitchell et al., 2011). Consequently, numerous studies have highlighted that tidal range is, at best, an imperfect indicator of sedimentary response.

Indicator	Size	Description	Tidal range
Delta morphology	10s - 100s km	Tide-dominated deltas display wide, landward-tapering river mouths, elongate shore-normal mouth bars, sinuous tidal creeks, tidal flats, saltmarsh and/or mangroves, and smaller-scale tidal indicators (e.g. Ganges-Brahmaputra, Mahakam, Irrawaddy, Fly deltas)	Mesotidal to macrotidal
		Fluvial-dominated deltas display digitate ('bird's-foot') to lobate morphologies and rapid progradation due to higher relative stream power compared to wave/tide reworking (e.g. Mississippi delta).	Microtidal to mesotidal
		Wave-dominated deltas display cuspate geometries with intermediate progradation rates due to wave action ('littoral energy fence') (e.g. Baram)	Microtidal to mesotidal
Open shelf tidal sand-sheets (including tidal sand ridges and ribbons)	10s - 100s km	Sheets are tabular sandbodies with planar tops and bases formed by open-shelf tidal currents. Super-imposed sedimentary bodies include tidal sand ridges, linear bedforms with long axes orientated up to 20 obliquely to tidal currents and distinguished from aeolian dunes by the presence of 2 main current directions at 180°, shelly debris, reactivation surfaces, low angle (3–6) cross-stratification and marine trace fossils (e.g. Norfolk Ridges, southern North Sea). Smaller superimposed bedforms include sand ribbons, scour hollows, longitudinal furrows, obstacle marks, sand waves, rippled sand sheets and longitudinal sand	Mesotidal to macrotidal

		patches.	
Furrows and gravel waves	L < 150 km; W < 50 km	Mostly erosional features with small (ca 1 m high, 10 m wavelength) gravel-rich subaqueous dunes, formed due to low sediment supply and strong tidal currents (e.g. Bristol Channel)	Macrotidal
Estuarine/incised valley-fill tidal sandbodies	W < 30 km; T ca 1 m	Outer estuary characterized by elongate sand ridges and tidal channels with super-imposed, smaller scale tidal indicators. Middle and inner estuary characterized by heterolithic strata with isolated sandbodies (e.g. Thames estuary, southern North Sea)	Microtidal to macrotidal
Saltmarsh	L 10 km; W < 5 km; T < 10 m	Gently sloping coastal wetland which extends landwards to the high-tide mark. Evaporating pools of saline water form localized 'salt-pans' and fauna and flora adapted to highly fluctuating salinities dominate.	Mesotidal to macrotidal
Mangroves	L <200 km; W <60 km; T <10 m	Densely vegetated forests occupying the lower intertidal zone (ca mean sea level to low-tide mark) of tide-dominated, typically mud-rich deltaic shorelines. Flora sub-zonations related to topography and often diverse fauna adapted to salinity variations (e.g. Mekong, Ganges-Brahmaputra deltas).	Mesotidal to macrotidal
Tidal creeks	W < 100 m; T 10	Shore-normal creeks which do not pass into a fluvial system landwards,	Microtidal to macrotidal

	m	often mud-rich.

Table 3. Larger-scale tidal indicators, ranging from depositional environments to systems, and their generalized implication for tidal-range prediction in the geological rock record (modified after Wells et al., 2005a).

2.2.3.3 Ancient bed shear stress analysis

Bed shear is a better indicator than tidal range of sedimentary response as it is a key variable for understanding the initiation and maintenance of grain motion, formation of bedforms (Fig. 5), and both competence-driven and capacity-drive deposition (Harms et al., 1982; Komar, 1987; Hiscott, 1994; Dalrymple, 2010a). Tidal currents that exceed the critical bed shear stress threshold for sediment entrainment will impact sedimentary processes and preserved sedimentary structures and grain size provide some information on ancient bed shear stress (Fig. 5). However, the type of sedimentary structures formed by currents of varying flow velocity is also strongly dependent on the available grain size and water depth during deposition (Fig. 5), which can only be estimated in the context of facies successions, permitted by the availability of appropriate rock record data. Less reliable predictions of available grain size range may be possible based on catchment area geology, interpreted palaeo-drainages and other indirect data sources (e.g. seismic geometries of clinoforms, seismic amplitudes, well logs and other borehole data). For a given water depth, if tidal bed shear stress was insufficient to rework the minimum grain size available, tides will not have influenced sediment transport. In contrast, the size, type and texture of sedimentary structures may vary depending on tidal current strength and the frequency with which the critical bed shear stress for entrainment of the available grain size range was exceeded.

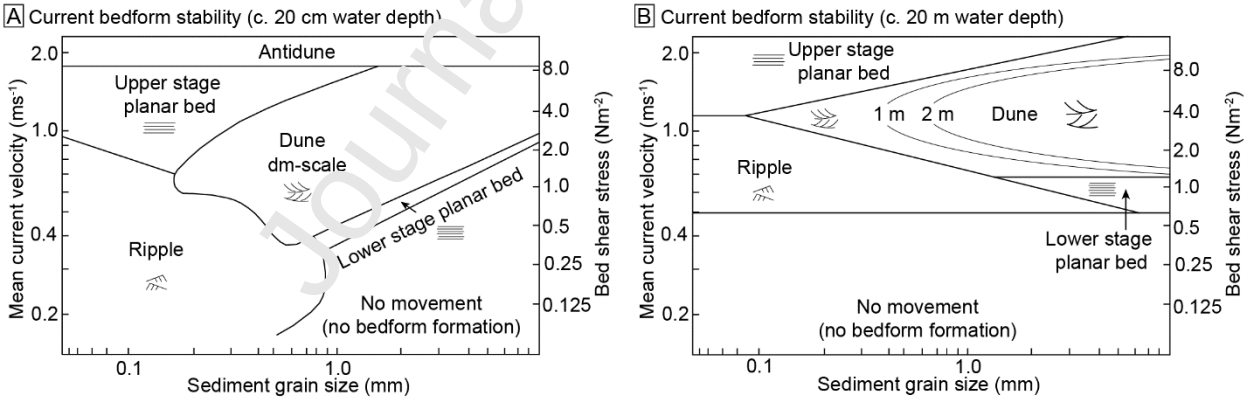

Fig. 5. (A) Bedform stability diagram, including bed shear stress, for unidirectional flow at approximately 20 cm water depth (flume tank) (Harms et al., 1982; Mitchell et al., 2010). (B) Bedform stability diagram, including bed shear stress, for unidirectional flow at approximately 2 m water depth (Rubin and McCulloch, 1980).

3 PALAEOTIDAL MODELLING CASE STUDIES

Several published palaeotidal modelling case studies each provide unique insights into the controls on tidal processes across a range of time periods and geological settings. Herein, we review three case studies that illustrate the range of physiographic controls on tides relevant for improving predictions of shoreline–shelf progress regime. Together these three case studies document changes in tidal processes: (1) across a wide range of spatial scales, from regional scale in open oceans (1000s km) through seaways and enclosed basins (100s – 1000s km), to local scale on continental shelves (10 – 100s km) and in shoreline features (1–10s km); (2) in different basin and tectonic settings; (3) across different time encompassing various changes in basin-to-shoreline physiography; and (4) at various times in Earth history. Below, each case study is summarized in turn, with a brief review of the geological setting followed by a synthesis and discussion of the palaeotidal model results in terms of the influence on tides by larger-scale basin physiography (100–1000 km), shelf width (c. 10–100 km) and shoreline geometry (c. 1–10 km).

3.1 Regional-scale controls on tidal deposition: Oligocene–Miocene South China Sea (SCS), Southeast Asia

3.1.1 Background

During the Oligo–Miocene, the SCS and wider Southeast Asia region experienced geologically rapid and extensive tectonic reorganization, impacting large-scale oceanic flow patterns, in response to major movements of the Indo-Australian, Eurasian, Pacific and Philippine Sea plates (Fig. 6) (Lee and Lawver, 1995; Hall, 1996; Hall, 2002). In summary, Oligocene–Early Miocene tectonism within the SCS was dominated by active seafloor spreading and broadly occur between c. 32–31 Ma and 20.5 Ma or 15 Ma (Briais et al., 1993; Barckhausen et al., 2014) (Barckhausen and Roeser, 2004). Post-collision uplift formed a foredeep along the NW Borneo margin by the Late Miocene (Hinz et al., 1989; Hall, 2002; Ingram et al., 2004; Franke et al., 2008; Hutchison, 2010), whilst the Sunda Shelf remained emergent throughout the Oligo–Miocene, in contrast to its present-day drowned state (Fig. 6) (van Hattum et al., 2006; Hall, 2013; Shoup et al., 2013) (e.g. Gordon et al., 2012; Hu et al., 2015). At the eastern SCS margin, clockwise rotation and northward movement of the Philippine Sea Plate and the Izu-Bonin-Mariana (IBM) arc formed the present-day Philippines by the Middle–Late Miocene and narrowed oceanic connections into the SCS from the Pacific Ocean north of the IBM arc, which is modelled as emergent in some palaeogeographies due to physiographic uncertainty (Fig. 6) (Collins et al., 2017a; Collins et al., 2018a; Collins et al., 2018b). At the western SCS margin, variable extension, compression, eustatic sea level and sediment supply impacted formation,

development and infill of several shelf basins (Doust and Sumner, 2007; Miller et al., 2011; Shoup et al., 2013; Morley, 2016; Collins et al., 2018a; Collins et al., 2018b).

Numerical palaeotidal modelling was undertaken to understand the spatial and temporal impact that regional-scale, tectonic-driven physiographic changes had on shoreline–shelf tides and the corresponding stratigraphic record during the Late Oligocene–Miocene interval. Palaeotidal modelling with Fluidity used full astronomical tidal forcing and global multi-scale meshes with a maximum *ca* 10 km resolution (Collins et al., 2017a; Collins et al., 2018a; Collins et al., 2018b). Model outputs included herein (Collins et al., 2018a) are maximum spring tidal range and maximum tidal bed shear stress, plotted as the equivalent grain size capable of being transported if present (see Section 2.2.3.3). 'Base case' models used the preferred palaeogeographic interpretations at sea level highstand for three time intervals in the Early, Middle and Late Miocene (Fig. 7). Sensitivity tests included tidal models for 50 m sea level lowstand palaeogeographies for Late Oligocene–Late Miocene time intervals, and a Late Miocene (6 Ma) tidal model for a palaeogeography with a submerged (10 m) IBM arc.

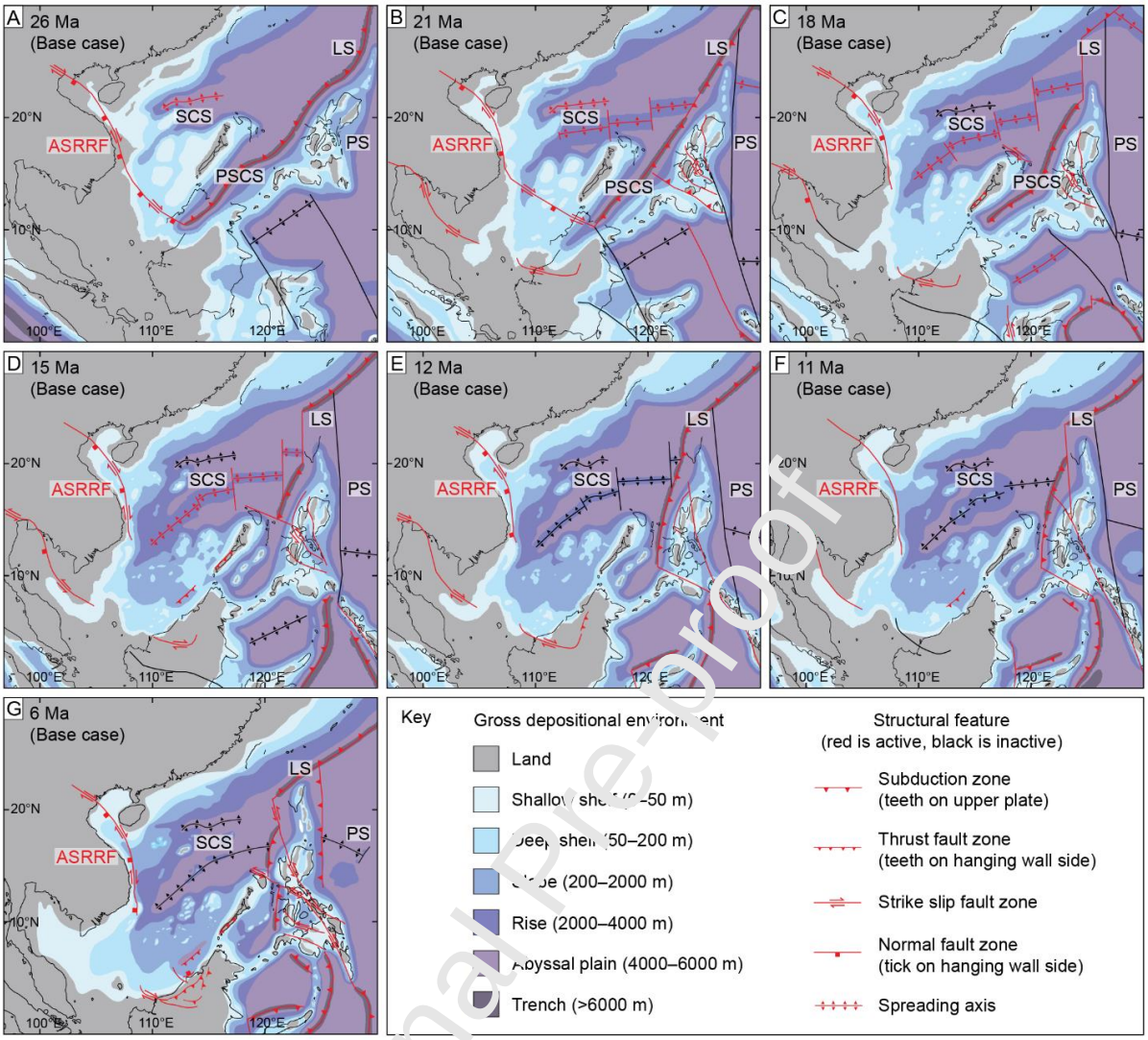

Fig. 6. Gross depositional environmental reconstructions for the Late Oligocene–Late Miocene in Southeast Asia based on sea-level highstand for eight time-slices: (A) 26 Ma (Chattian); (B) 21 Ma (Aquitanian); (C) 18 Ma (Burdigalian); (D) 15 Ma (Langhian); (E) 12 Ma (Serravallian); (F) 11 Ma (Tortonian); (G) 6 Ma (Messinian). Alternative gross depositional environmental reconstructions include a submerged Palawan: (H) 26 Ma (Chattian); (I) 21 Ma (Aquitanian); (J) 18 Ma (Burdigalian). After Collins et al. (2018a).

3.1.2 Model results and rock-record integration

In the Oligocene–Miocene SCS, regional (100–1000s km) and tectonic-driven palaeogeographic changes caused a significant decrease in the overall extent and magnitude of tidal processes. Most notably during the Miocene, reduced oceanic inflow and boundary tide related to narrowing of the Pacific Ocean connection via the Luzon Strait (from c. 1500 km to 350 km) and north of the IBM arc (from c. 1600 km to 370 km) coincided with no ocean outflow from the SW SCS due to the emergent Sunda Shelf. Consequently, tides in the central SCS decreased from macrotidal (>4 m), and capable of coarse sand to gravel transport in the Early Miocene, to mesotidal (>2 to 4 m), and capable of fine

sand to silt transport in the Middle–Late Miocene (Fig. 7). The importance of regional-scale ocean inflow on tides is further indicated by sensitivity analyses. Shutdown of oceanic throughflow into the Sea of Japan during lowstands increased tidal inflow and boundary tides to the SCS, resulting in larger and stronger tides than during equivalent highstands (Fig. 8A–B). Likewise, submerging the IBM arc (to only 10 m water depth) in the Late Miocene causes substantially larger and stronger tides across the SCS (Fig. 8C–D). Overall, tides were diurnal to mixed diurnal dominated (F-ratio >1.5), reflecting amplification and dominance of diurnal tides in the Pacific Ocean, similar to the present day.

On a local-scale, tidal range and bed shear stress maxima in the Oligo–Miocene SCS invariably occurred within embayed shoreline areas, particularly those with (1) relatively wide and deep entrances open to the incoming tide, and (2) high resonance and theoretical funnelling potential (Collins et al., 2018a). For example, widening and deepening the entrance to the Gulf of Thailand (western SCS) permitted greater tidal inflow and a larger tidal prism, potentially enhanced by resonance effects, resulting in an increase from microtidal to low mesotidal conditions during the Miocene (Collins et al., 2018a).

Model results are supported by sedimentological and micropalaeontological data (Fig. 9) and are consistent with previous Miocene palaeoenvironmental stratigraphic interpretations (e.g. Doust and Sumner, 2007), including the distribution of interpreted mangrove-related facies in the western SCS (Morley et al., 2011; Shoup et al., 2013). Preserved Oligocene–Middle Miocene strata in several basins within areas of high modelled tidal range and bed shear stress include interpretable evidence for tidal processes on different scales (e.g. facies to facies successions), and mangrove palynomorph data, notably acmes in mangrove pollen (Fig. 8) (Morley et al., 2011; Shoup et al., 2013). Tidal processes are commonly interpreted to have operated together with river processes, and to a lesser extent wave processes. Mixed fluvial and tidal preservations is often expressed within heterolithic facies and facies associations, where variations in sandstone-bed thickness, the ratio of sandstone-to-mudstone, and bioturbation on a cm-to-metre scale can be attributed to variations in river discharge and tides (Amir Hassan et al., 2013; Amir Hassan et al., 2016; Collins et al., 2018c; Collins et al., 2020). Tidal processes are also interpreted for sandstone-dominated facies associations and successions predominantly characterised by trough-cross stratification, often but not exclusively with long rippled toesets and/or bi-modal palaeocurrent directions. Significantly, this occurs in association with paralic coals and mudstones deposited within or in close relation to mangroves, including *in situ* occurrences (Morley et al., 2011; Amir Hassan et al., 2013; Togunwa et al., 2015; Amir Hassan et al.,

2016; Murtaza et al., 2018). Tidal signals are less widespread in Middle–Late Miocene strata (Fig. 9), preferentially occurring in embayed shoreline settings coincident with relative highs in modelled tidal range and bed shear stress, such as in the Gulf of Thailand (Morley et al., 2011; Ridd et al., 2011; Shoup et al., 2013) and in areas of NW Borneo (Hadley et al., 2006; Collins et al., 2018c). Preserved sections in open-coastline systems are mostly interpreted to have been dominated by wave processes, even in areas of modelled high tidal bed shear stress such as along SE Vietnam (Morley et al., 2011; Chung et al., 2015), suggesting wave processes may have overprinted evidence of tides.

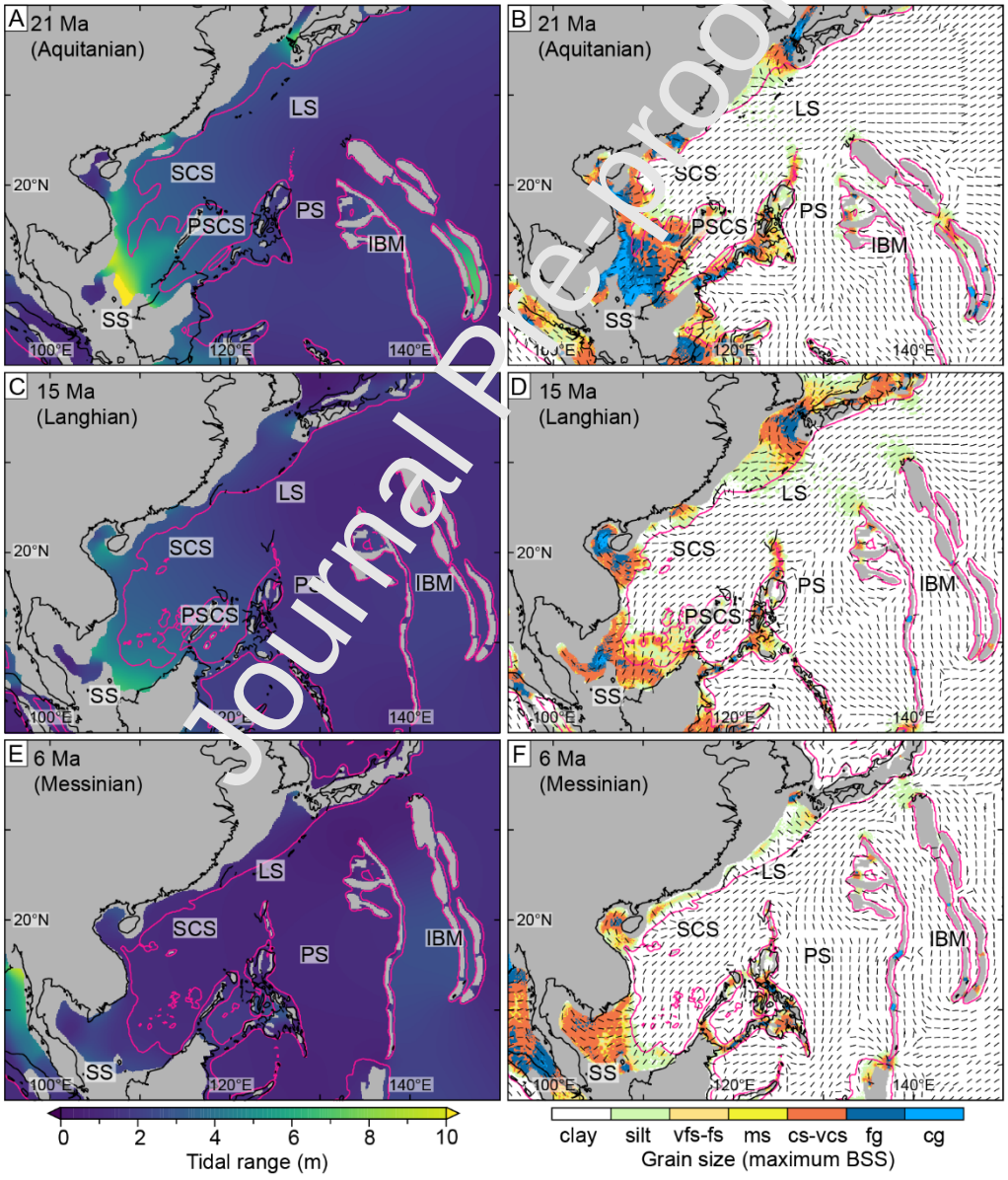

Fig. 7. Palaeotidal model results in the Oligo–Miocene South China Sea for tidal range (A, C, E) and maximum tidal bed shear stress plotted as the maximum sediment caliber entrained (B, D, F), for three 'base case' palaeogeographic reconstructions: (A, B) Early Miocene at 21 Ma; (C, D) Middle Miocene at 15 Ma; and (E, F) Late Miocene at 6 Ma (see Fig. 6). The thicker black line (A–F) is the reconstructed present-day coastline. The thinner black lines in the bed shear stress plots indicate the orientation of maximum tidal bed shear stress. The pink lines (A–F) indicate the interpreted 200 m palaeobathymetric contour and approximate palaeo-shelf edge. See Collins et al. (2018a) for all model results and sensitivity analyses. Map abbreviations: IBM – Izu-Bonin-Mariana Arc; LS – Luzon strait; PS – Philippine Sea; SCS – South China Sea; SS – Sunda Shelf. Grain size abbreviations: vfs = very fine sand; fs = fine sand; ms = medium sand; cs = coarse sand; vcs = very coarse sand; fg = fine gravel; cg = coarse gravel.

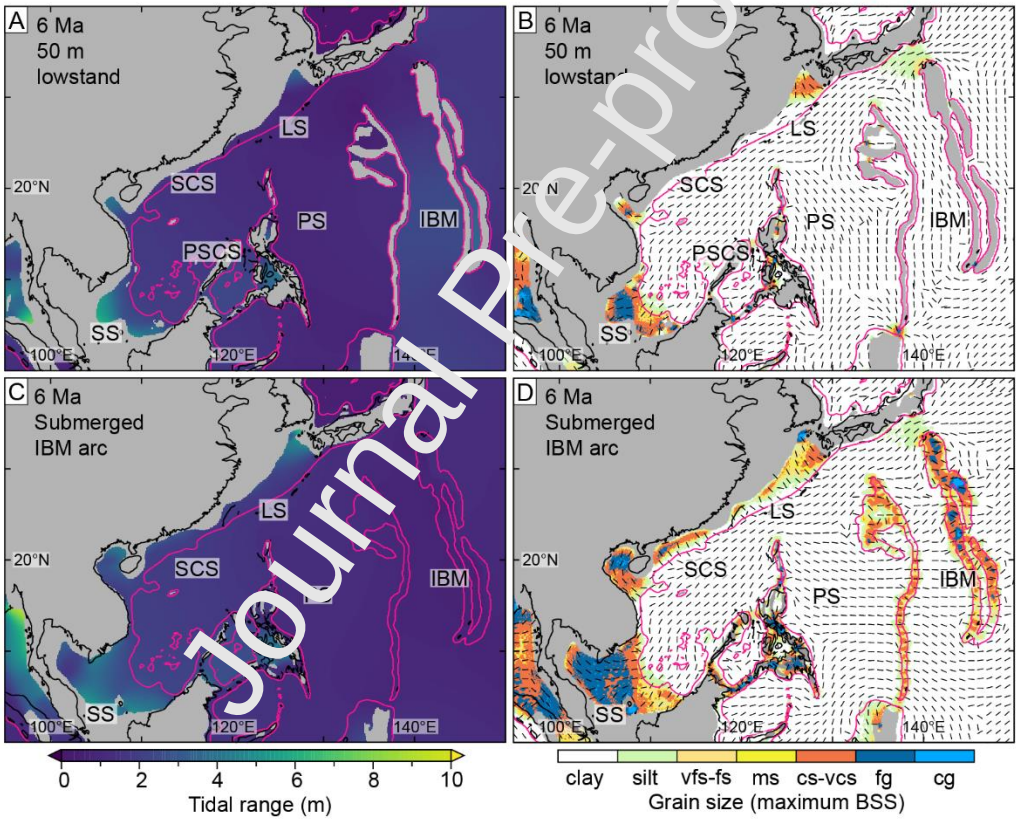

Fig. 8. Sensitivity analyses of the base-case for the Late Miocene (6 Ma) base case palaeogeographic reconstruction (cf. Fig. 7E, F) showing modeled tidal range (A, C) and maximum tidal bed shear stress, plotted as the maximum sediment caliber entrained (B, D), for a 50 m sea-level lowstand reconstruction (A, B) and submerged Izu-Bonin-Mariana (IBM) arc (C, D). Refer to Fig. 7 for abbreviations.

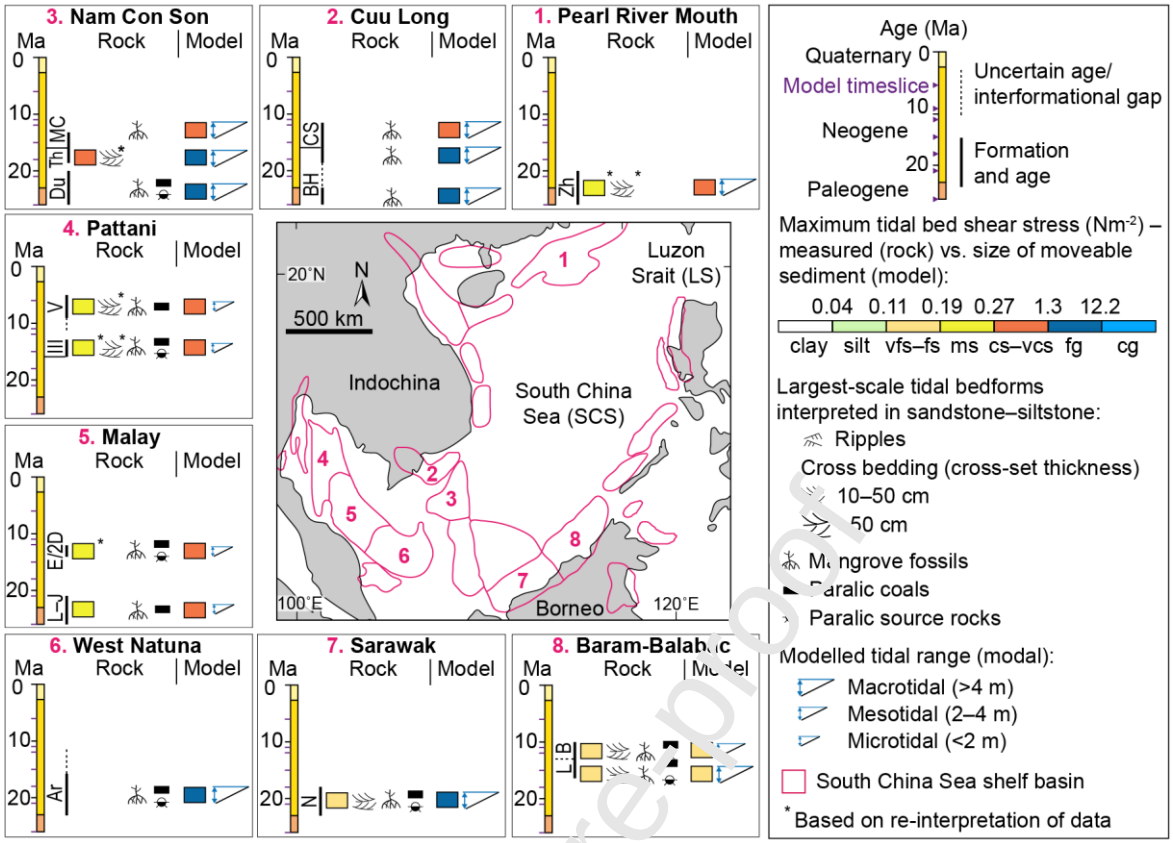

Fig. 9. Evidence of tide-influenced deposition based on sedimentological and micropalaeontological data, mainly from petroleum exploration wells, and comparison to base case tidal model results (Fig. 7) in South China Sea shelf basins. Rock-record data include grain size, cross lamination (ripples) and/or cross bedding interpreted to preserve evidence of tidal process (e.g. bidirectional palaeocurrents, scoop-shaped foresets, mudstone drapes), mangrove pollen acmes and the occurrence of paralic, mangrove-bearing coals and source rocks. Studied formations and key references for each basin are: (1) Upper Zhuhai (Zh) Formation, Pearl River Mouth Basin (Zheng and Deng, 2012); (2) Bach Ho (BH) and Con Son (CS) formations, Cuu Long Basin (Morley et al., 2011); (3) Dua (Du), Thong (Th) and Mang Cau (MC) formations, Nam Con Son Basin (Tin and Ty, 1995; Morley et al., 2011); (4) Sequences II–IV, Pattani Basin (Jardine, 1997; Lockhart et al., 1997); (5) Groups L–J and E, Malay Basin (Morley et al., 2011); (6) Arang (Ar) Formation, West Natuna Basin (Morley et al., 2011); (7) Nyalau (Ny) Formation, Balingian Province, Sarawak Basin (Amir Hassan et al., 2013; Amir Hassan et al., 2016); (8) Lambir (L) and Belait (B) formations, Baram Delta Province, Baram-Balabac Basin (Lambiase et al., 2003; Collins et al.).

3.2 Regional- to local-scale controls on tidal deposition: Early Cretaceous (Aptian–Albian) Lower Greensand Seaway, north-west Europe

3.2.1 Background

The Early Cretaceous (Aptian–Albian) 'Lower Greensand Seaway' (LGS), used here to refer to the interconnected network of three main seaways connecting with larger marine bodies (i.e. Boreal, proto-Atlantic and Neothys; Fig. 10A–B), contrasts markedly to the SCS example: it covers a much smaller area, it was part of a larger epicontinental sea and it was entirely shallow water, far removed from coeval oceanic basins. The larger-scale (10–100s km) basin physiography was determined by a series of precursor, west-east-trending, rift basins (*c.* 50–100 km long and 10–30 km wide; e.g. Weald, Wessex and Channel basins; Fig. 10 C–D) that were initiated during the Early Cretaceous (e.g. Ziegler, 1990; Hawkes et al., 1998). Aptian-Albian deposits in the LGS comprise shallow-marine sandstones (Lower Greensand Group; Fig. 10E), divided informally herein into two stratigraphic intervals: (1) the upper part of the *fissicostatus–martinioides* Zone (labelled 'FH', Fig. 10E) comprising deposits with negligible evidence of tidal currents, suggesting low tidal range (microtidal–low mesotidal) (Ruffell and Wach, 1991; Wells et al., 2010b); (2) the mid-to-upper part of the *upper martinioides– lower tardefurcata* Zone (labelled 'FSW' in Fig. 10E), represented by several units, with exemplary evidence of deposition by strong tidal currents within an inferred macrotidal, ebb-dominated diurnal, or mixed, predominantly diurnal tidal regime (e.g. De Raaf and Boersma, 1977) (Allen, 1982a; Bridges, 1982; Johnson and Level, 1995; Wonham and Elliott, 1996; Yoshida et al., 2004). These 'greensands' deposits are overlain by offshore marine mudstones (Gault Clay Formation). Hence, the Aptian-Albian succession reflects overall marine transgression, which was accompanied by an overall increase in basin width, length, bathymetry and connectivity. Consequently, predicting tidal circulation in this setting is complicated by several uncertainties, most notably: (1) variability in palaeobathymetry caused by the drowning of previously separate rift basins (potentially forming various 'straits') with differing initial water depths (Fig. 10C–D); and (2) complex marine flooding of these basins, with competing marine incursions entering the LGS through connections to the Boreal Sea (to the north), proto-Atlantic Ocean (to the south-west), and Neotethys Ocean (to the south-east) (Fig. 10A–B).

Palaeotidal modelling and comparison to the Lower Greensand Group in the two stratigraphic intervals outlined above ('FH' and 'FSW' in Fig. 10E) allows uncertainty analyses across a range of different age, palaeobathymetric and palaeogeographic scenarios (Wells et al., 2010b). Regional-scale tidal simulations for tidal amplitude and phase represent both astronomical (M_2, S_2, K_1, and O_1) and boundary tidal forcing, the latter generated using a global Aptian model (Wells et al., 2010a). Two base-case palaeogeographies ('Scenario 1'), based on modified published interpretations (see Wells, 2008; Wells et al., 2010b), were generated for the 'FH' and 'FSW' stratigraphic intervals (Fig. 10E),

referred to as FH1 (Fig. 11A–B) and FSW1 (Fig. 11C–D), respectively. A key difference between the 'base case' scenarios for these two timeslices is widening of the oceanic connections, especially through the Paris Basin, in the upper *martinioides*–lower *tardefurcata* Zone due to transgression in the *nutfieldensis* Zone (Casey, 1961; Wells et al., 2010b). Four out of seven sensitivity analyses for each base-case palaeogeography are discussed herein, corresponding to scenarios 2, 4, 6 and 8 in Wells et al. (2010b): Scenario 2 has closure of the Paris Basin connection to the Neotethys Ocean (FH2 and FSW2); Scenario 4 has a connection through the Pewsey Basin to the proto-Atlantic Ocean (FH4 and FSW4); Scenario 6 has opening of all oceanic connections (FH6 and FSW6); and Scenario 8 has a doubled water depth between 0 and 200 m (FH8 and FSW8).

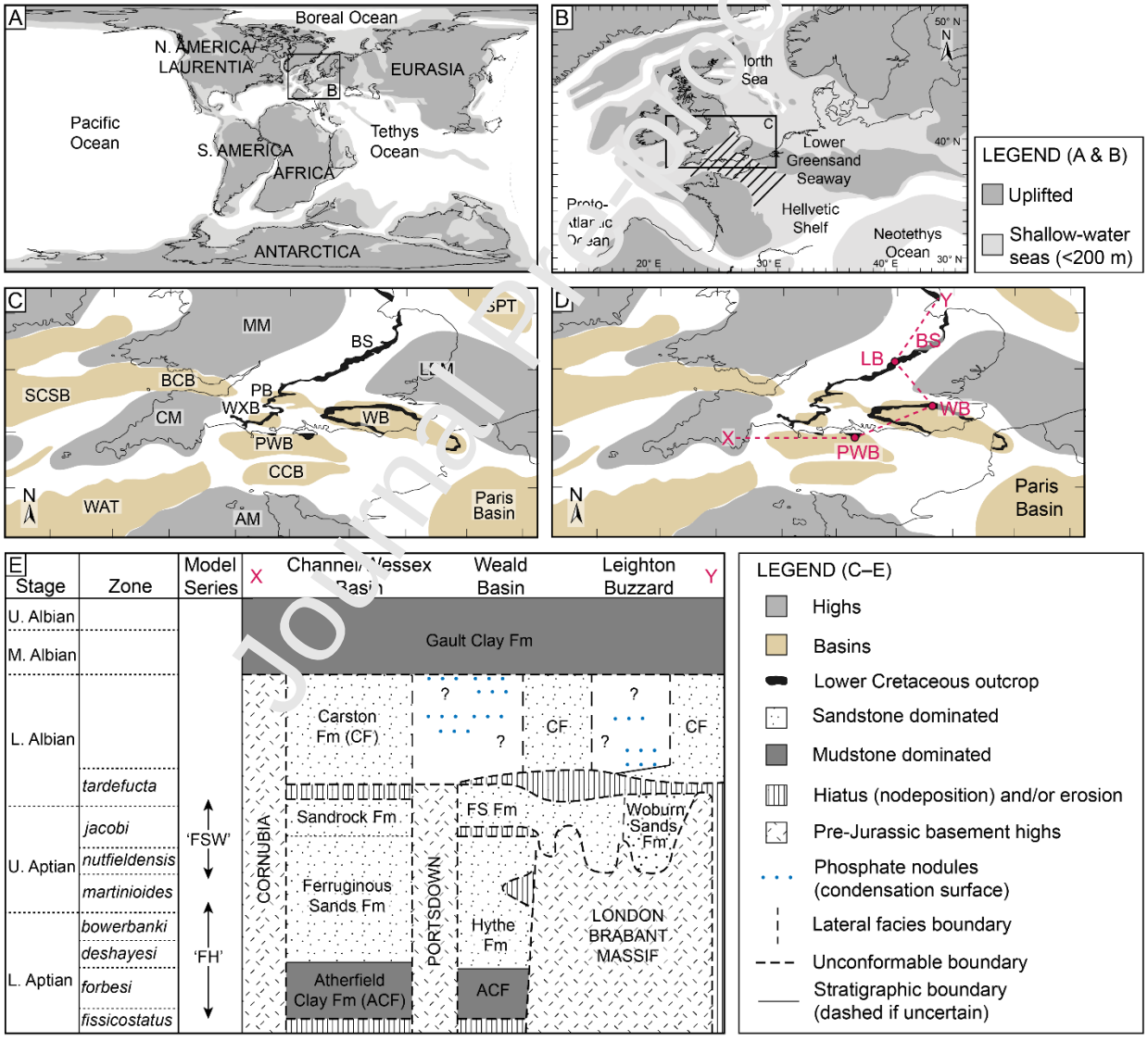

Fig. 10. Geological and stratigraphic framework of the Early Cretaceous 'Lower Greensand Seaway', NW Europe. (A) Global Aptian palaeogeographic framework. (B) Aptian palaeogeographic framework of northwest

Eurasia. In A and B, darker grey are significant uplifted highs and lighter grey shallow-water seas (< 200 m depth). (C) Aptian palaeogeographic map of southern UK and northern France with significant uplifted highs in dark grey and basins in light brown. Basin abbreviations: BCB – Bristol Channel Basin; BS – Bedfordshire Strait; CCB – Central Channel Basin; PB – Pewsey Basin; PWB – Purbeck-Wright Basin; SCSB – South Celtic Sea Basin; WAT – Western Approaches Trough; WB – Weald Basin. High abbreviations: AM – Armorcian Massif; CM – Cornubian Massif; LBM – London-Brabant Massif; MM – Midlands Massif. (D) Aptian palaeogeographic map illustrating key locations for the chronostratigraphic and lithostratigraphic framework of the Lower Greensand Group (section X–Y in E). Location abbreviations in addition to those labelled in C: LB – Leighton Buzzard. (E) Illustrative chronostratigraphic and lithostratigraphic section of the Lower Greensand Group in southern England. Two ‘‘base case’’ palaeogeographies are considered (Fig. 11): ‘FH’ represents the upper part of the *fissicostatus–martinioides* Zone depositional sequence, corresponding to the Ferruginous Sands Formation on the Isle of Wight and the Hythe Formation in the Weald; ‘FSW’ represents the mid to upper part of the upper *martinioides*–lower *tardefurcata* Zone depositional sequence, corresponding to the Folkestone Sands Formation in the Weald, the Sandrock Formation on the Isle of Wight, and the Woburn Sands Formation around Leighton Buzzard. After Wells et al. (2010b), Yoshida et al. (2004) and references therein.

3.2.2 Model results and rock-record integrati…

The range of tidal model scenarios illustrates the regional-scale (100s km) interplay between tidal inflow and outflow. This has a first-order control on tides in smaller-scale (10s km) areas and can supersede funnelling effects within some smaller physiographic constrictions, such as in straits and embayments. In the LGS, predicted tidal ranges in simulations of the upper *martinioides*–lower *tardefurcata* Zone (‘FSW’) (Figs. 11B, D, 12B, D, F, H) are consistently higher than in equivalent base-case and sensitivity simulations of the *fissicostatus–martinioides* Zone (‘FH’; Figs. 11 A, C, 12A, C, E, G), and are interpreted to relate to increased inflow of tidal energy due to the greater width of the seaway and its ocean connections in 'FSW’ simulations. This is especially pronounced for the Paris Basin, because the maximum depth is similar in equivalent FSW and FH simulations and the same open tidal boundary conditions are used in both cases. In addition, for all scenarios and both timeslices, tidal range is higher along the eastern margins of the seaway and the Paris Basin, due to Coriolis deflection of the northward propagating tidal wave from the Neotethys Ocean.

Modelled high mesotidal to low macrotidal conditions for the FSW interval are supported by widespread interpreted tidal deposits throughout the seaway at this time. Evidence of tidal processes ranges in scale from facies (e.g. sedimentary structures, palaeocurrents and ichnology), through facies associations to facies successions (see Section 2.2.3), and include various combinations of tidal indicators such as the following: (1) mudstone draped cross-set, including some double-drapes and possible spring-neap bundles; (2) compound cross-stratification; (3) bidirectional palaeocurrent

directions on a range of scales, including ebb- and flood-dominated patterns in 10s m-thick intervals; (4) reactivation surfaces; (5) wavy-, flaser- and lenticular-bedded heterolithic cross-bed toesets; (6) shallow-marine, variable intensity, low diversity ichnofauna; and (7) vertical and lateral facies and facies association relationships, including grain size trends and the geometry of bounding surfaces e.g. (Bridges, 1982; Johnson and Levell, 1995; Wonham and Elliott, 1996; Yoshida et al., 2004; Wells et al., 2010b), (Allen, 1982a; Bridges, 1982). Overall, these deposits are interpreted to record deposition under strong tidal currents, with probable mesotidal to macrotidal ranges (Allen, 1981b), in tidal estuarine to embayment environments (Yoshida et al., 2004). This is consistent with palaeotidal model results that include local-scale amplification through shoaling and funnelling effects (Fig. 12B and 13). Furthermore, the predicted diurnal-dominated tidal regime in the LGS in all modelled scenarios (Fig. 13) matches the interpretation of diurnal-dominated spring–neap tidal bundles in the Folkestone Sands Formation (Allen, 1981a; Allen, 1982a).

Modelled microtidal to low mesotidal conditions for the FH interval is broadly consistent with little evidence of tidal influence in the time-equivalent stratigraphic record (see review in Wells et al. (2010b). The only putative tidal deposits of this age, occurring in the western Weald Basin, are limited in areal extent and contain no published evidence of bidirectional currents or mud drapes, decreasing the confidence in interpretation (Casey, 1961; Narayan, 1971; Bridges, 1982; Ruffell and Wach, 1991; Rawson, 2006).

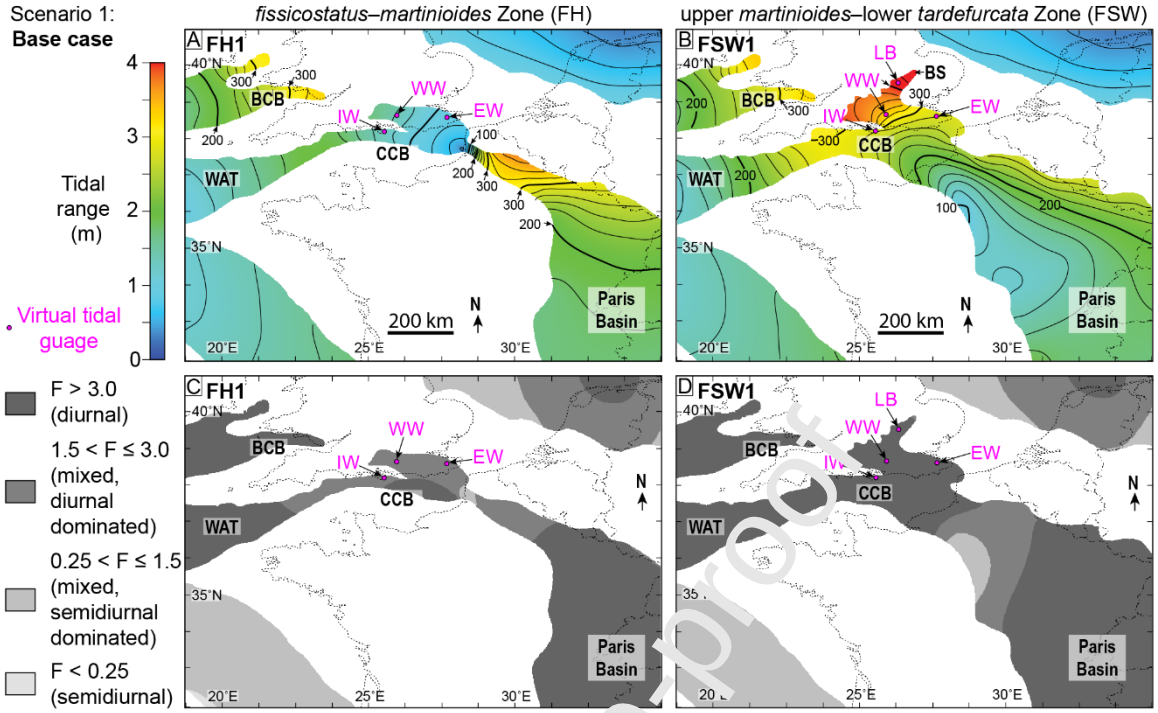

Fig. 11. Base case palaeotidal model results in the Early Cretaceous Lower Greensand Seaway for the *fissicostatus–martinioides* Zone (A, C) and upper *martinioides*–lower *tardefurcata* Zone (B, D) timeslices (respectively 'FH' and 'FSW' in Fig. 10D) showing modelled tidal range (0–4 m) for the four principal tidal constituents ($M_2 + S_2 + K_1 + O_1$), with 20 cm contours and bold, annotated contours every 100 cm (A–B), and the 'F-ratio' between the amplitudes of diurnal and semidiurnal tidal constituents (C–D). After Wells et al. (2010b). Pink labelled dots show positions of 'virtual tidal gauges' in the East Weald Basin (EW), Isle of Wight (IW), Leighton Buzzard (LB) and West Weald Basin (WW). Basin abbreviations: CCB – Central Channel Basin; BCB – Bristol Channel Basin; BS – Bedfordshire Strait; CCB – Central Channel Basin; PB – Pewsey Basin; WAT – Western Approaches Trough. Modified from Wells et al. (2010b).

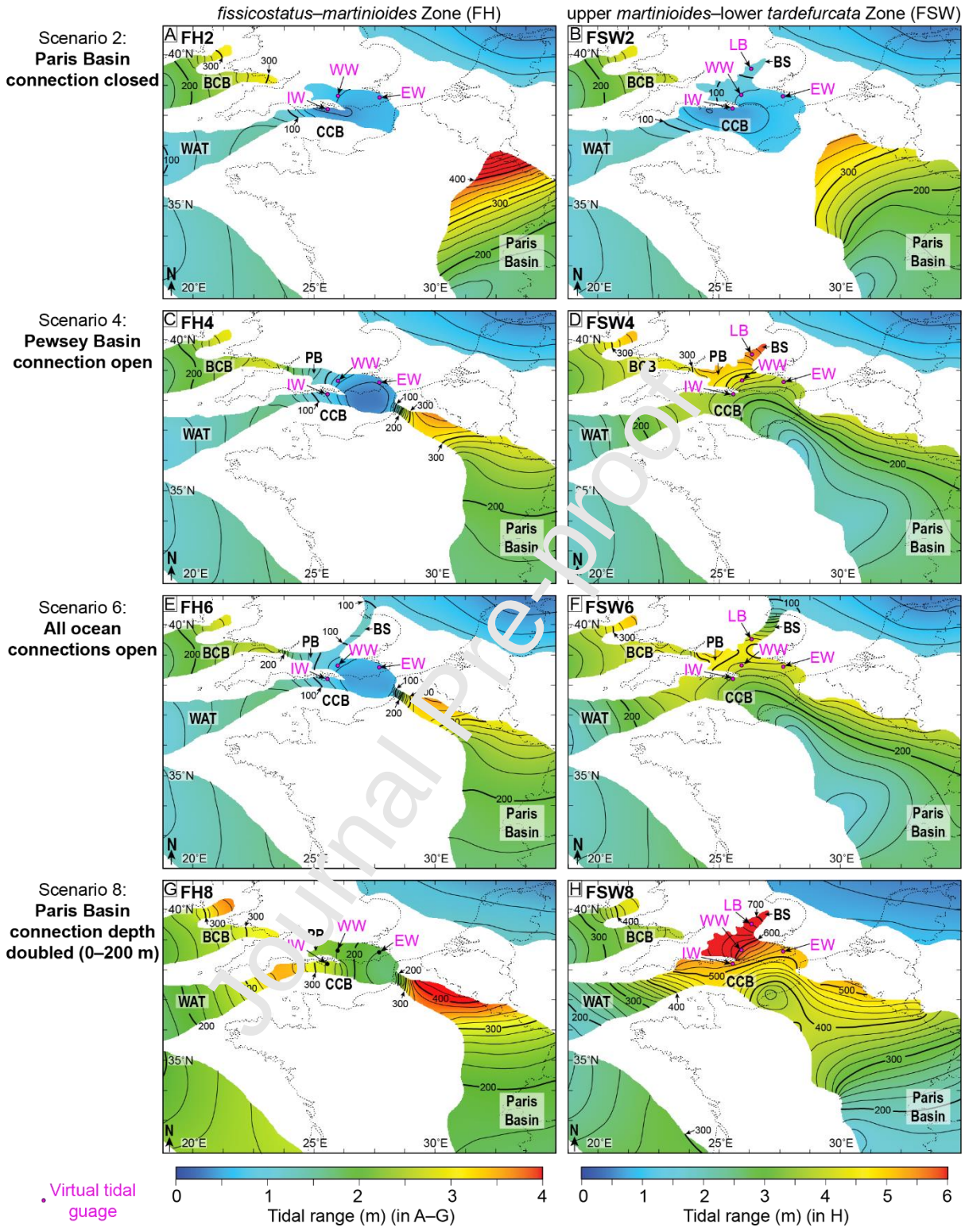

Fig. 12. Modelled tidal range for the four principal tidal constituents ($M_2 + S_2 + K_1 + O_1$) in sensitivity analyses of base-case reconstructions for the *fissicostatus–martinioides* Zone (A, C, E, G) and upper *martinioides*–lower *tardefurcata* Zone (B, D, F, H) timeslices in the Early Cretaceous Lower Greensand Seaway (respectively 'FH' and 'FSW' in Fig. 10D); tidal range contours are drawn for 20 cm intervals and bold, annotated contours every

100 cm. Pink labelled dots show positions of 'virtual tidal gauges' in the East Weald Basin (EW), Isle of Wight (IW), Leighton Buzzard (LB) and West Weald Basin (WW).Basin abbreviations: CCB – Central Channel Basin; BCB – Bristol Channel Basin; BS – Bedfordshire Strait; CCB – Central Channel Basin; PB – Pewsey Basin; WAT – Western Approaches Trough. Modified from Wells et al. (2010b).

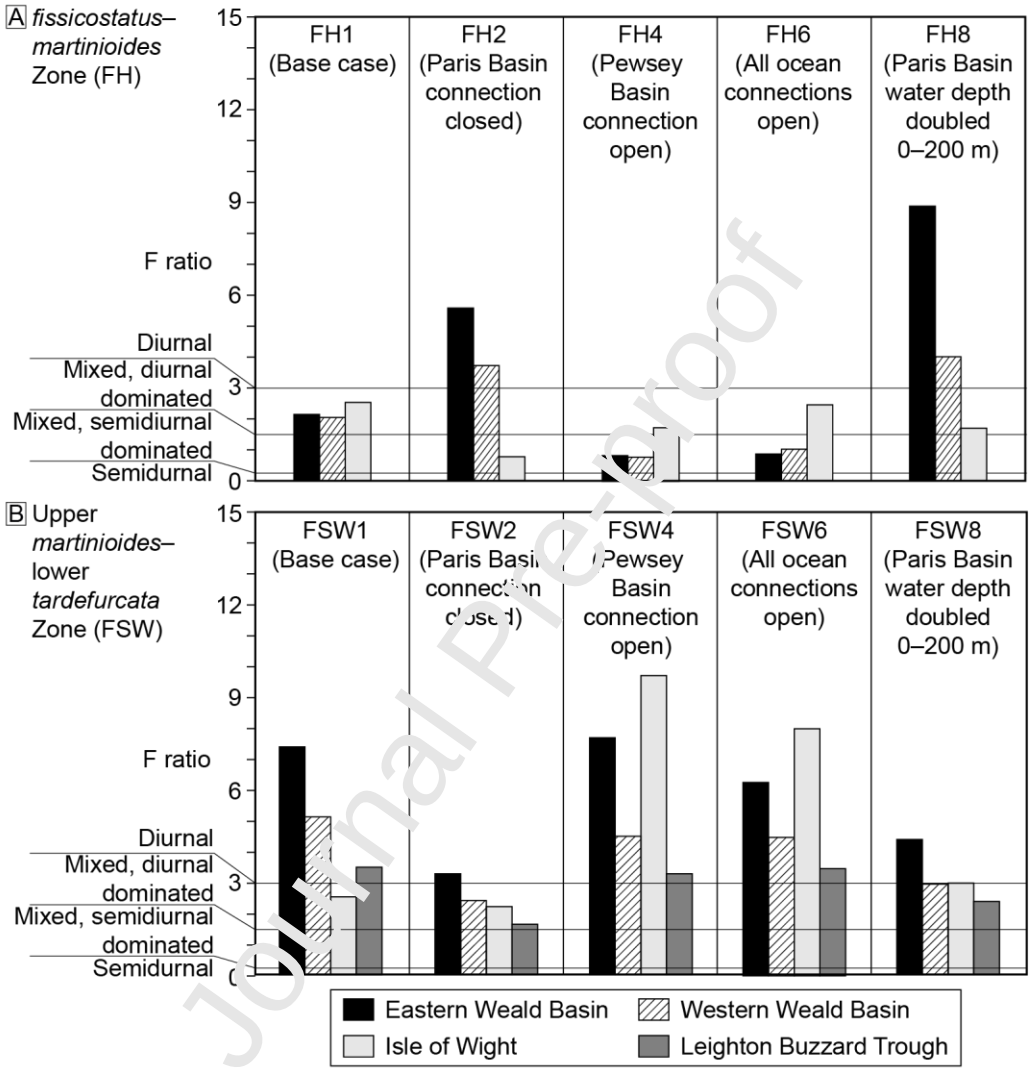

Fig. 13. Bar graphs of modelled tidal range at 'virtual tide gauge' locations (see Fig. 11 & 12) for base-case (Fig. 11) and sensitivity simulations (Fig. 12) for the *fissicostatus*– *martinioides* Zone (A) and upper *martinioides*–lower *tardefurcata* Zone (B) timeslices (respectively 'FH' and 'FSW' in Fig. 10D). Modified from Wells et al. (2010b).

3.3 Local-scale controls on tidal deposition: Late Cretaceous (Turonian-Cenomanian), Bohemian Cretaceous Basin, Central Europe

3.3.1 Background

The Bohemian Cretaceous Basin (BCB) was a slowly subsiding, transtensional basin that linked with other basins to form the large and shallow Mid-Cretaceous European Epicontinental Sea (MCEES) (e.g. Ziegler, 1990; Mitchell et al., 2010). As with the LGS example presented above, the BCB was far removed from coeval oceanic basins; over a thousand kilometres from the Neotethys Ocean to the southeast and the Proto-Atlantic Ocean to the west (Fig. 14) (e.g. Ziegler, 1990; Mitchell et al., 2010). Several emergent landmasses lay in between these oceans and the BCB (Fig. 14), such that boundary tides are likely to have been significantly blocked and damped by seabed friction (Mitchell et al., 2010). However, funnelling and shoaling effects in local-scale straits (c. 10s km wide) may have been important within the basin (Fig. 15). In this context, two depositional models have been proposed for Turonian-to-early-Coniacian shallow-marine sandstones in the BCB. An early model of large offshore bedforms sculpted by storms and tides (cf. tidal sand banks or ridges) (e.g. Jerzykiewicz and Wojewoda, 1986) has been superseded by one of top-truncated, coarse-grained deltaic shorelines that were reworked by tidal currents (Uličný, 2001; Uličný et al., 2009); both models are discussed here.

Palaeotidal modelling in the MCEES and BCB has focused on the early Middle Turonian interval ('TUR 2' genetic sequence of Uličný et al. (2009) with two main aims: (1) to understand how boundary tides from the Neotethys and Proto-Atlantic oceans were expressed as tidal circulation in the BCB, by considering regional-scale (10–100s km) basin physiography (Fig. 14); and (2) to assess whether modelled tidal bed shear stress was capable of generating the grain-size distributions, bedform types and palaeocurrent orientations observed at local-scale (1s–10s km) in the Turonian-to-early-Coniacian shallow-marine sandstones (Fig. 15) (Mitchell et al., 2010). A dataset combining outcrops and densely spaced boreholes provides good constraint on the basin-fill thickness and syn-depositional physiography of the BCB (Uličný et al., 2009), which contained islands with intervening, 10s km-wide straits (e.g. 'Elbe Strait'; Fig. 15). However, the physiography of many areas in the wider epicontinental sea is uncertain, with differences of up to 100 m water depth in basin centres outside the BCB (Fig. 14B–C) (Ziegler, 1990). Palaeotidal model simulations for the MCEES and BCB were forced with both astronomical (M_2, S_2, K_1 and O_1). and co-oscillating boundary tides adjacent to the deep, and expansive Proto-Atlantic and Neotethys oceans (Fig. 14) (Wells et al., 2007; Mitchell et al., 2010). The co-oscillating boundary tide was set in phase with the natural resonance at each respective boundary to give the maximum tidal potential in the seaway. Two sensitivity cases of tides in the MCEES were considered: (1) palaeobathymetric uncertainty was tested using 'minimum' and maximum' depth scenarios (Fig. 14D, E); and (2) resonance of different tidal constituents was

tested by imposing different boundary tides weighted towards semi-diurnal (M_2, S_2) and diurnal components (K_1, O_1). These regional-scale tidal simulations were subsequently investigated on a more local scale in the BCB.

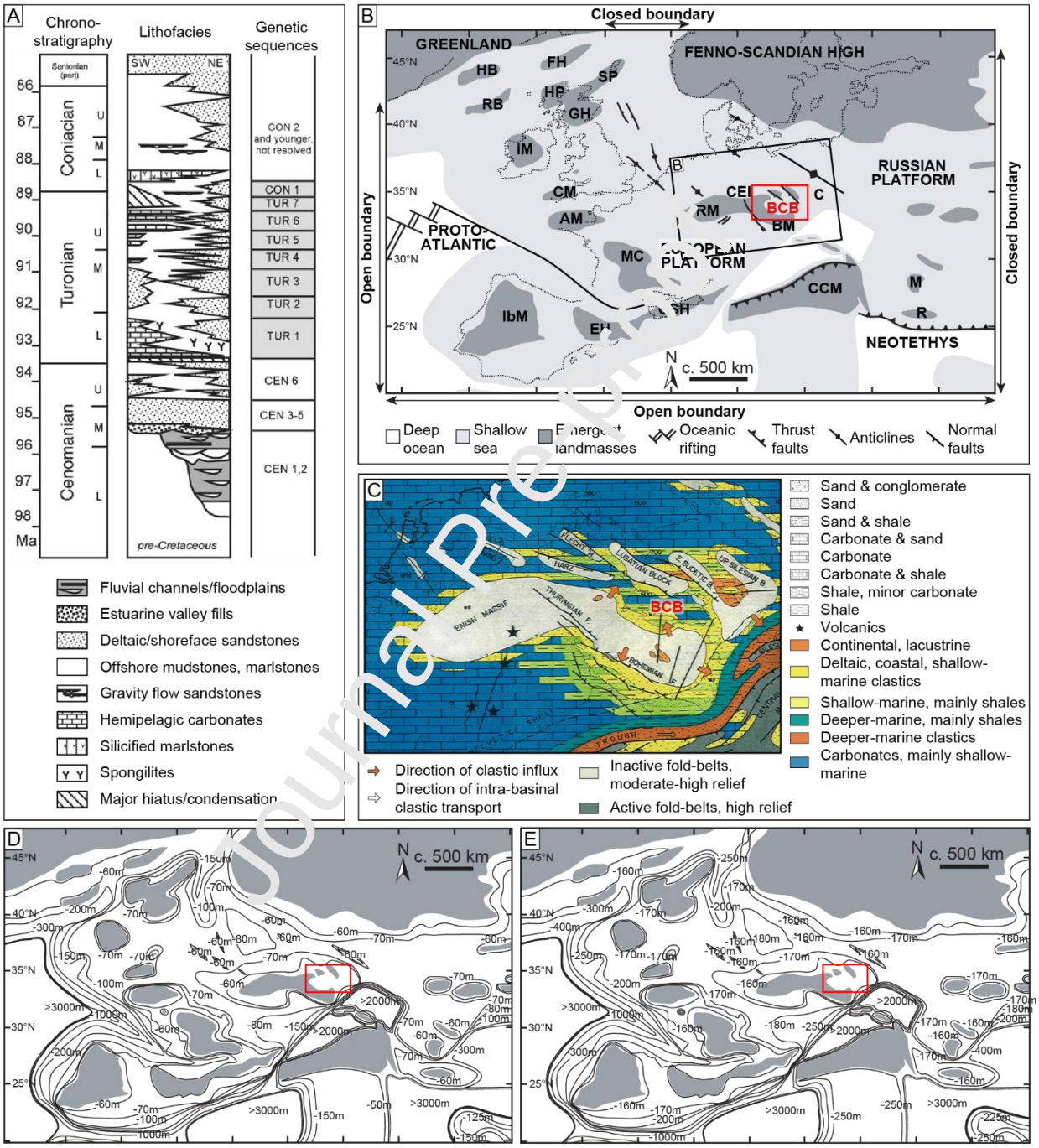

Fig. 14. (A) Stratigraphic chart showing the chronostratigraphy (modified after Ogg et al. (2004)), main lithofacies in the Lužice-Jizera Sub-basin (see Fig. 15A), genetic sequences recognized in this paper, and phases of basin evolution (after Uličný et al., 2009). (B) Regional palaeogeography for the Mid-Cretaceous European

Epicontinental Sea (Ziegler, 1990; Dercourt et al., 2000; Golonka, 2004; Gil et al., 2006; Golonka et al., 2006; Golonka, 2007; Mitchell et al., 2010). The approximate outline of the Bohemian Cretaceous Basin (BCB) is shown in red. (c) Gross depositional environmental map of central-western mainland Europe for the Cenomanian–Turonian (from Ziegler, 1990). (D–E Regional palaeobathymetries for palaeotidal modelling of the Mid-Cretaceous European Epicontinental Sea (MCEES), showing major contours for (D) minimum and (E) maximum depth scenarios (after Mitchell et al., 2010). Red box shows the position of the BCB. Abbreviations: AM = Amorican Massif; BCB = Bohemian Cretaceous Basin; BM = Bohemian Massif; C = Cracow Swell; CM = Cornubian Massif; CCM = Central Carpathian Massif; CSH = Corso-Sardinian High; EH = Ebro High; FH = Faeroe High; GH = Grampian High; HB = Hatton Bank; HP = Hebrides Platform; IbM = Iberian Massif; IM = Irish Massif; M = Moesia; MC = Massif Central; SP = Shetland Platform; R = Rodopes; RB = Rockall Bank; RM = Rhenish Massif.

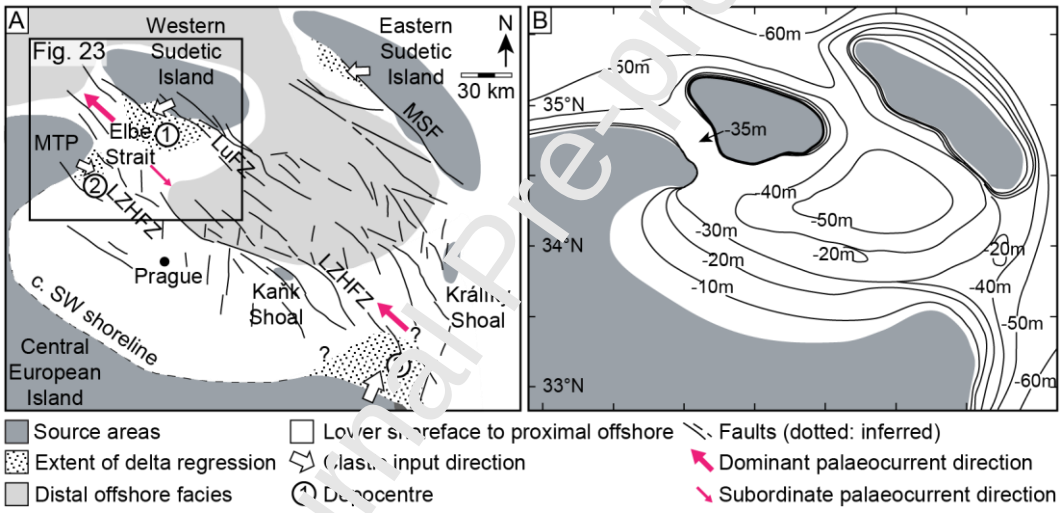

Fig. 15. Local scale palaeogeography (A) and palaeobathymetric (B) for the early Middle Turonian Bohemian Cretaceous Basin (onset of *Collignoniceras woollgarii* Zone). The extent of deltaic depocenters correspond to intermediate regression of the 'TUR 2' siliciclastic wedge (see Fig. 19A). Circled numbers (1) to (3) indicate the three main depocenters: (1) the Lužice-Jizera Sub-basin; (2) the Ohře Ramp; and (3) the Orlice-Žďár Sub-basin. MTP – Most-Teplice Palaeohigh; LuFZ – Lužice (Lausitz) Fault Zone; LZHFZ – Labe-Železné Hory Fault Zone. Modified after (Uličný et al., 2009). (B) Palaeobathymetric interpretation based on facies analysis of preserved outcrop and subsurface data (Uličný, 2001; Uličný et al., 2009). The heights of delta-front clinoforms suggests minimum depths of c. 35 m in the Elbe Strait, whereas a maximum depth of c. 50 m is estimated for the basin interior as inferred from trace fossil assemblages. After Mitchell et al. (2010).

3.3.2 Model results and rock-record integration

On a regional scale, modelled tidal range in the MCEES interior is consistently microtidal to mesotidal (Fig. 16), which supports attenuation of the tidal wave by seabed friction and emergent landmasses during propagation across the continental shelf (Shaw, 1964; Hallam, 1981; Wells et al., 2005a; Mitchell et al., 2010). These results could be consistent with early interpretations of Turonian-to-early-Coniacian sandstones as large tidal bedforms, which do not necessarily require macrotidal conditions cf. (Stride, 1973; Stride, 1982; Jerzykiewicz and Wojewoda, 1986). Tidal amplification forming macrotidal conditions is limited to embayments and straits, however, this only occurs with specific boundary and bathymetric conditions, consistent with the influence of tidal resonance (Wells et al., 2007). Overall, these results more closely support a tide-influenced deltaic depositional model (Uličný, 2001; Uličný et al., 2009; Mitchell et al., 2010), in which fluvio-deltaic sediment supplied laterally from the basin margins was reworked along the basin axis by strong, locally constricted tidal currents. This model is similar to mixed fluvial and tidal deposition in other tidal straits (e.g. Longhitano and Steel, 2017; Rossi et al., 2017a).

At a local-scale, modelled tidal range in the BCB varies from microtidal to mesotidal (Fig. 16) and modelled maximum tidal bed shear stress is consistently elevated within palaeogeographic constrictions between islands, including the Elbe Strait (Fig. 17). All modelled scenarios with forced boundary conditions generated maximum bed shear stresses in excess of c. 2.0 Nm^{-2} in the Elbe Strait (Fig. 17), which is capable of forming 3D dunes in coarse sand in up to c. 20 m water depths. These predicted tidal processes are more than sufficient to form the dm-scale cross bedding with common reactivation surfaces, finer-grained foreset drapes (some in doublets) and WNW-dominated to bidirectional palaeocurrents observed in age-equivalent sandstones within the Elbe Strait and north-western Lužice-Jizera Sub basin (Figs 20 & 22) (e.g. Harms et al., 1982; Jerzykiewicz and Wojewoda, 1986; Southard and Boguchwal, 1990; Uličný, 2001; Uličný et al., 2009; Mitchell et al., 2010). Sensitivity analysis suggests that modelled maximum bed shear stress values significantly increase for a higher boundary tide magnitude (Fig. 17A–B). Furthermore, water depth in the regional seaway influences the modelled maximum bed shear stresses locally in the BCB: modelled values are higher in the minimum depth scenario for the semi-diurnal regime, but higher in the maximum depth scenario for the diurnal tidal regime (Fig. 17C, D). This result suggests variations in resonance potential between boundary tide and palaeobathymetry scenarios, likely a result of relatively complex, constructive interaction between different co-oscillating boundary tides (Mitchell et al., 2010). Nonetheless, instantaneous bed shear stress vectors in all models show clear northwest- and southeast-directed transport patterns in the Elbe Strait, consistent with measured palaeocurrent directions (Fig. 18) (Voigt and Tröger, 1996; Uličný et al., 2009; Mitchell et al., 2010).

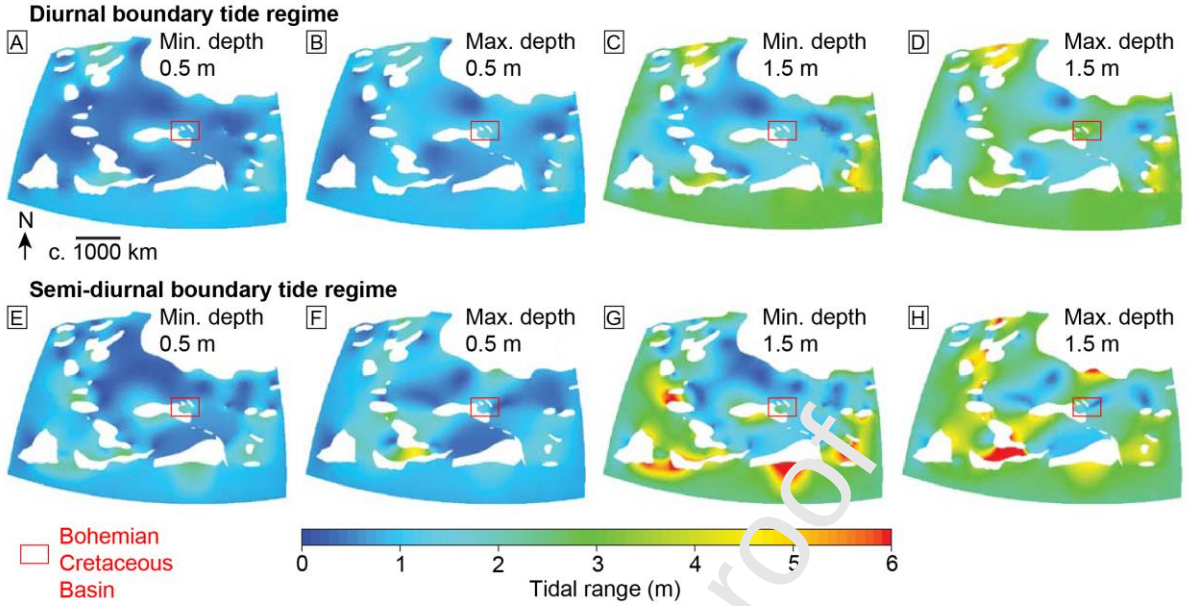

Fig. 16. Modelled tidal range in the Mid-Cretaceous European Epicontinental Sea (MCEES) for eight sensitivity tests for co-oscillating diurnal (A–D) versus semi-diurnal (E–H) boundary tide regimes, 0.5 m (A, B, E, F) versus 1.5 m (C, D, G, H) boundary tidal range, and minimum (min.) (A, C, E, G) and maximum (max.) (B, D, F, H) regional palaeobathymetry in the MCEES. Fidelity consistently predicts a microtidal to mesotidal range in the interior of the seaway, suggesting attenuation of the boundary tidal waves across the continental shelf by bed friction and blocking by emergent landmasses. After Mitchell et al. (2010).

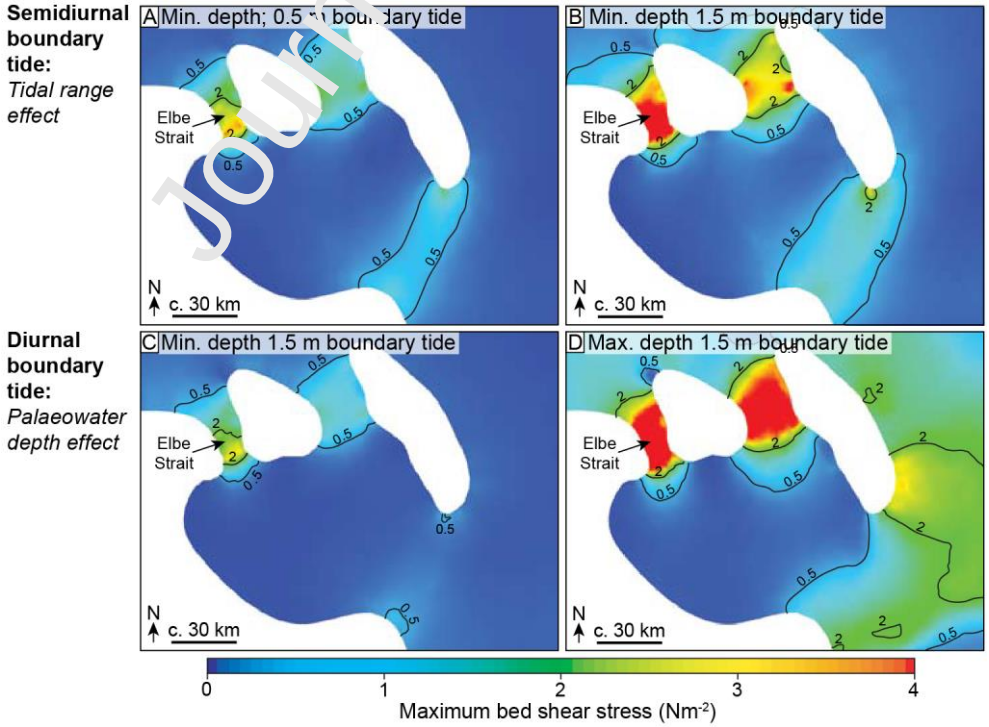

Fig. 17. Modeled maximum bed shear stress in the Bohemian Cretaceous Basin. The 0.5 Nm^{-2} contours show the approximate minimum bed shear stress required for the formation of dunes in coarse sand (Fig. 5) (Harms et al., 1982), whereas 1.0 Nm^{-2} is the approximate minimum bed shear stress required to form the observed scale of 3D dunes in coarse-grained sand in the Elbe Strait. Results for a 0.5 m (A) and 1.5 m (B) semi-diurnal boundary tide regime in the minimum (min.) depth regional palaeobathymetric domain (Fig. 14D) indicate that the modeled maximum bed shear stress is strongly dependent on the amplitude of the co-oscillating boundary tide. Results for the 1.5 m diurnal boundary tide regime in (C) minimum and (D) maximum (max.) regional palaeobathymetries indicate that the modeled maximum bed shear stress is strongly dependent on regional palaeobathymetry (Fig. 14D, E). After Mitchell et al. (2010).

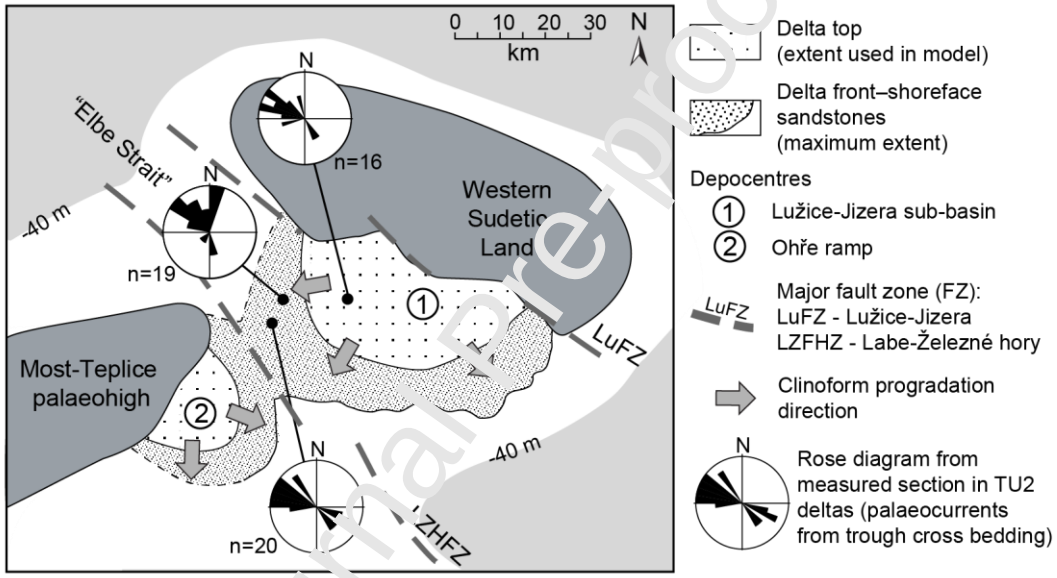

Fig. 18. Close-up view of the Elbe Strait area within the BCB (Fig. 15), showing the progradation extent and direction of sandy clinoforms (Voigt and Tröger, 1996; Uličný et al., 2009), and typical palaeocurrent rose diagrams for small-scale cross-sets in clinoforms recording intermediate regression of TUR 2 deltas. Circled numbers indicate (1) the Lužice-Jizera Sub-basin; (2) the Ohře Ramp.

4 DISCUSSION

4.1 Comparing tidal model and rock record data

The comparison of palaeotidal model to rock-record data involves the evaluation of different data types with contrasting dimensions and spatial-temporal scales (Fig. 19). This review has highlighted favourable comparisons between palaeotidal model predictions of tidal range and tidal bed shear stress with the occurrence of tidally-influenced strata in the spatial and temporal domains of the respective models. However, the comparison of palaeotidal model results and the time-equivalent rock record is limited by three key challenges: (1) confidently recognising tidal influence in the rock record, (2) inferring ancient bed shear stress and, especially, tidal range, and (3) the spatial and temporal resolutions of palaeogeographic data and subsequent interpretations underpinning palaeotidal simulations (e.g. basin morphology, palaeobathymetry, gross depositional environments).

Palaeogeographic reconstructions underpinning palaeotidal simulations involve combining, simplifying and averaging multiple geological data types (e.g. sedimentological, biostratigraphic, seismic). Each data type contains uncertainties, especially the quality and resolution of age dating and geological interpretations (Markwick and Valdes, 2004). With increasing spatial extent, the minimum temporal resolution of the geologic data underpinning palaeogeographic maps generally coarsens, becomes more variable and forms a composite 'time-slice' rather than a single 'time plane' (Fig. 19A).

Palaeotidal modelling provides areal (2D) and temporal data on three main parameters: (1) tidal amplitude, (2) tidal range and (3) tidal bed shear stress (magnitude and direction of instantaneous, mean and maximum values). In existing palaeotidal simulations, the maximum spatial resolution of computational meshes is of the order of 10 km and the temporal duration represented by a composite 'timeslice' (i.e. time interval) is typically c. 2–5 Ma (Fig. 19B and C), but both vary on a case-by-case basis (Table 3). Rock record data is typically one-dimensional (e.g. stratigraphic logs, core and well data), occasionally two-dimensional (e.g. outcrop panels, well-log correlation panels, seismic cross-sections and maps) and rarely three-dimensional (e.g. curvilinear and/or multiple outcrop panels, multiple and closely-spaced cores and wells, 3D seismic volumes) (Fig. 19B). Such data may lie at spatial resolutions much smaller than those of palaeotidal model meshes and model timeslices. It is possible to address the discrepancy in spatial scales between rock record data and palaeotidal models by combining rock record data from multiple locations, although such amalgamation of data should be carried out carefully so as not to obscure important local patterns. For example, in palaeotidal models of the BCB (Section 3.3), instantaneous bed shear stress provides a more reliable model output for

comparison with rock-record palaeocurrent data than values of mean and maximum bed shear stress collated over multiple tidal cycles (Mitchell et al., 2010).

Facies modelling aimed at deciphering the relative influence of tide, wave and fluvial processes involves analysis at a wide range of scales, from facies (mm–m) to systems tracts (10–100s km) (Van Wagoner et al., 1990; Walker and James, 1992; Posamentier and Walker, 2006; Hampson et al., 2008). Vakarelov and Ainsworth (2013) have formalized this approach for shoreline depositional systems into five stratigraphic hierarchical levels, each with different spatial resolutions and dimensions (Fig. 20): (1) facies (element), a component of a depositional element; (2) facies association (element set), a depositional environment; (3) a facies model for part of a depositional system (element complex assemblage); (4) a facies model for a whole depositional system (element complex assemblage set); and (5) a transgressive-regressive tongue or parasequence, which captures the temporal evolution of the facies model for a whole depositional system during one episode of shoreline advance and subsequent retreat. Comparing tidal model and rock-record data most often occurs at the facies, facies-association and parasequence levels, and possibly at larger scales (e.g. parasequence set). This is due in part to data availability, but also because the variability in process dominance and preservation typically increases up the stratigraphic levels. For example, mixed-energy depositional systems (level 4 and above) often comprise several depositional sub-environments (level 3) with varying degrees of tide, wave and/or fluvial influence (e.g. Ainsworth et al., 2011; Vakarelov and Ainsworth, 2013).

Deciphering the degree and extent of tidal influence is further complicated by incomplete stratigraphic preservation, including preservational bias. Tidal deposits may be preferentially preserved in a wide range of depositional environments but with variable extent and significance. For example, such deposits are often particularly significant in coastal embayments and at the mouths of fluvially incised valleys, but geographically restricted elsewhere, such as in tidal inlets within larger barrier-lagoon systems. However, the maximum resolution of computational meshes used in palaeotidal modelling, especially for regional-scale studies, is significantly larger than the typical spatial dimensions of facies (mm–m) and facies associations (1–100s m) (Fig. 19B). Furthermore, across all spatial scales, the topographically lower components of these depositional systems have higher preservation potential and, generally, their deposits tend to be coarser grained (Dalrymple, 2010a). Hence there is an almost inevitable bias in the preserved sedimentary and stratigraphic features indicative of certain depositional processes and sub-environments. For example, in a mixed fluvial-tidal setting with channel-bar topography, fluvial currents are likely to preferentially influence coarser-grained

deposition in deeper channel axes, with variable superimposed influence of tides, especially ebb tidal currents. These coarser-grained deposits are likely to have a higher preservation potential compared to finer-grained, typically more heterolithic and more strongly tide-influenced deposits of topographically higher parts of tidal bars (e.g. Levell et al., 2020). Consequently, despite a depositional environment reflecting mixed river and tidal processes, fluvially influenced deposits may be preferentially preserved and the record of tidal deposition diminished. This is further supported by the frequent paucity of intertidal deposits and dominance of subtidal deposits in many ancient tide-dominated successions (Legler et al., 2013; van Cappelle et al., 2016; Archer et al., 2019; Collins et al., 2020; Levell et al., 2020). Consequently, the comparison of model to rock-record data may be biased by the varying preservation of tide-influenced deposits in relation to spatial and temporal changes in depositional processes across a range of scales. These primary depositional biases are further exacerbated where limited rock-record data is available in the present-day and where data are selectively compared to model results.

For one- and two-dimensional stratigraphic data, interpretation of areal depositional morphology and its relationship to the depositional system scale are typically guided by comparison to process-based interpretations of modern shoreline environments (Fig. 20B). Process-based classifications of modern shoreline systems are principally based on 2D areal morphology, ideally supported by data on hydrodynamics and sediment type (e.g. Coleman and Wright, 1975; Galloway, 1975; Hayes, 1979; Boyd et al., 1992; Hori and Saito, 2007; Ainsworth et al., 2011; Nyberg and Howell, 2016) and sedimentary facies characteristics (e.g. Dalrymple et al., 2002a; Lambiase et al., 2003; Salahuddin and Lambiase, 2013; Fanget et al., 2014; Gugliotta et al., 2018). Hence, the 2D morphologies of end-member tide-, wave- and fluvial-dominated shorelines are embedded in ternary-process models of shoreline depositional systems (Ainsworth et al., 2011; Vakarelov and Ainsworth, 2013; Nyberg and Howell, 2016).

Tide-dominated shorelines typically display the following morphological characteristics: (1) complex and intricately branching networks of funnel-shaped (seaward-flaring) tidal channels, (2) elongate tidal bars (mainly subtidal but often with subaerial tops), which partly infill tidal channels and often extend seaward from channel mouths, and (3) more extensive ('land-fringing') intertidal and supratidal areas with, depending principally on latitude, salt marsh or mangrove colonization (e.g. Ainsworth et al., 2011; Nyberg and Howell, 2016). Tide-dominated shorelines are more likely to be rugose to funnel shaped, and *vice versa*, whereas straighter shorelines are more likely to be wave-dominated, and *vice versa* (e.g. Fig. 2) (e.g. Ainsworth et al., 2011; Nyberg and Howell, 2016). These

generalized relationships are useful but oversimplified, especially when they are an intrinsic component of algorithms for classifying modern shoreline process regime (Nyberg and Howell, 2016). For example, this relationship does not include quantifiable variations in tidal range, tidal prism and/or tidal bed shear with shoreline rugosity, or complex related feedbacks (e.g. D'Alpaos et al., 2010). A more rigorous, albeit ambitious, approach for determining the process regime along shorelines would be to compare measured values of tidal strength (bed shear stress), tidal range, wave strength, wave height and fluvial discharge (Harris et al., 2002) with those from numerical models, preferably including data assimilation.

The temporal resolution of rock-record data is highly dependent on the methodology of absolute dating and the degree of interpolation between control ages (Fig. 1C). For example, in the Cretaceous of the Western Interior Basin of North America, an estimated temporal resolution of c. 200 ka has been achieved because high-resolution ammonite biozones have been calibrated to radiometric age dates (Obradovich, 1993) (Krystinik and DeJarnett, 1995). In contrast, a paucity of absolute age dates in the Miocene–Pliocene Baram Delta Province, and the vast majority of similar Tertiary delta provinces around the world, means biostratigraphic zones have a temporal resolution of >1 Ma (Sandal, 1996).

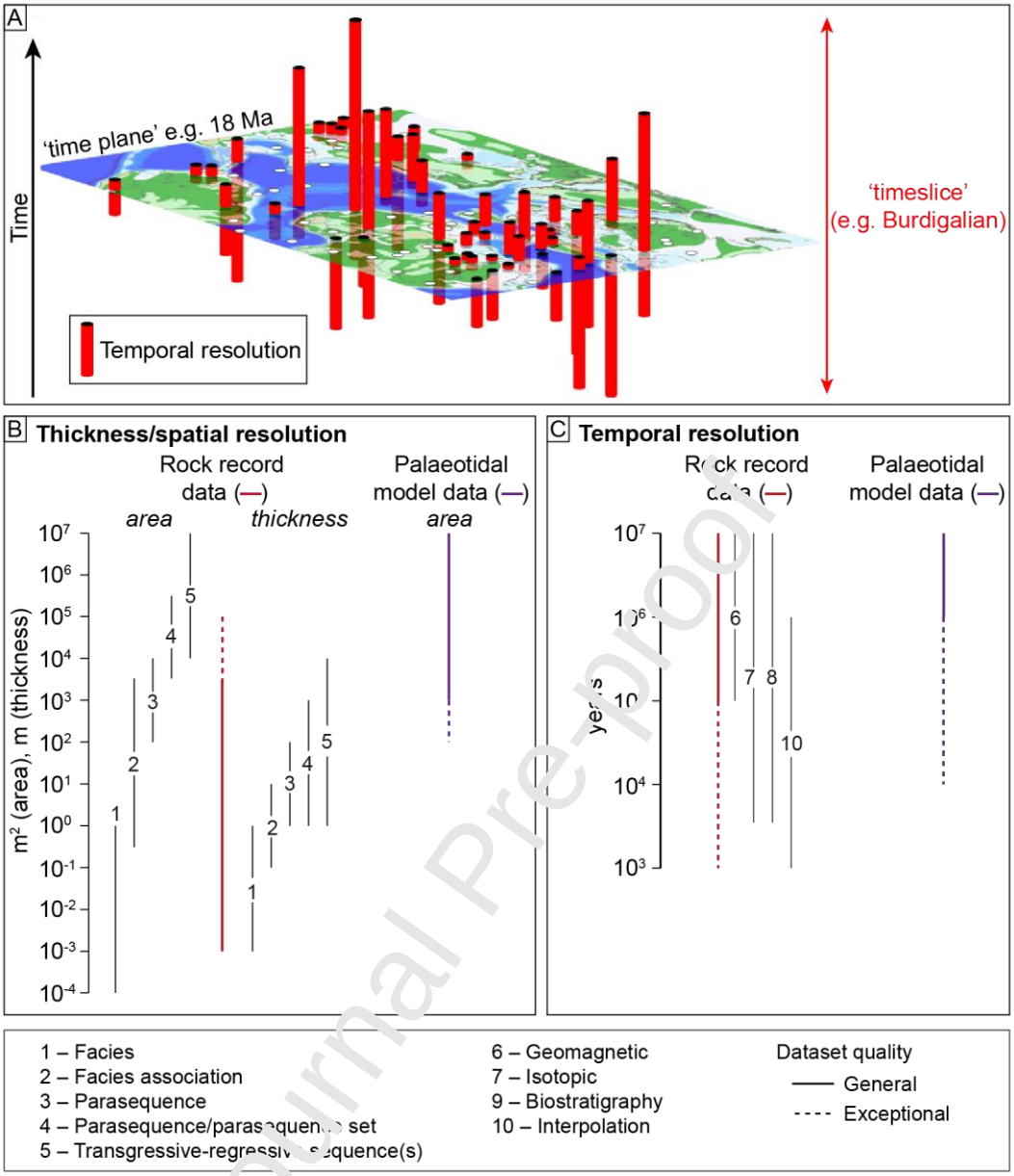

Fig. 19. Variable resolution of palaeogeographic, tidal modelling and rock record data. (A) Illustration of the minimum temporal resolution of geologic data underpinning a palaeogeographic 'timeslice' (after (after Markwick and Valdes, 2004). Each data point is assumed to represent a single observation of equivalent area, but the temporal resolution of each point is generally variable (red cylinders), due in part to imprecise or uncertain dating and correlation. Defining a timeslice instead of a time-plane maximizes data density. (B) Thickness and spatial resolution of rock and model data. Rock data are differentiated by general versus exceptional dataset quality: in this context, exceptional means extensive and continuous outcrops or several tens of correlated cores and well logs. Numbers 1-5 represent five hierarchical levels of rock data (e.g. the "levels" of (or levels; e.g. Vakarelov and Ainsworth, 2013), showing varying areal and thickness scales (see full text and legend in the bottom panel). Tidal model data is area based. (C) Temporal resolution of rock and model data, showing (i) five hierarchical levels of rock data (Vakarelov and Ainsworth, 2013); (ii) the most common

methods of absolute rock dating include geomagnetic, isotopic, biostratigraphy (calibrated to absolute dates), and interpolation between dates; and (iii) data quality types.

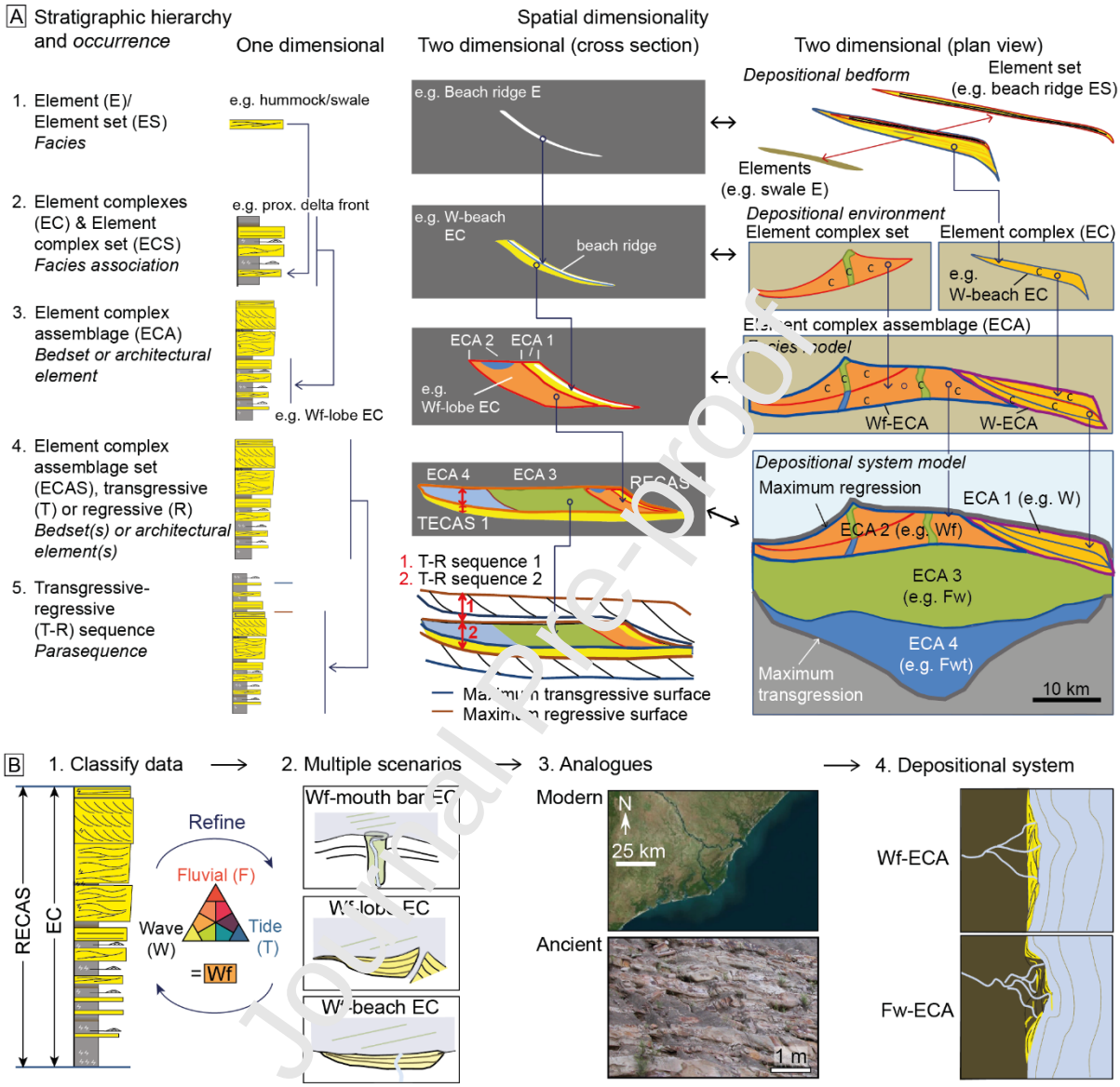

Fig. 20. Scale and methodology of process classification and depositional model reconstruction (after Vakarelov and Ainsworth, 2013). (A) Five hierarchical levels of process-based architectural classification based on one-dimensional thickness and two-dimensional cross-section and plan-view data. For stratigraphic hierarchy levels 3 and 4, the stratigraphic occurrence–bedset(s) or architectural element(s) varies case-by-case. (B) Simplified workflow for determining process depositional model from one-dimensional rock-record data. Refer to Vakarelov and Ainsworth (2013) for further information.

4.2 Controls on tidal processes and sedimentation

4.2.1 Basin physiography

The overall physiography – size, shape and bathymetry – of the Earth's global ocean, and constituent ocean basins (at present, the Pacific, Atlantic, Southern and Arctic oceans) is the first-order, largest-scale (1000s km) control on astronomical tides. A key consideration for understanding tidal processes and sedimentation along shorelines directly facing ocean basins (i.e. open-ocean shoreline systems) is therefore to estimate the influence of ocean-basin width and depth in controlling tidal resonance (Section 2.2.1). On geological timescales, of the order of 10s–100s Myr plate movements, ocean basins can move in and out of tidal resonant states in response to changing physiography (Green et al., 2017). For present-day open-ocean systems, there is no obvious systematic, qualitative relationship between tidal amplitude and latitude (e.g. Fig. 4) (Dalrymple and Padman, 2019). This is due to strong modification of tidal circulation by rotational, funnelling, shoaling and resonance effects, especially in shallower bathymetric areas and shoreline constrictions (Allen, 1997; Wells, 2008; Dalrymple and Padman, 2015; Dalrymple and Padman, 2019). These effects are complicated and difficult to predict. However, numerical tidal modelling provides a proven, robust method to understand the cumulative influence of these effects. This results in more rigorous and quantitative predictions of tidal potential in modern and ancient, open-ocean systems.

Shoreline systems facing water bodies that are partly enclosed by land, referred to herein as 'partly enclosed' systems, have variable degrees of connectivity to adjacent open ocean basin(s), and display a large variation in size (100s to 1000s km) (e.g. present-day North Sea). The case studies presented earlier (Section 3) are all partly enclosed systems. For partly enclosed systems, the foremost control on shoreline tides is the balance between the amount of tidal energy entering and exiting the basin – the tidal inflow and outflow (Fig. 21). Tidal potential is highest when tidal inflow exceeds outflow. Tidal inflow is mainly controlled by the physiography of the basin entrance(s) and the angle between the basin entrance(s) and tidal flow in the adjacent open ocean (Fig. 21A), which principally depends on latitude and Coriolis rotation (Leeder, 2011). Tidal inflow will be relatively high where open-ocean tides flow directly towards the basin entrance, minimizing loss of tidal energy to frictional damping, and/or the entrance is relatively wide, deep and unobstructed (Fig. 21A). Tidal outflow depends on the number, size, configuration and physiography of outflow connections (Fig. 21B). Tidal outflow is highest if there are multiple, wide, deep and unobstructed outflow connections (Fig. 27B). The tidal energy distribution within partly enclosed systems depends on the relative locations of inflow positions versus outflow positions and embayments, and the tidal flow dynamics within the

basin. This point is clearly illustrated in palaeotidal modelling sensitivity tests of the Lower Greensand Seaway (section 4.2), in which the number and location of tidal inflow and outflow positions is varied (Fig. 12).

Partly enclosed systems may also include relatively shallow (up to a few hundreds of metres) but wide (up to several 100s km) basins, for example, the present-day Baltic Sea and ancient epicontinental seaways. The physiography of these systems may also result in tidal resonance of the incoming boundary tide due to the tidal periodicity matching a natural oscillation frequency of water within the basin. Tidal resonance potential has been approximated for simple, rectangular-shaped, open-ended water bodies (Wells, 2008). However, more complex ancient basin physiographies can be modelled to provide quantitative information on integrated resonance potential for all tidal constituents.

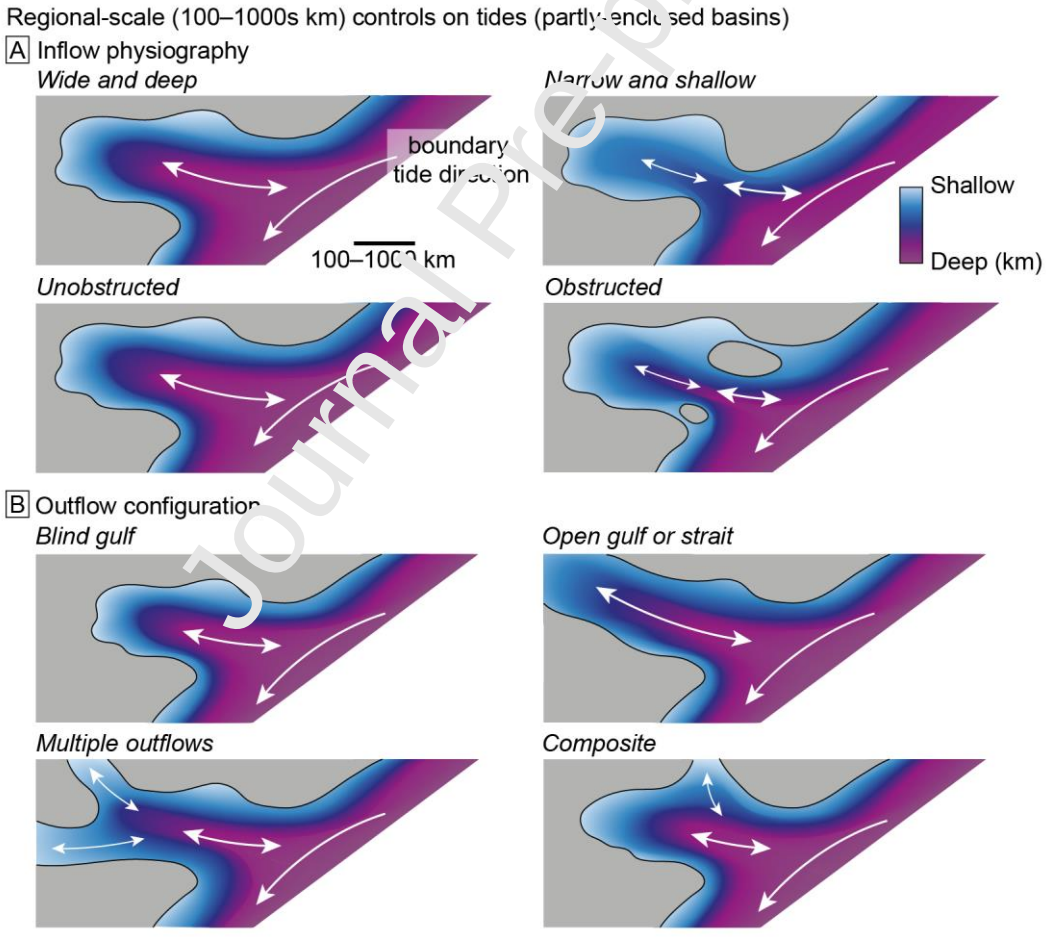

Fig. 21. Regional-scale (100–1000s km) basin physiographic controls on tidal energy potential in partly-enclosed basins, related to the balance in tidal energy flux into (inflow) and out (outflow) of the partly enclosed basin. (A) The control of inflow physiography on tidal inflow includes the width, depth and degree of

obstruction of the main tidal inflow position to the basin. Larger, thicker arrows indicate higher tidal energy flux into the partly enclosed basin. (B) The control of outflow physiography on tidal outflow includes the number, width, depth and degree of obstruction of main tidal outflow positions and their configuration with respect to the main tidal inflow positions and boundary tide pathway.

4.2.2 Tidal resonance on continental shelves

Funnelling, shoaling and resonance effects across continental shelves are widely recognised 10s–100s km-scale controls on tides (sections 2.1.4 and 2.2.1). Analysis of modern tides suggests that the relative importance of tides compared to wave and fluvial processes increases with shelf width perpendicular to the coastline (e.g. Redfield, 1958; Cram, 1979; Howarth, 1982; Ainsworth et al., 2011). This is principally due to an increase in tidal resonance with shelf width (Section 2.2.1) (Howarth, 1982; Ainsworth et al., 2011), but some tidal energy will be lost to frictional drag on wider shelves (Allen, 1997). Furthermore, the relationship between shelf width, tidal range and tidal dominance (Nyberg and Howell, 2016) varies globally due to changes in the following controls (Fig. 22): (1) the relative amplitude of semi-diurnal to diurnal tidal constituents, which have significantly different wavelengths (e.g. Kowalik and Luick, 2013); (2) the geometry of continental shelves; (3) the incidence angle of tides and tidal flow patterns, which partly relates to latitude and Coriolis rotation; and (4) frictional effects, which may exceed tidal amplification across wide shelves and seaways. Continental shelf width may change significantly on short geological timescales due to relative sea level changes related to global eustasy, isostatic adjustment, and tectonic subsidence and uplift (e.g. Miller et al., 2005; Haq, 2014; Sames et al., 2016). Furthermore, within short-term eustatic sea level changes (10–100s ka), shelf width may change due to shoreline progradation, which is likely to be pronounced adjacent to major delta systems (e.g. Burgess and Hovius, 1998; Hori et al., 2001; Ta et al., 2002a; Chamberlain et al., 2018). In addition, changes to regional-scale tidal flow can supersede the effect of shelf width change on shelf tidal resonance. For example, despite a decrease in shelf width during 50 m sea-level lowstands, tidal range along northern SCS coastlines was higher during the Late Oligocene–Late Miocene because the boundary tide had a higher tidal range (section 3.1; Figs. 7, 8). Likewise, resonance of the M2 tide in the modern Atlantic Ocean provides a higher boundary tide to the higher latitude Arctic Ocean (Fig. 4A).

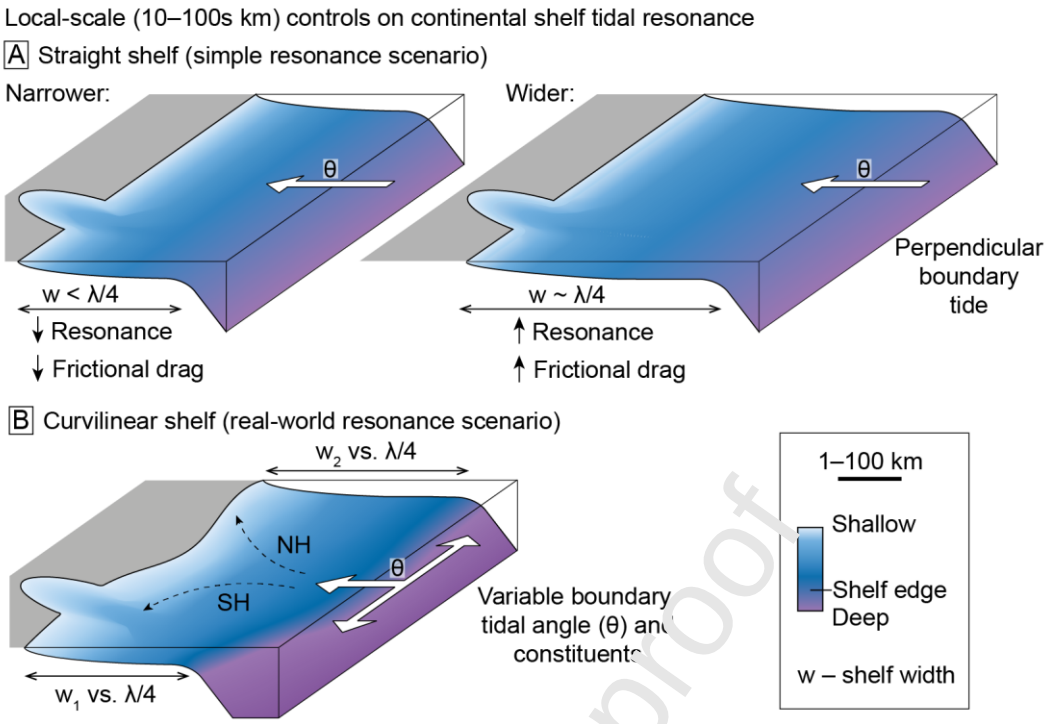

Fig. 22. Local-scale (10–100s km) controls on continental shelf tidal resonance. (A–B) Simple resonance scenario for a straight shelf, perpendicular boundary tide and uniform shelf width (w), where maximum tidal resonance occurs when shelf width is one-quarter the tidal wavelength (λ) (after Howarth, 1982). (C) A more realistic resonance scenario for a curvilinear shelf, variable angle (θ) and dominant tidal constituent of the boundary tide, Coriolis rotation and variable shelf width (w_1 versus w_2) compared to one-quarter the tidal wavelength. NH = Northern Hemisphere. SH = Southern Hemisphere.

4.2.3 Shoreline geometry

Tidal amplification due to funnelling, shoaling and resonance effects in shoreline embayments are potentially very important smaller-scale (1–10s km) controls on tides (e.g. Slingerland, 1986; Dalrymple, 1992; Wells et al., 2007; Ainsworth et al., 2011). However, as outlined below, modern tides and palaeotidal modelling suggest that tidal amplification in coastal embayments is variable and depends on the balance between tidal amplification and frictional damping.

Modern river-linked embayments (e.g. estuaries and interdistributary bays) are typically classified as either hyposynchronous, where tidal range decreases landward because frictional damping exceeds tidal amplification, or hypersynchronous, where tidal range initially increases landward due tidal amplification exceeding frictional damping, before decreasing to the tidal limit (e.g. Godin, 1999; Dalrymple and Choi, 2007). The degree of tidal amplification versus frictional damping can vary between adjacent embayments and show complex patterns within embayments, as seen along eastern

North America and western India (Fig. 23). Differentiating between ancient hypersynchronous and hyposynchronous embayments is difficult and requires interpretation of the process balance and extent of turbidity maximum zone in the fluvial-to-marine transition zone (e.g. Gugliotta et al., 2016a). However, palaeotidal modelling can reveal spatial and temporal variations in tidal processes within ancient embayments. For example, as the entrance to the palaeo-Gulf of Thailand became wider and deeper during the Miocene, greater tidal inflow and reduced frictional damping shifted the tidal maximum landward (Fig. 7).

The relative strength of tidal amplification versus frictional damping depends on several factors:

(1) The geometry and bathymetry of the embayment, especially its sinuosity (e.g. Slingerland, 1986; Allen, 1997). Frictional effects will be higher in more sinuous and rapidly shallowing embayments compared to straighter, gently shallowing embayments (Fig. 23, 24A).
(2) The geometry and bathymetry of the embayment entrance impacts inflow and outflow of tidal energy. A narrower, shallower and obstructed entrance increases dissipation and reflection of tidal energy (e.g. Mediterranean Ocean; Chesapeake Bay), whereas a wider, deeper and unobstructed entrance permits greater tidal inflow (e.g. Bay of Fundy) (Figs. 23, 24C).
(3) The angle between the embayment axis and incoming tide influences tidal inflow. Tidal inflow increases and frictional effects decrease when the incoming tide is more parallel to the embayment axis (Fig. 23, 24B).
(4) Embayment physiography and the dominant tidal constituent control the resonance potential of embayment tides (Section 2.3)

Hyposynchronous embayments are more likely if the tidal inflow and resonance potential are low and frictional drag potential is high (Fig. 23A). Hypersynchronous embayments are more likely if tidal inflow and resonance potential are high and frictional drag potential is low (Fig. 23B). However, even if tidal amplification exceeds frictional effects, embayments may be dominated by fluvial or wave processes (Dalrymple, 1992).

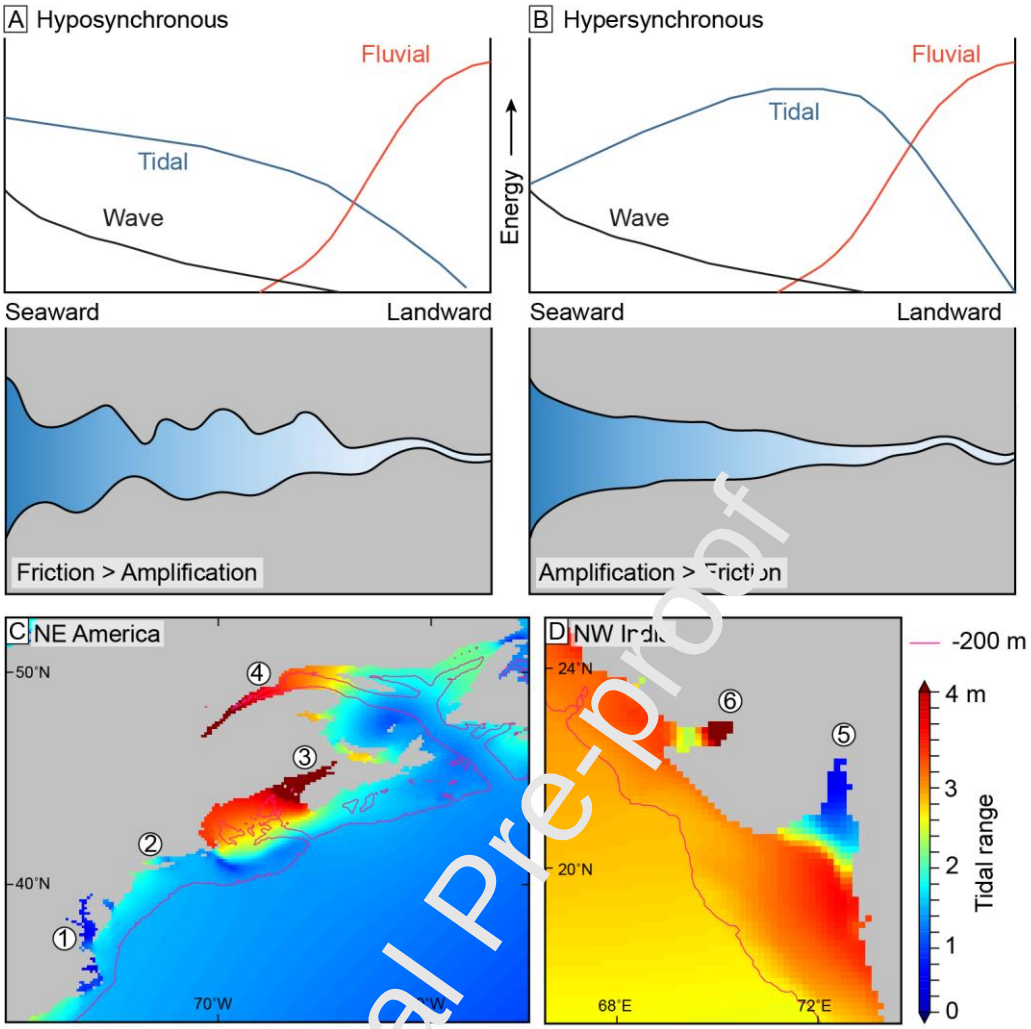

Fig. 23. Tides in shoreline embayments. (A) A hyposynchronous system in which frictional damping exceeds amplification of tides due to funneling, shoaling and resonance effect, resulting in a seaward to landward decrease in tidal range and tidal current speed. (B) A hypersynchronous system in which tidal amplification exceeds friction, causing a seaward-to-landward increase in tidal range and current speed, before friction causes tidal range and current speed to decrease to zero at the tidal limit (after Dalrymple and Choi, 2007). (C, D) Modeled tidal range from FES 2012 for north-east America (C) and north-west India (D) illustrating the varying relationship between tidal range and position within adjacent embayments: (1) hyposynchronous Chesapeake Bay; (2) moderately hypersynchronous Long Island Sound; (3) strongly hypersynchronous Bay of Fundy; (4) strongly hypersynchronous St. Lawrence River mouth; (5) strongly hyposynchronous Gulf of Khambhat; and (6) complex hyposynchronous and hypersynchronous Gulf of Kutch.

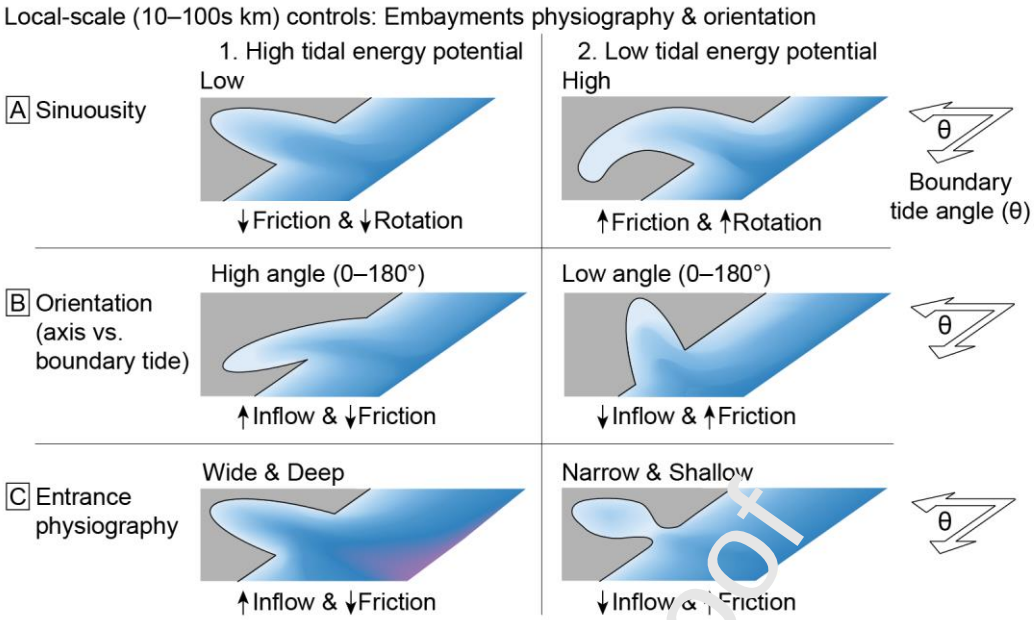

Fig. 24. Physiographic controls on tides in shoreline embayments. A schematic matrix includes the influence of (A) shoreline geometry, for example, sinuosity and rugosity, (B) the relative orientation of the embayment axis and incoming tide, and (C) the physiography of the embayment entrance, on (1) high versus (2) low tidal energy potential within the embayment. Note this matrix excludes the influence of wave or fluvial processes.

4.3 Modified decision tree for prediction of shoreline–shelf depositional process regime

The original process-based, decision tree hierarchy for predicting shoreline-shelf systems uses the following sequential assessment procedure (Ainsworth et al., 2011) (Fig. 3A): (1) tidal resonance potential, (2) fluvial versus wave effectiveness, (3) low versus high A/S, (4) shoreline geometry (relative degree of rugosity), and (5) coastal process dominance (relative degree of fluvial, wave and tidal processes). We propose replacing this procedure with one that uses two decision trees, reflecting low and high wave energy potential, respectively. The procedure for using each decision tree comprises the following hierarchy (compare Figs. 3A and 26): (1) wave energy potential, (2) tidal energy potential, (3) shelf tidal resonance potential, (4) fluvial potential, and (5) shoreline geometry. The justification for this revision is outlined below, based on the preceding review of tidal theory, the physiographic influence on modern tides and present-day shoreline process regimes (e.g. Nyberg and Howell, 2016), and the physiographic controls on tides highlighted by palaeotidal modelling studies and the time-equivalent stratigraphic record with preserved tidal indicators.

The dominance of wave-dominated process regimes along present-day depositional shorelines (Fig. 2) (Nyberg and Howell, 2016) supports this being the first decision for predicting shoreline process regime (hierarchical query #1 in Fig. 25). In modern systems, the height and strength of wind-generated surface waves are primarily controlled by the speed, duration and fetch of the wind (e.g. Allen, 1997). Wave dominance also depends on the frequency of larger-magnitude storms, overall meteorological conditions and the orientation of the shoreline relative to the wave-generating standing body of water. In ancient domains, determining the speed and duration of wind, and the effect on wave processes, would ideally require sophisticated analyses integrating palaeogeographic reconstructions and numerical climate and wave modelling. More generally, predicting wave energy potential along ancient shorelines relies on larger scale palaeogeographic reconstructions. If a system is open to a large water body or ocean, wave fetch and consequently wave potential would be relatively high. Any protection that restricts access to oceanic waves will lower wave potential (e.g. Ainsworth et al., 2011). Protection from ocean waves may be tectonic (e.g. emergent fault blocks, tectonically controlled seaways) or depositional (e.g. rugose coastal morphology, depositional headland, barrier islands, asymmetrical deltas).

The tidal energy potential of a basin (hierarchical query #2 in Fig. 25) is first dependent on whether the connected open ocean is at resonance with a particular tidal constituent (thus impacting the boundary tide amplitude), and second, whether the study area directly faces the open ocean or instead faces a partly enclosed water body. For systems facing an open ocean, tidal energy potential is assumed to be relatively high because of the relative lack of dissipation effects compared to partly enclosed systems. However, the absolute amount and distribution of tidal energy in an open-ocean basin relates to its size, shape, bathymetry, which together determine resonance, and only partly relates to latitude (Dalrymple and Padman, 2019). As discussed (Section 4.2.1), the tidal energy potential in partly enclosed systems depends on the balance of tidal energy inflow versus outflow (Fig. 21), as well as resonance (Section 2.2.1).

Shelf resonance potential (hierarchical query #3 in Fig. 25) is related to shelf width and the dominant tidal constituent of the incoming tide (Figs. 4, 23). Analysis of modern shoreline processes suggest a cut-off of c. 75 km between mainly tide-dominated (>75 km) and wave-dominated (<75 km) systems (Ainsworth et al., 2011). However, tides only dominate on c. 50% of depositional shorelines associated with shelf widths of >75 km, with 47% being wave dominated (Fig. 2) (Nyberg and Howell, 2016). This suggests that a more representative shelf width threshold may be even higher, which would be closer to the theoretical shelf width for resonance of the typically dominant semi-

diurnal M_2 or diurnal K_1 tidal components (Fig 23). However, without a more accurate and globally applicable cut-off value, the 75 km cut-off is retained in the proposed process prediction decision tree (Fig. 25). Nevertheless, this should be critically assessed on a case-by-case basis, considering other local geological factors.

Assessing fluvial potential (hierarchical query #4 in Fig. 25) relies on (1) measured or inferred drainage area, hinterland relief and rock types (Milliman and Syvitski, 1992; Syvitski and Milliman, 2007; Sømme et al., 2009); (2) palaeoclimate and its effects on water and sediment discharge (Hovius, 1998; Syvitski et al., 2003; Milliman and Farnsworth, 2011), and/or (3) observational evidence of fluvial influence in the rock record (Bhattacharya and Walker, 1992; MacEachern and Bann, 2008; Ainsworth et al., 2016). In general, large drainage basins would have higher fluvial potential than smaller drainage basins. Conversely, large rivers may have a disproportionate likelihood of being strongly tide influenced, or even tide dominated, at their mouth because of the larger tidal prism that is generated by the width of the river channel and its flat gradient, promoting long-distance penetration of the tide (Dalrymple, 2010b). An exception may be river systems with short, steep drainage basins subject to high rainfall storms, which often preserve river-influenced shoreline deposits (e.g. Bhattacharya and MacEachern, 2009; Collins et al., 2017b). The overwhelming dominance of wave- and tide-dominated shoreline morphologies along present-day coastlines indicates effective reworking of riverine sediment by marine processes (Fig. 6). However, sedimentary dynamics and deposition may still be dominated by river floods, even in deltas with lobate-to-cuspate geometries typical of wave dominance (Rodriguez et al., 2000; Fielding et al., 2005; Gani and Bhattacharya, 2007). Consequently, for ancient shoreline systems, any information indicating close proximity to a river system may suggest relatively high potential for river influence (Fig. 25).

Shoreline geometry (hierarchical query #5 in Fig. 25) mainly relates to the degree of rugosity, recognizing that tides are commonly amplified in many modern embayments and along embayed shorelines. However, modern embayments and those in palaeotidal simulations are not exclusively tide dominated (e.g. Figs. 2, 4, 26; cf. Fig. 2) due to variations in the balance between frictional damping and tidal amplification, due to funnelling, shoaling and/or resonance (as discussed in Section 4.2.3). Embayed shorelines are also inevitably more protected from direct wave processes. However, wave processes may still be dominant along the back of moderately embayed shorelines, especially where embayment mouths allow direct access to open ocean waves (Fig. 25). In fluvially linked

embayments, river processes may dominate over tides and waves (e.g. Dalrymple and Choi, 2007). Therefore, shoreline geometry can have a variable potential influence on depositional processes.

The A/S ratio of a shoreline–shelf system is a widely-used theoretical concept that links tectonics, eustatic sea-level change and sediment supply (Muto and Steel, 1997), and features prominently in the original process-based decision tree of Ainsworth et al. (2011) (hierarchical query #3 in Fig. 3A). However, A/S ratio has been removed from our revised predictive decision tree (Fig. 25) due to limitations with the concept. For example, identifying relatively 'high' and 'low' A/S ratio relies on generalized relationships between A/S ratio and sequence stratigraphic systems tracts, which in turn relies on extensive datasets for sequence stratigraphic and/or shoreline trajectory analysis (Ainsworth et al., 2008). Quantification of 'high' versus 'low' A/S ratios also relies upon sufficient well log, core and/or outcrop data to calculate the thickness of a sedimentary unit to approximate accommodation and the sand-to-shale ratio and approximate coarse sediment supply rate (Ainsworth, 2003; Ainsworth, 2005; Ainsworth et al., 2008; Ainsworth et al., 2013). However, even if sufficient data are available, the exact ratios for 'high' and 'low' A/S regimes are yet to be determined. The reliance on available data and interpretations reduces the applicability of the A/S ratio for predicting shoreline processes in ancient systems, especially where data are limited. Furthermore, the A/S ratio is a subordinate control on tides compared to the tidal energy potential of a basin, shelf tidal resonance potential and shoreline geometry. Process changes relating to A/S ratio only apply for moderately- to highly-embayed shorelines and are captured in changes to shoreline geometry (Section 1.2) (Ainsworth et al., 2011).

We propose to replace the original three-tier process prediction scheme (Figs. 3A) (Ainsworth et al., 2011) with a two-tier scheme that reflects the primary and secondary processes (Figs. 1, 26). Analysis of modern shorelines suggests the thresholds for process classification in a three-tier scheme can be ambiguous (e.g. Fig. 2) (Nyberg and Howell, 2016). While a three-tier scheme has the superficial appearance of greater precision (Figs. 1A, 3) (Ainsworth et al., 2011), it requires definitive process classification and potential quantification of formative processes for sedimentary structures that is rarely, if ever, possible. At present, the range of mixed-process sedimentary structures and variability between different modern and ancient depositional systems is incomplete, including ambiguities in the process interpretations of several sedimentary structures (Section 2.2). A more holistic framework for interpreting mixed-process deposition and preservation would also include the effect of grain size availability on sedimentary facies characteristics and preservation, plus integration with a range of observational and interpretational techniques from both modern and ancient systems (including

numerical modelling). However, such holistic analysis of the ancient record is still limited by several factors, notably preservation bias, dataset quality, and time available for data study. The process prediction scheme proposed herein provides a quick, easily applied and robust interpretation of shoreline–shelf process regime to use, test and refine in subsequent studies. The scheme directly incorporates learnings from several numerical tidal modelling studies and can therefore be applied with a fair degree of confidence in the absence of potentially time-consuming and expensive numerical modelling.

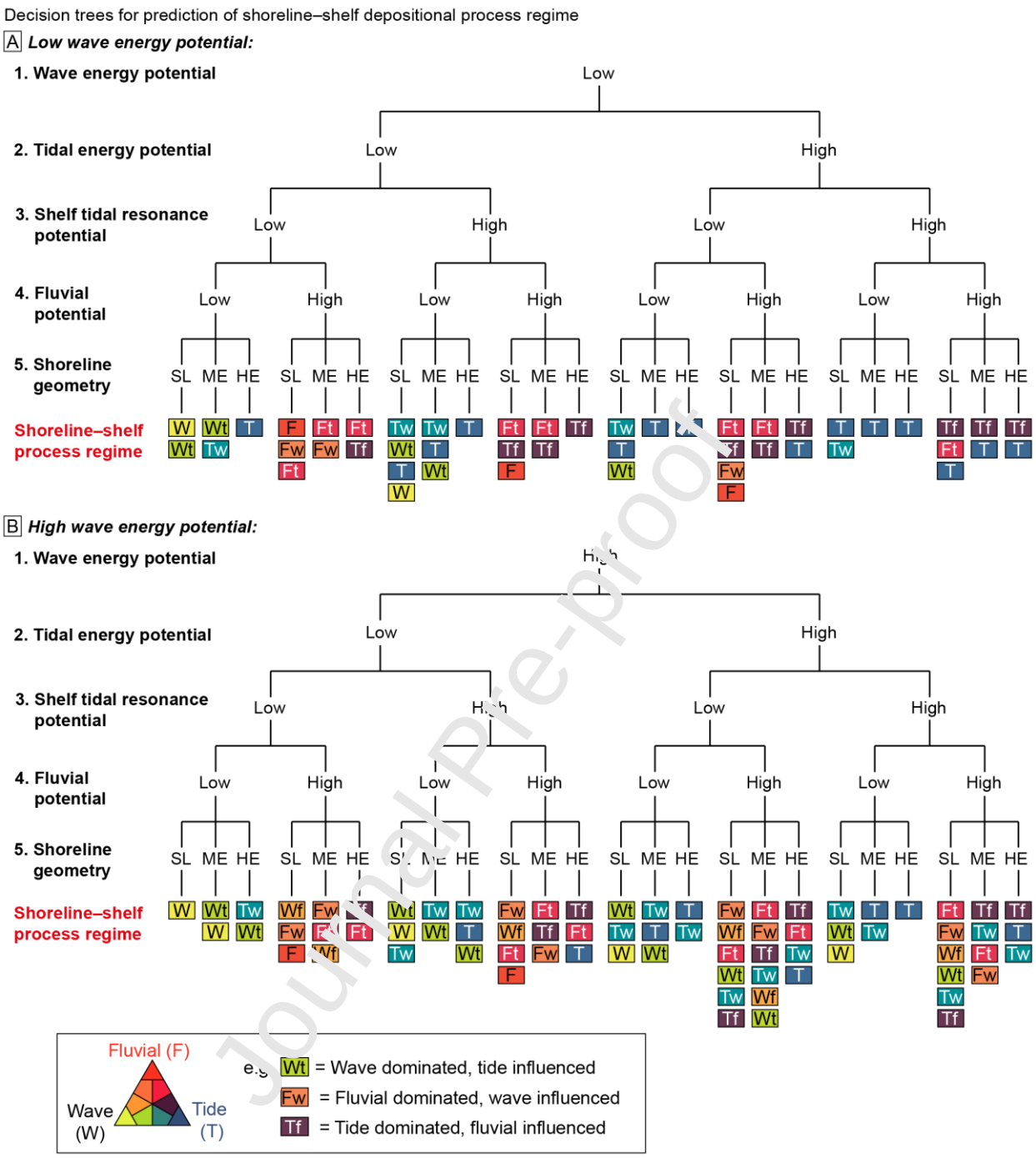

Fig. 25. Proposed revision to decision trees for predicting shoreline process dominance (cf. Fig. 3A) (after Ainsworth et al., 2011) for systems with (A) low wave energy potential, and (B) high wave energy. The two decision trees each include five hierarchical queries: (1) wave energy potential of the basin; (2) tidal energy potential of the basin; (3) shelf tidal resonance potential; (4) fluvial potential; and (5) shoreline geometry. Key to colour coding is shown in the inset. Shoreline geometry abbreviations: SL-straight/lobate; ME-moderately embayed; HE-highly embayed.

5 CONCLUSIONS

For shoreline–shelf systems, river, wave (including storm) and tide interactions are the primary determinants of sediment transport, morphodynamics and sedimentary preservation and are the cornerstones of process classification schemes. The preserved sedimentary record of these process interactions is widely interpreted, though the range of characteristics and corresponding process interpretation are debated and often ambiguous. Understanding the controls on river, wave and tidal processes benefits from an integrated approach combining numerical modelling and traditional facies analysis, which in turn improves prediction of shoreline–shelf processes classifications. We illustrate this approach in three case studies that combine palaeotidal modelling with process-based facies analysis of time-equivalent stratigraphy. The inferred controls on tides are discussed in the context of modern tidal processes and shoreline–shelf process regimes, resulting in a modification of predictive classification schemes for shoreline–shelf systems.

Tides are controlled by the following physiographic controls: (1) the impact of physiography – size, shape and bathymetry – on tidal resonance in the Earth's global ocean and constituent ocean basins (1000s km-scale), (2) in partly-enclosed water bodies, the physiography of ocean connections controls the balance between the amount of tidal energy entering and exiting the basin – the tidal inflow and outflow; (3) shelf physiography (10–100 km-scale) and the boundary tide orientation and dominant tidal constituent control shelf tidal resonance; and (4) embayment physiography (1–10 km-scale), especially at the entrance, and the relative orientation of the incoming tide, control tidal amplification (funnelling and shoaling) versus frictional effects in shoreline embayments. Validation of palaeotidal simulations using the rock record requires observations and process interpretations across a range of scales, from facies to depositional sequences, ideally integrating diverse data types. However, the validation is limited by three main uncertainties: (1) ancient tidal range prediction from stratigraphic data; (2) determining the processes of primary sedimentary structures, and (3) preservational bias in the stratigraphic record. In contrast, numerical modelling of tides and other hydrodynamic processes are uniquely powerful tools in providing quantitative insights into the nature and intensity of ancient hydrodynamic processes. We show how this can significantly reduce ambiguities in palaeoenvironmental interpretations in a range of contrasting geological settings.

The overwhelming dominance of waves along modern shorelines indicates existing shoreline–shelf process regime models overstate the role of tides relative to waves. We propose a modified classification scheme for shoreline–shelf process regime that places wave fetch and associated meteorological conditions as the first-order control, with two initial strands for low and high wave energy potential, respectively. These two decision trees each include five hierarchical queries: (1)

wave energy potential of the basin; (2) tidal energy potential of the basin; (3) shelf tidal resonance potential; (4) fluvial potential; and (5) shoreline geometry. The tidal prediction elements of both decision trees can be significantly enhanced by calibration with numerical palaeotidal modelling, as demonstrated by the case studies.

Determining process regime from ancient shoreline successions continues to be limited by two critical aspects: (1) uncertainty and biases in the process classification of common sedimentary structures; and (2) skewed preservation of certain depositional processes in different environments and on different timescales. These aspects, combined with the challenges in unravelling modern mixed-process regimes, lends support to a two-tier, rather than a three-tier, process classification of shoreline–shelf systems, in which emphasis is placed on only primary and secondary processes. Wider utilisation of this simpler yet robust predictive classification should enable more consistent and structured comparisons between ancient shoreline–shelf systems.

ACKNOWLEDGEMENTS

The authors acknowledge financial support from Natural Environment Research Council (NERC), Leverhulme Trust, Shell International Exploration and Production, and the Academy of Sciences of the Czech Republic. The authors thank Bob Dalrymple and Zheng Zhou for thorough, constructive reviewers and Jingping Xu for editorial comments. We also acknowledge support of Getech and Imperial College's Grantham Institute and High-Performance Computing Service. D.M. Hodgson, B.K. Levell, R.B. Ainsworth and B.K. Valkarelov are thanked for valuable comments and discussion.

SUPPLEMENTARY MATERIAL

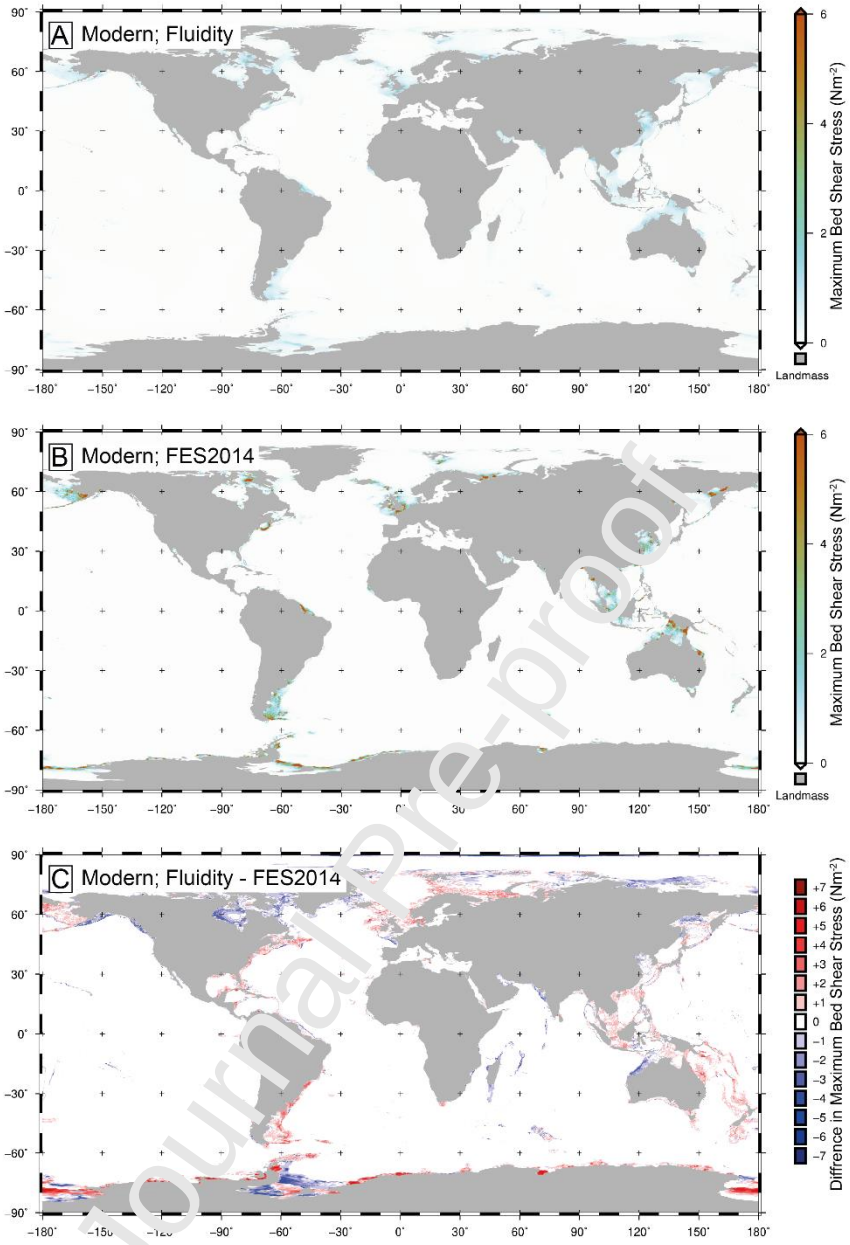

Supplementary Fig. 1. Global map of modern tidal bed shear stress calculated from (A) tidal modelling using Fluidity and (B) tidal velocity magnitude from FES2014. C) Difference in maximum tidal bed shear stress between (A) Fluidity and (B) FES2014; Blue indicates FES2014 has a higher maximum tidal bed shear stress.

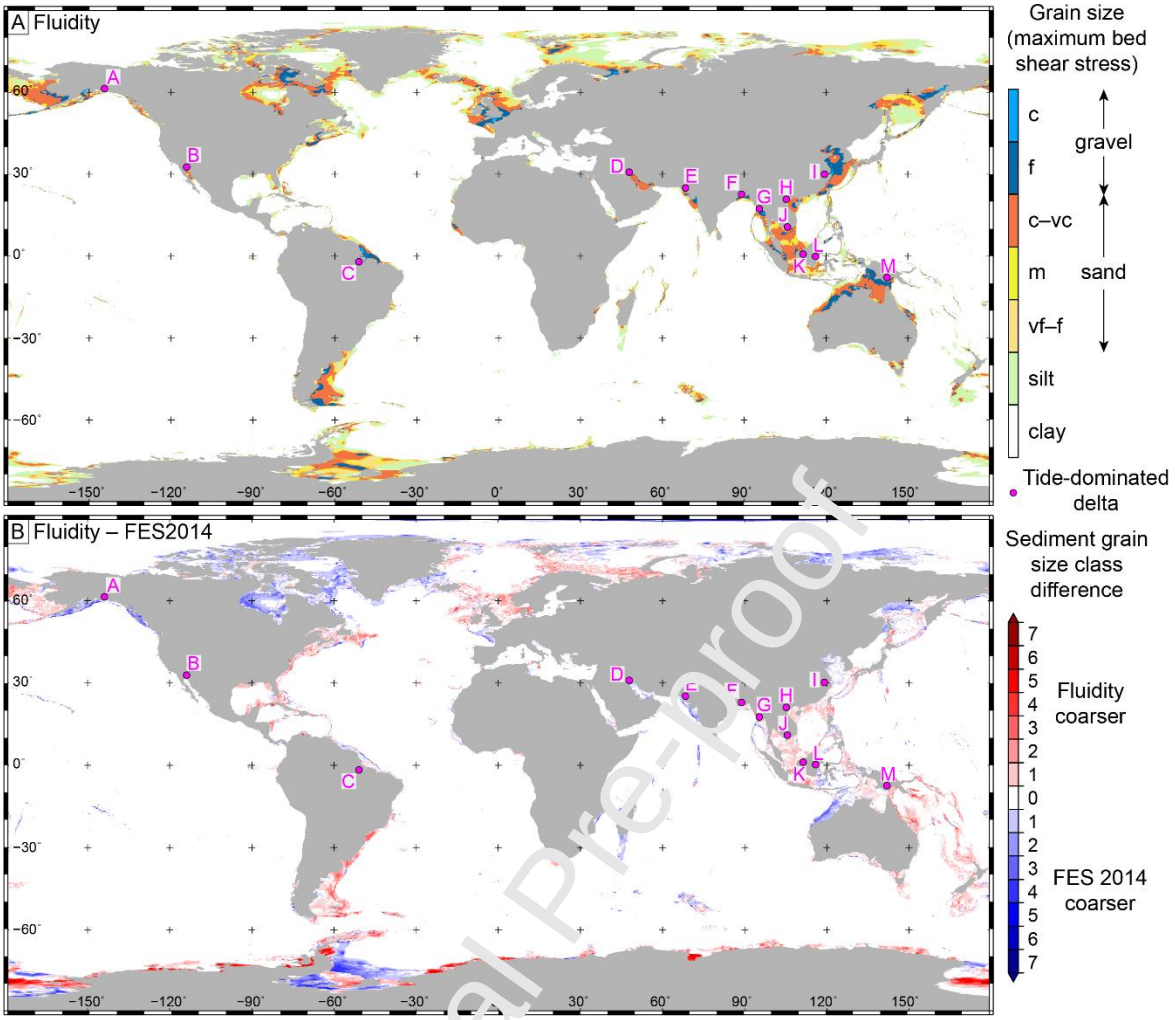

Supplementary Fig. 2. (A) Maximum tidal bed shear stress modeled using Fluidity, plotted as the equivalent grain size that could be entrained if available. (B) Difference in sediment grain size class between maximum tidal bed shear stress for Fluidity (A) and FES2014 (Fig. 2D) (Carrère et al., 2015). Grain size abbreviations: vf = very fine; f = fine; m = medium; c = coarse; vc = very coarse. Pink dots show location of tide-dominated deltas (Goodbred and Saito, 2012): A) Copper; B) Colorado; C) Amazon; D) Shatt-al-Arab; E) Indus; F) Ganges-Brahmaputra; G) Irrawaddy; H) Red River; I) Yangtze; J) Mekong; K) Rajang; L) Mahakam; and M) Fly.

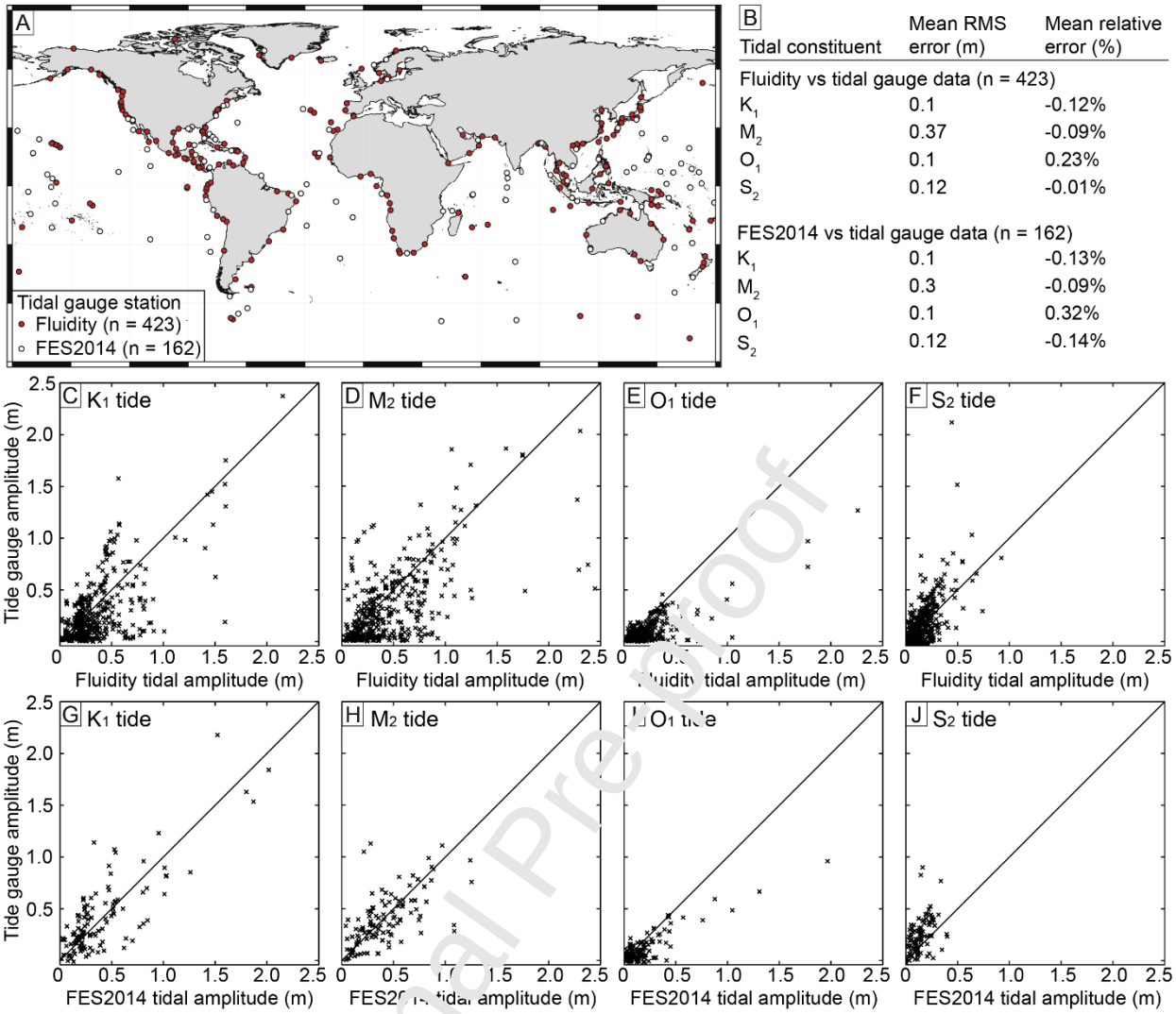

Supplementary Fig. 3. Validation of modeled tidal amplitude using Fluidity and FES2014 (Carrère et al., 2015). (A) Number (n) and position of a global set of tidal stations used for the comparisons to FES2014 (white circles, n = 162) and Fluidity (red circles, n = 423) model data. (B) Summary of root-mean-squared (RMS) and relative percentage errors between the model and tidal gauge data of tidal constituent amplitude. Tidal gauge amplitude data was derived by tidal harmonic analysis of sea surface elevation data. (C–J) Plots of tidal gauge versus modeled tidal amplitude for the K_1 (C, G), M_2 (D, H), O_1 (E, I) and S_2 (F, J) tidal constituents using Fluidity (C–F) and FES2014 (G–J).

REFERENCES

Ainsworth, R.B., 2003. Sequence stratigraphic-based analysis of depositional connectivity using 3-D reservoir modelling techniques, University of Liverpool, UK, 310 pp.

Ainsworth, R.B., 2005. Sequence stratigraphic-based analysis of reservoir connectivity: influence of depositional architecture – a case study from a marginal marine depositional setting. Petroleum Geoscience, 11: 257–276.

Ainsworth, R.B., Flint, S.S. and Howell, J.A., 2008. Predicting coastal depositional style: influence of basin morphology and accommodation to sediment supply ratio within a sequence stratigraphic framework. In: G.J. Hampson, R.J. Steel, P.M. Burgess and R.W. Dalrymple (Editors), Recent Advances in Models of Siliclastic Shallow-Marine Stratigraphy. SEPM Special Publication, pp. 237–263.

Ainsworth, R.B., McArthur, J.B., Lang, S.C. and Vonk, A.J., 2018. Quantitative sequence stratigraphy. AAPG Bulletin, 102: 1913-1939.

Ainsworth, R.B., Vakarelov, B.K., Lee, C., MacEachern, J.A., Montgomery, A.E., Ricci, L.P. and Dashtgard, S.E., 2015. Architecture and evolution of a regressive, tide-influenced marginal marine succession, Drumheller, Alberta, Canada. Journal of Sedimentary Research, 85: 596–625.

Ainsworth, R.B., Vakarelov, B.K., MacEachern, J.A., Nanson, R.A., Lane, T.I., Rarity, F. and Dashtgard, S.E., 2016. Process-Driven Architectural Variability In Mouth-Bar Deposits: A Case Study From A Mixed-Process Mouth-Bar Complex, Drumheller, Alberta, Canada. Journal of Sedimentary Research, 86: 512-541.

Ainsworth, R.B., Vakarelov, B.K. and Nanson, R.A., 2011. Dynamic spatial and temporal prediction of changes in depositional processes on clastic shorelines: Toward improved subsurface uncertainty reduction and management. AAPG Bulletin, 95: 267–297.

Allen, G.P. and Chambers, J.L.C., 1998. Sedimentation in the modern and Miocene Mahakam Delta. Indonesian Petroleum Association, Jakarta, 236 pp.

Allen, G.P. and Posamentier, H.W., 1993. Sequence stratigraphy and facies model of an incised valley fill; the Gironde Estuary, France. Journal of Sedimentary Research, 63: 378-391.

Allen, J., 1981a. Lower Cretaceous tides revealed by cross-bedding with mud drapes. Nature, 289: 579.

Allen, J.R.L., 1968. Current Ripples: their relation to patterns of water and sediment motion. North Holland, Amsterdam, 433 pp.

Allen, J.R.L., 1981b. Palaeotidal speeds and ranges estimated from cross-bedding sets with mud drapes. Nature, 293: 394-396.

Allen, J.R.L., 1982a. Mud drapes in sand-wave deposits: a physical model with application to the Folkestone Beds (early Cretaceous, southeast England). Philosophical Transactions of the Royal Society of London A: Mathematical, Physical and Engineering Sciences, 306: 291-345.

Allen, J.R.L., 1982b. Sedimentary structures, their character and physical basis, 1. Elsevier, Amsterdam, 592 pp.

Allen, P. and Homewood, P., 1984. Evolution and mechanics of a Miocene tidal sandwave. Sedimentology, 31: 63-81.

Allen, P.A., 1997. Earth Surface Processes. Blackwell Scientific Publications, Oxford, U.K., 404 pp.

Amir Hassan, M.H., Johnson, H.D., Allison, P.A. and Abdullah, W.H., 2013. Sedimentology and stratigraphic development of the upper Nyalau Formation (Early Miocene), Sarawak, Malaysia: A mixed wave- and tide-influenced coastal system. Journal of Asian Earth Sciences, 76: 301–311.

Amir Hassan, M.H., Johnson, H.D., Allison, P.A. and Abdullah, W.H., 2016. Sedimentology and stratigraphic architecture of a Miocene retrogradational, tide-dominated delta system: Balingian Province, offshore Sarawak, Malaysia. In: G.J. Hampson, A.D. Reynolds, B. Kostic and M.R. Wells (Editors), Sedimentology of Paralic Reservoirs: Recent Advances. Special Publications. Geological Society of London, London, UK, pp. SP444.12, 36 p.

Anderton, R., 1976. Tidal-shelf sedimentation: an example from the Scottish Dalradian. Sedimentology, 23: 429-458.

Androsov, A., Kagan, B., Romanenkov, D. and Voltzinger, N., 2002. Numerical modelling of barotropic tidal dynamics in the strait of Messina. Advances in Water Resources, 25: 401-415.

Anthony, E.J. and Orford, J.D., 2002. Between wave-and tide-dominated coasts: the middle ground revisited. Journal of Coastal Research, 36: 8-15.

Anthony, E.J., Oyédé, L.M. and Lang, J., 2002. Sedimentation in a fluvially infilling, barrier-bound estuary on a wave-dominated, microtidal coast: the Ouémé River estuary, Benin, west Africa. Sedimentology, 49: 1095-1112.

Archer, A.W., 1995. Modeling of cyclic tidal rhythmites based on a range of diurnal to semidiurnal tidal-station data. Marine Geology, 123: 1-10.

Archer, A.W., Kvale, E.P. and Johnson, H.R., 1991. Analysis of modern equatorial tidal periodicities as a test of information encoded in ancient tidal rhythmites. In: S. DG, R. GE, Z. BA and R. RA (Editors), Clastic Tidal Sedimentology. Memoir of the Canadian Society of Petroleum Geologists, pp. 189–196.

Archer, S.G., Steel, R.J., Mellere, D., Blackwood, S. and Cullen, B., 2019. Response of Middle Jurassic shallow-marine environments to syn-depositional block tilting: Isles of Skye and Raasay, NW Scotland. Scottish Journal of Geology, 55: 35-68.

Arnott, R.W.C. and Southard, J.B., 1990. Exploratory flow-duct experiments on combined-flow bed configurations, and some implications for interpreting storm-event stratification. Journal of Sedimentary Research, 60: 211-219.

Avdis, A., Candy, A.S., Hill, J., Kramer, S.C. and Piggott, M.D., 2018. Efficient unstructured mesh generation for marine renewable energy applications. Renewable Energy, 116: 842-856.

Banks, N., 1973. Tide-dominated offshore sedimentation, Lower Cambrian, north Norway. Sedimentology, 20: 213-228.

Barckhausen, U., Engels, M., Franke, D., Ladage, S. and Pubellier, M., 2014. Evolution of the South China Sea: Revised ages for breakup and seafloor spreading. Marine and Petroleum Geology, 58: 599-611.

Barckhausen, U. and Roeser, H.A., 2004. Seafloor spreading anomalies in the South China Sea revisited. In: P. Clift, W. Kuhnt, P. Wang and D. Hayes (Editors), Continent-Ocean Interactions Within East Asian Marginal Seas. Geophysical Monograph Series. AGU, Washington, DC, pp. 121-125.

Basilici, G., de Luca, P.H.V. and Poiré, D.G., 2012. Hummocky cross-stratification-like structures and combined-flow ripples in the Punta Negra Formation (Lower-Middle Devonian, Argentine Precordillera): A turbiditic deep-water or storm-dominated prodelta inner-shelf system? Sedimentary Geology, 267-268: 73-92.

Belderson, R., Johnson, M., Kenyon, N. and Stride, A., 1982. Bedforms. In: A.H. Stride (Editor), Offshore tidal sands, processes and deposit. Chapman and Hall, pp. 27-57.

Bhattacharya, J.P., 2010. Deltas. In: N.P. James and R.W. Dalrymple (Editors), Facies Models 4. Geotext 6. Geological Association of Canada, pp. 233-264.

Bhattacharya, J.P. and Giosan, L., 2003. Wave-influenced deltas: Geomorphological implications for facies reconstruction. Sedimentology, 50: 187–210.

Bhattacharya, J.P. and MacEachern, J.A., 2009. Hyperpycnal Rivers and Prodeltaic Shelves in the Cretaceous Seaway of North America. Journal of Sedimentary Research, 79: 184-209.

Bhattacharya, J.P. and Walker, R.G., 1992. Deltas. In: R.G. Walker and N.P. James (Editors), Facies Models: Response to Sea-Level Change. Geological Association of Canada, St. John's, NL, pp. 157–177.

Boersma, J. and Terwindt, J., 1981. Neap–spring tide sequences of intertidal shoal deposits in a mesotidal estuary. Sedimentology, 28: 151-170.

Boersma, J.R., 1969. Internal structure of some tidal mega-ripples on a shoal in the Westerschelde estuary, the Netherlands: report of a preliminary investigation. Geologie en Mijnbouw (Netherlands Journal of Geosciences), 48: 409-414.

Boyd, R., Dalrymple, R.W. and Zaitlin, B.A., 1992. Classification of clastic coastal depositional environments. Sedimentary Geology, 80: 139-150.

Boyd, R., Dalrymple, R.W. and Zaitlin, B.A., 2006. Estuarine and incised-valley facies models. In: H.W. Posamentier, Walker, R.G. (Editor), Facies Models Revisited. SEPM Special Publication, pp. 171-234.

Briais, A., Patriat, P. and Tapponnier, P., 1993. Updated interpretation of magnetic anomalies and seafloor spreading stages in the south China Sea: Implications for the Tertiary tectonics of Southeast Asia. Journal of Geophysical Research, 98: 6299-6328.

Bridges, P.H., 1982. Ancient offshore tidal deposits. In: A.H. Stride (Editor), Offshore Tidal Sands, Processes and Deposits. Chapman & Hall, London, UK, pp. 172-192.

Buatois, L.A., Santiago, N., Herrera, M., Plink-Björklund, P., Steel, R.J., Espin, M. and Parra, K., 2012. Sedimentological and ichnological signatures of changes in wave, river and tidal influence along a Neogene tropical deltaic shoreline. Sedimentology, 59: 1568–1612.

Burgess, P.M. and Hovius, N., 1998. Rates of delta progradation during highstands: consequences for timing of deposition in deep-marine systems. Journal of the Geological Society, 155: 217-222.

Carrère, L., Lyard, F., Cancet, M. and Guillot, A., 2015. FES 2014, a new tidal model on the global ocean with enhanced accuracy in shallow seas and in the Arctic regio, EGU General Assembly 2015, Vienna, Austria.

Casey, R., 1961. The stratigraphical palaeontology of the Lower Greensand. Palaeontology, 3: 487-621.

Chamberlain, E.L., Törnqvist, T.E., Shen, Z., Mauz, B. and Wallinga, J., 2018. Anatomy of Mississippi Delta growth and its implications for coastal restoration. Science advances, 4: eaar4740.

Chen, S., Steel, R.J., Dixon, J.F. and Osman, A., 2014. Facies and architecture of a tide-dominated segment of the Late Pliocene Orinoco Delta (Morne L'Enfer Formation) SW Trinidad. Marine and Petroleum Geology, 57: 208–232.

Choi, K.S., Dalrymple, R.W., Chun, S.S. and Kim, S.-P., 2004. Sedimentology of modern, inclined heterolithic stratification (IHS) in the macrotidal Han River delta, Korea. Journal of Sedimentary Research, 74: 677–689.

Chung, N.H., Quang, C.D. and Tham, N.T., 2015. A Review of Tertiary Palynomorph Assemblage in Cuu Long Basin: Case Study of Palynomorphs in Miocene–Oligocene Sediments. International Journal of Sciences: Basic and Applied Research, 24: 103-111.

Clifton, H.E., 1983. Discrimination between subtidal and intertidal facies in Pleistocene deposits, Willapa Bay, Washington. Journal of Sedimentary Research, 53: 353-369.

Coates, L. and MacEachern, J.A., 2007. The ichnological signatures of river-and wave-dominated delta complexes: differentiating deltaic and non-deltaic shallow marine successions, Lower Cretaceous Viking Formation and Upper Cretaceous Dunvegan Formation, west-central Alberta. In: J.A. MacEachern, K.L. Bann, M.K. Gingras and S.G. Pemberton (Editors), Applied Ichnology. Short Course Notes 52. SEPM, Tulsa, Oklahoma, pp. 227–254.

Coleman, J.M. and Wright, L.D., 1975. Modern river deltas: variability of processes and sand bodies. In: M.L. Broussard (Editor), Deltas: Models for Exploration. Houston Geological Society, Houston, Texas, pp. 99-149.

Collins, D.S., Avdis, A., Allison, P.A., Johnson, H.D., Hill, J. and Piggott, M.D., 2018a. Controls on tidal sedimentation and preservation: Insights from numerical tidal modelling in the Late Oligocene–Miocene South China Sea, Southeast Asia. Sedimentology, 65: 2468-2505.

Collins, D.S., Avdis, A., Allison, P.A., Johnson, H.D., Hill, J., Piggott, M.D., Amir Hassan, M.H. and Damit, A.R., 2018b. Controls on Tidal Sedimentation and Preservation: Insights from Numerical Tidal Modelling in the Late Oligocene–Miocene South China Sea, Southeast Asia. Sedimentology, Accepted; In Press.

Collins, D.S., Avdis, A., Allison, P.A., Johnson, H.D., Hill, J., Piggott, M.D., Hassan, M.H.A. and Damit, A.R., 2017a. Tidal dynamics and mangrove carbon sequestration during the Oligo–Miocene in the South China Sea. Nature Communications, 8: 15698.

Collins, D.S., Johnson, H.D., Allison, P.A. and Damit, A.R., 2018c. Mixed Process, Humid-Tropical, Shoreline–Shelf Deposition: Middle Miocene–Modern Baram Delta Province, North-West Borneo. Journal of Sedimentary Research, 88: 399–430.

Collins, D.S., Johnson, H.D., Allison, P.A., Guilpain, P. and Damit, A.R., 2017b. Coupled 'storm-flood' depositional model: Application to the Miocene–Modern Baram Delta Province, north-west Borneo. Sedimentology, 64: 1203–1235.

Collins, D.S., Johnson, H.D. and Baldwin, C.T., 2020. Architecture and preservation in the fluvial to marine transition zone of a mixed-process humid-tropical delta: Middle Miocene Lambir Formation, Baram Delta Province, north-west Borneo. Sedimentology, 67: 1-46.

Collinson, J. and Mountney, N.P., 2019. Sedimentary Structures. Dunedin Academic Press Ltd, 320 pp.

Colombera, L. and Mountney, N.P., 2020a. Accommodation and sediment-supply controls on clastic parasequences: A meta-analysis. Sedimentology, 67: 1667-1709.

Colombera, L. and Mountney, N.P., 2020b. On the geological significance of clastic parasequences. Earth-Science Reviews, 201: 103062.

Cooper, J., 2001. Geomorphological variability among microtidal estuaries from the wave-dominated South African coast. Geomorphology, 40: 99-122.

Cooper, J.A.G., 1993. Sedimentation in a river dominated estuary. Sedimentology, 40: 979-1017.

Cram, J.M., 1979. The influence of continental shelf width on tidal range: paleoceanographic implications. The Journal of Geology, 87: 441-447.

Curray, J.R., 1964. Transgressions and regressions. In: R.J. Miller (Editor), Papers in Marine Geology. Macmillan, New York, pp. 175-203.

D'Alpaos, A., Lanzoni, S., Marani, M. and Rinaldo, A., 2010. On the tidal prism–channel area relations. Journal of Geophysical Research: Earth Surface, 115: F01003.

d'Anglejan, B. and Brisebois, M., 1978. Recent sediments of the St. Lawrence middle estuary. Journal of Sedimentary Research, 48: 951-964.

Dalrymple, R.W., 1992. Tidal depositional systems. In: R.G. Walker and N.P. James (Editors), Facies Models: Response to Sea Level Change. Geological Association of Canada, St. John's, Newfoundland, pp. 195-218.

Dalrymple, R.W., 2006. Incised valleys in time and space: an introduction to the volume and an examination of the controls on valley formation and filling. In: R.W. Dalrymple, D.A. Leckie and R.W. Tillman (Editors), Incised Valleys in Time and Space. SEPM Special Publication, pp. 5–12.

Dalrymple, R.W., 2010a. Interpreting sedimentary successions: facies, facies analysis and facies models. In: N.P. James and R.W. Dalrymple (Editors), Facies Models 4. Geological Association of Canada, pp. 3-18.

Dalrymple, R.W., 2010b. Tidal depositional systems. In: R.W. Dalrymple and N.P. James (Editors), Facies models 4. Geological Association of Canada, St. Johns, NL, pp. 201–231.

Dalrymple, R.W., 2021. Sedimentation on high-energy sand flats in the Bay of Fundy: The record of tidal-bore activity and deposition from high-concentration suspensions of sand. Sedimentology, Accepted Article.

Dalrymple, R.W., Baker, E.K., Harris, P.T. and Hughes, M.G., 2003. Sedimentology and stratigraphy of a tide-dominated, foreland-basin delta (Fly River, Papua New Guinea). In: F.H. Sidi, D. Nummedal, P. Imbert, H. Darman and H.W. Posamentier (Editors), Tropical Deltas of Southeast Asia—Sedimentology, Stratigraphy, and Petroleum Geology. SEPM Spec. Publ., pp. 147–173.

Dalrymple, R.W. and Choi, K., 2007. Morphologic and facies trends through the fluvial–marine transition in tide-dominated depositional systems: A schematic framework for environmental and sequence-stratigraphic interpretation. Earth-Science Reviews, 81: 135–174.

Dalrymple, R.W., Kurcinka, C.E., Jablonski, B.V.J., Ichaso, A.A. and Mackay, D.A., 2015. Deciphering the relative importance of fluvial and tidal processes in the fluvial–marine transition. In: P.J. Ashworth, J.L. Best and D.R. Parsons (Editors), Fluvial–Tidal Sedimentology. Developments in Sedimentology. Elsevier, pp. 3–45.

Dalrymple, R.W., Mackay, D.A., Ichaso, A.A. and Choi, K.S., 2012. Processes, morphodynamics, and facies of tide-dominated estuaries. In: R.A.J. Davis and R.W. Dalrymple (Editors), Principles of Tidal Sedimentology. Springer, New York, pp. 79-108.

Dalrymple, R.W. and Padman, L., 2015. Tides at high latitudes, AAPG Hedberg Research Conference, Latitudinal Controls on Stratigraphic Models and Sedimentary Concept. AAPG Search and Discovery Article #120178, Banff.

Dalrymple, R.W. and Padman, L., 2019. Are tides controlled by latitude? . In: C. Fraticelli, A.W. Martinius, J.R. Suter and P.J. Markwick (Editors), Latitudinal controls on stratigraphic models and sedimentary concepts. SEPM Special Publication 108, pp. 29-45.

Dalrymple, R.W. and Rhodes, R.N., 1995. Estuarine dunes and bars. In: P. G.M.E. (Editor), Geomorphology and Sedimentology of Estuaries. Developments in Sedimentology. Elsevier, Amsterdam, pp. 359–422.

Dalrymple, R.W., Zaitlin, B.A. and Boyd, R., 1992. Estuarine facies models: conceptual basis and stratigraphic implications: perspective. Journal of Sedimentary Petrology, 62: 1130–1146.

Davis, R.A. and Dalrymple, R.W., 2012. Principles of Tidal Sedimentology. Springer, New York, 621 pp.

Davis, R.A. and Hayes, M.O., 1984. What is a wave-dominated coast? Marine Geology, 60: 313-329.

De Boer, P.L., Oost, A. and Visser, M., 1989. The diurnal inequality of the tide as a parameter for recognizing tidal influences. Journal of Sedimentary Research, 59: 912-921.

De Raaf, J.F.M. and Boersma, J.R., 1977. Tidal deposits and their sedimentary structures (seven examples from Western Europe). Geologie en Mijnbouw, 50: 479-504.

de Vriend, H.J., Capobianco, M., Chesher, T., De Swart, H.d., Latteux, B. and Stive, M., 1993. Approaches to long-term modelling of coastal morphology: a review. Coastal engineering, 21: 225-269.

de Vries Klein, G., 1977. Tidal circulation model for deposition of clastic sediment in epeiric and mioclinal shelf seas. Sedimentary Geology, 18: 1-12.

Dean, C.D., Collins, D.S., van Cappelle, M., Avdis, A. and Hampson, G.J., 2019. Regional-scale paleobathymetry controlled location, but not magnitude, of tidal dynamics in the Late Cretaceous Western Interior Seaway, USA. Geology, 47: 1083-1087.

Defant, A., 1961. Physical Oceanography, 11. Pergamon, New York, 598 pp.

Dercourt, J., Gaetani, M., Vrielynck, B., Barrier, E., Biju-Duval, B., Brunet, M.-F., Cadet, J.P., Crasquin, S. and Sandulescu, M., 2000. Atlas Peri-Tethys Palaeogeographical Maps, I-XX. CCGM/CGMW, 269 pp.

Dott, R.H. and Bourgeois, J., 1982. Hummocky stratification: significance of its variable bedding sequences. Geological Society of America Bulletin, 93: 663–680.

Doust, H. and Sumner, H.S., 2007. Petroleum systems in rift basins—a collective approach in Southeast Asian basins. Petroleum Geoscience, 13: 127-144.

Dumas, S. and Arnott, R.W.C., 2006. Origin of hummocky and swaley cross-stratification— The controlling influence of unidirectional current strength and aggradation rate. Geology, 34: 1073–1076.

Egbert, G.D., Ray, R.D. and Bills, B.G., 2004. Numerical modeling of the global semidiurnal tide in the present day and in the last glacial maximum. Journal of Geophysical Research: Oceans, 109.

Elliott, T., 1986. Deltas. In: H.G. Reading (Editor), Sedimentary environments and facies. Blackwell Scientific Publications, Oxford, UK, pp. 113-154.

Ericksen, M.C. and Slingerland, R., 1990. Numerical simulations of tidal and wind-driven circulation in the Cretaceous Interior Seaway of North America. Geological Society of America Bulletin, 102: 1499-1516.

Fanget, A.-S., Berné, S., Jouet, G., Bassetti, M.-A., Dennielou, B., Maillet, G.M. and Tondut, M., 2014. Impact of relative sea level and rapid climate changes on the architecture and lithofacies of the Holocene Rhone subaqueous delta (Western Mediterranean Sea). Sedimentary Geology, 305: 35-53.

Fielding, C.R., Trueman, J. and Alexander, J., 2005. Sedimentology of the modern and Holocene Burdekin River Delta of north Queensland, Australia–controlled by river output, not by waves and tides. In: L. Giosan and J.P. Bhattacharya (Editors), River Deltas—Concepts, Models, and Examples
Special Publication 18, pp. 467–496.
Franke, D., Barckhausen, U., Heyde, I., Tingay, M. and Ramli, N., 2008. Seismic images of a collision zone offshore NW Sabah/Borneo. Marine and Petroleum Geology, 25: 606-624.
Galloway, W.E., 1975. Process framework for describing the morphologic and stratigraphic evolution of deltaic depositional systems. In: M.L. Broussard (Editor), Deltas: Models for Exploration. Houston Geological Society, Houston, USA, pp. 87–98.
Gani, M.R. and Bhattacharya, J.P., 2007. Basic building blocks and process variability of a Cretaceous delta: Internal facies architecture reveals a more dynamic interaction of river, wave, and tidal processes than is indicated by external shape. Journal of Sedimentary Research, 77: 284–302.
Gao, C. and Adcock, T.A., 2017. On the tidal resonance of the Bristol Channel. International Journal of Offshore and Polar Engineering, 27: 177-183.
Gardner, M.H., Cross, T.A., Levorsen, M., Chidsey, T., Adams, R. and Morris, T., 2004. Stacking patterns, sediment volume partitioning, and facies differentiation in shallow-marine and coastal-plain strata of the Cretaceous Ferron Sandstone, Utah. In: T.C. Chidsey, R.D. Adams and T.H. Morris (Editors), Regional to Wellbore Analog for Fluvial–Deltaic Reservoir Modeling: The Ferron Sandstone of Utah. American Association of Petroleum Geologists, Studies in Geology pp. 95–124.
Garrett, C., 1972. Tidal resonance in the Bay of Fundy and Gulf of Maine. Nature, 238: 441-443.
Geleynse, N., Storms, J.E.A., Walstra, D.-J.R., Jagers, H.R.A., Wang, Z.B. and Stive, M.J.F., 2011. Controls on river delta formation: insights from numerical modelling. Earth and Planetary Science Letters, 302: 217–226.
Geuzaine, C. and Remacle, J.F., 2009. Gmsh: A 3-D finite element mesh generator with built-in pre- and post-processing facilities. International Journal for Numerical Methods in Engineering, 79: 1309-1331.
Gil, J., García-Hidalgo, J., Segura, M., Garcia, A. and Carenas, B., 2006. Stratigraphic architecture, palaeogeography and sea-level changes of a third order depositional sequence: the late Turonian–early Coniacian in the northern Iberian Ranges and Central System (Spain). Sedimentary Geology, 191: 191-225.
Gingras, M.K. and MacEachern, J.A., 2012. Tidal ichnology of shallow-water clastic settings. In: R.A. Davis and R.W. Dalrymple (Editors), Principles of Tidal Sedimentology. Springer, New York, pp. 57-77.
Gingras, M.K., MacEachern, J.A. and Dashtgard, S.E., 2012. The potential of trace fossils as tidal indicators in bays and estuaries. Sedimentary Geology, 279: 97-106.
Godin, G., 1993. On tidal resonance. Continental Shelf Research, 13: 89-107.
Godin, G., 1999. The propagation of tides up rivers with special considerations on the upper Saint Lawrence River. Estuarine, Coastal and Shelf Science, 48: 307-324.
Golonka, J., 2004. Plate tectonic evolution of the southern margin of Eurasia in the Mesozoic and Cenozoic. Tectonophysics, 381: 235-273.
Golonka, J., 2007. Late Triassic and Early Jurassic palaeogeography of the world. Palaeogeography, Palaeoclimatology, Palaeoecology, 244: 297-307.
Golonka, J., Gahagan, L., Krobicki, M., Marko, F. and Oszczypko, N., 2006. Plate-tectonic evolution and paleogeography of the circum-Carpathian region. In: J. Golonka and F.J. Picha (Editors), The Carpathians and their Foreland: Geology and Hydrocarbon Resources. AAPG Memoir, pp. 11–46.
Gomis-Cartesio, L.E., Poyatos-Moré, M., Flint, S.S., Hodgson, D.M., Brunt, R.L. and Wickens, H.D., 2016. Anatomy of a mixed-influence shelf edge delta, Karoo Basin, South Africa. In: G.J. Hampson, A.D. Reynolds, B. Kostic and M.R. Wells (Editors), Sedimentology of Paralic

Reservoirs: Recent Advances. Special Publication 444. Geological Society of London, pp. SP444.5.
Goodbred, S.L. and Saito, Y., 2012. Tide-dominated deltas. In: R.A. Davis and R.W. Dalrymple (Editors), Principles of Tidal Sedimentology. Springer, New York, pp. 129-149.
Gordon, A.L., Huber, B.A., Metzger, E.J., Susanto, R.D., Hurlburt, H.E. and Adi, T.R., 2012. South China Sea throughflow impact on the Indonesian throughflow. Geophysical Research Letters, 39: 1-7.
Gorman, G.J., Piggott, M. and Pain, C.C., 2007. Shoreline approximation for unstructured mesh generation. Computers & geosciences, 33: 666-677.
Gorman, G.J., Piggott, M., Wells, M., Pain, C.C. and Allison, P., 2008. A systematic approach to unstructured mesh generation for ocean modelling using GMT and Terreno. Computers & Geosciences, 34: 1721-1731.
Greb, S.F. and Archer, A.W., 1995. Rhythmic sedimentation in a mixed tide and wave deposit, Hazel Patch sandstone (Pennsylvanian), eastern Kentucky coal field. Journal of Sedimentary Research, 65: 96-106.
Green, J. and Huber, M., 2013. Tidal dissipation in the early Eocene and implications for ocean mixing. Geophysical Research Letters, 40: 2707-2713.
Green, J.A.M., Huber, M., Waltham, D., Buzan, J. and Wells, M., 2017. Explicitly modelled deep-time tidal dissipation and its implication for Lunar history. Earth and Planetary Science Letters, 461: 46-53.
Grindrod, J., 1988. The palynology of Holocene mangrove and saltmarsh sediments, particularly in northern Australia. Review of Palaeobotany and Palynology, 55: 229-245.
Gugliotta, M., Flint, S.S., Hodgson, D.M. and Veiga, G.D., 2015. Stratigraphic record of river-dominated crevasse subdeltas with tidal influence (Lajas Formation, Argentina). Journal of Sedimentary Research, 85: 265–284.
Gugliotta, M., Flint, S.S., Hodgson, D.M. and Veiga, G.D., 2016a. Recognition criteria, characteristics and implications of the fluvial to marine transition zone in ancient deltaic deposits (Lajas Formation, Argentina). Sedimentology, 63: 1971–2001.
Gugliotta, M., Kurcinka, C.E., Dalrymple, R.W., Flint, S.S. and Hodgson, D.M., 2016b. Decoupling seasonal fluctuations in fluvial discharge from the tidal signature in ancient deltaic deposits: an example from the Neuquén Basin, Argentina. Journal of the Geological Society of London, 173: 94–107.
Gugliotta, M., Saito, Y., Nguyen, V.L., Oanh Ta, T.K. and Tamura, T., 2018. Sediment distribution and depositional processes along the fluvial to marine transition zone of the Mekong River delta, Vietnam. Sedimentology, Accepted; In Press.
Hadley, D.F., Arochukwu, F.C., Nishi, K., Sarginson, M.J., Salleh, H. and Omar, M., 2006. Depositional Modelling of Champion Field, Brunei, Society of Petroleum Engineers Asia Pacific Oil and Gas Conference and Exhibition. Society of Petroleum Engineers, Adelaide, Australia.
Hall, R., 1996. Reconstructing Cenozoic SE Asia. In: R. Hall and D. Blundell (Editors), Tectonic Evolution of Southeast Asia. Geological Society, London, Special Publications, London, UK, pp. 153-184.
Hall, R., 2002. Cenozoic geological and plate tectonic evolution of SE Asia and the SW Pacific: computer-based reconstructions, model and animations. Journal of Asian Earth Sciences, 20: 353-431.
Hall, R., 2013. The palaeogeography of Sundaland and Wallacea since the Late Jurassic. Journal of Limnology, 72: 1-17.
Hallam, A., 1981. Facies Interpretation and the Stratigraphic Record. W.H. Freeman, Oxford, 291 pp.
Hampson, G.J., 2016. Towards a sequence stratigraphic solution set for autogenic processes and allogenic controls: Upper Cretaceous strata, Book Cliffs, Utah, USA. Journal of the Geological Society, 173: 817-836.

Hampson, G.J., Rodriguez, A.B., Storms, J.E.A., Johnson, H.D. and Meyer, C.T., 2008. Geomorphology and High-Resolution Stratigraphy of Progradational Wave-Dominated Shoreline Deposits: Impact on Reservoir-Scale Facies Architecture. 117-142.

Hansen, C.D., MacEachern, J.A., Bann, K., Gingras, M. and Pemberton, S., 2007. Application of the asymmetric delta model to along-strike facies variations in a mixed wave-and river-influenced delta lobe, Upper Cretaceous Basal Belly River Formation, central Alberta. In: J.A. MacEachern, K.L. Bann, M.K. Gingras and S.G. Pemberton (Editors), Applied Ichnology. SEPM Short Course Notes 52. SEPM, Tulsa, Oklahoma, pp. 255–271.

Haq, B.U., 2014. Cretaceous eustasy revisited. Global and Planetary Change, 113: 44-58.

Harms, J.C., Southard, J.B. and Walker, R.G., 1982. Structures and Sequences in Clastic Rocks. Short Course 9. SEPM, Tulsa, Oklahoma, 249 pp.

Harris, P.T., Heap, A.D., Bryce, S.M., Porter-Smith, R., Ryan, D.A. and Heggie, D.T., 2002. Classification of Australian Clastic Coastal Depositional Environments Based Upon a Quantitative Analysis of Wave, Tidal, and River Power. Journal of Sedimentary Research, 72: 858-870.

Harris, P.T., Hughes, M.G., Baker, E.K., Dalrymple, R.W. and Keene, J.B., 2004. Sediment transport in distributary channels and its export to the pro-deltaic environment in a tidally dominated delta: Fly River, Papua New Guinea. Continental Shelf Research, 24: 2431-2454.

Hawkes, P., Fraser, A. and Einchcomb, C., 1998. The tectono-stratigraphic development and exploration history of the Weald and Wessex basins, Southern England, UK, Development, Evolution and Petroleum Geology of the Wessex Basin. Special Publications 133. Geological Society, London, pp. 39-65.

Hayes, M.O., 1975. Morphology of sand accumulations in estuaries: an introduction to the symposium. In. In: L.E. Cronin (Editor), Estuarine Research. Academic Press, New York, N.Y., pp. 3–22.

Hayes, M.O., 1979. Barrier island morphology as a function of tidal and wave regime. In: S.P. Leatherman (Editor), Barrier Islands. Academic Press, New York, pp. 1-27.

Hayes, M.O., 1980. General morphology and sediment patterns in tidal inlets. Sedimentary geology, 26: 139-156.

Heap, A.D., Bryce, S. and Ryan, D.A., 2004. Facies evolution of Holocene estuaries and deltas: a large-sample statistical study from Australia. Sedimentary Geology, 168: 1-17.

Hinz, K., Fritsch, J., Kempter, E., Mohammad, M.A.M., Meyer, J., Mohamed, M.D., Vosberg, D.G.H., Weber, D.I.J. and Benavidez, M.J., 1989. Thrust tectonics along the north-western continental margin of Sabah/Borneo. Geologische Rundschau, 78: 705-730.

Hiscott, R.N., 1994. Loss of capacity, not competence, as the fundamental process governing deposition from turbidity currents. Journal of Sedimentary Research, 64: 209-214.

Holgate, N.E., Jackson, C.A.L., Hampson, G.J. and Dreyer, T., 2013. Sedimentology and sequence stratigraphy of the Middle-Upper Jurassic Krossfjord and Fensfjord formations, Troll Field, northern North Sea. Petroleum Geoscience, 19: 237-258.

Honig, C. and Boyd, R., 1992. Estuarine sedimentation on the eastern shore of Nova Scotia. Journal of Sedimentary Research, 62: 569-583.

Hori, K. and Saito, Y., 2007. Classification, architecture, and evolution of large-river deltas. In: A. Gupta (Editor), Large rivers: geomorphology and management. John Wiley & Sons, Chichester, UK, pp. 75-96.

Hori, K., Saito, Y., Zhao, Q., Cheng, X., Wang, P., Sato, Y. and Li, C., 2001. Sedimentary facies of the tide-dominated paleo-Changjiang (Yangtze) estuary during the last transgression. Marine Geology, 177: 331-351.

Hori, K., Saito, Y., Zhao, Q. and Wang, P., 2002. Architecture and evolution of the tide-dominated Changjiang (Yangtze) River delta, China. Sedimentary Geology, 146: 249-264.

Hovikoski, J., Räsänen, M., Gingras, M., Ranzi, A. and Melo, J., 2008. Tidal and seasonal controls in the formation of Late Miocene inclined heterolithic stratification deposits, western Amazonian foreland basin. Sedimentology, 55: 499–530.

Hovius, N., 1998. Controls on sediment supply by large rivers. In: K.W. Shanley and P.J. McCabe (Editors), Relative Role of Eustasy, Climate and Tectonics in Continental Rocks SEPM Special Publication 59, pp. 3-16.

Howarth, M.J., 1982. Tidal currents of the continental shelf. In: A.H. Stride (Editor), Offshore Tidal Sands: Processes and Deposits. Chapman & Hall, London, pp. 10-26.

Hu, D., Wu, L., Cai, W., Gupta, A.S., Ganachaud, A., Qiu, B., Gordon, A.L., Lin, X., Chen, Z. and Hu, S., 2015. Pacific western boundary currents and their roles in climate. Nature, 522: 299–308.

Hubbard, S.M., Smith, D.G., Nielsen, H., Leckie, D.A., Fustic, M., Spencer, R.J. and Bloom, L., 2011. Seismic geomorphology and sedimentology of a tidally influenced river deposit, Lower Cretaceous Athabasca oil sands, Alberta, Canada. AAPG bulletin, 95: 1123-1145.

Hutchison, C.S., 2010. The North-West Borneo Trough. Marine Geology, 271: 32-43.

Ingram, G.M., Chisholm, T.J., Grant, C.J., Hedlund, C.A., Stuart-Smith, P. and Teasdale, J., 2004. Deepwater North West Borneo: hydrocarbon accumulation in an active fold and thrust belt. Marine and Petroleum Geology, 21: 879-887.

Jablonski, B.V.J. and Dalrymple, R.W., 2016. Recognition of strong seasonality and climatic cyclicity in an ancient, fluvially dominated, tidally influenced point bar: Middle McMurray Formation, Lower Steepbank River, north-eastern Alberta, Canada. Sedimentology, 63: 552–585.

James, N.P. and Dalrymple, R.W., 2010. Facies Models 4. Geological Association of Canada, 586 pp.

Jardine, E., 1997. Dual petroleum systems governing the prolific Pattani Basin, offshore Thailand. In: J.V.C. Howes and R.A. Noble (Editors), International Conference on Petroleum Systems of SE Asia and Australasia, Indonesian Petroleum Association, Jakarta, Indonesia, pp. 351-363.

Jerzykiewicz, T. and Wojewoda, J., 1986. The Radków and Szczeliniec sandstones: an example of giant foresets on a tectonically controlled shelf of the Bohemian Cretaceous Basin (Central Europe). In: J.R. Knight and J.R. McLean (Editors), Shelf Sands and Sandstones. Canadian Society of Petroleum Geologists, Memoir 11, pp. 1-15.

Johnson, H.D., 1975. Tide-and wave-dominated inshore and shoreline sequences from the late Precambrian, Finnmark, North Norway. Sedimentology, 22: 45-74.

Johnson, H.D. and Baldwin, C.T., 1996. Shallow Clastic Seas. In: H. Reading (Editor), Sedimentary Environments: processes, facies and stratigraphy. Blackwell Scientific Publications, Oxford, pp. 236-286.

Johnson, H.D. and Levell, B.K., 1995. Sedimentology of a transgressive, estuarine sand complex: the Lower Cretaceous Woburn Sands (Lower Greensand), southern England. In: A.G. Plint (Editor), Sedimentary Facies Analysis: a Tribute to the Research and Teaching of Harold G. Reading. IAS Special Publication 22. Blackwell Publishing Ltd., Oxford, UK, pp. 17-46.

Jouanneau, J.-M. and Latouche, C., 1981. The Gironde Estuary. Contributions to Sedimentology, 10. E. Sehweizerbart'sche Verlagsbuchhandlung, Stuttgart.

Klein, G.d., 1970a. Depositional and dispersal dynamics of intertidal sand bars. Journal of Sedimentary Research, 40: 1095-1127.

Klein, G.D., 1970b. Tidal origin of a Precambrian quartzite; the Lower Fine-grained quartzite (middle Dalradian) of Islay, Scotland. Journal of Sedimentary Research, 40: 973-985.

Klein, G.D., 1971. A sedimentary model for determining paleotidal range. Geological Society of America Bulletin, 82: 2585-2592.

Komar, P.D., 1987. Selective gravel entrainment and the empirical evaluation of flow competence. Sedimentology, 34: 1165-1176.

Kowalik, Z. and Luick, J., 2013. The Oceanography of Tides. University of Alaska Fairbanks, Fairbanks, Alaska, 157 pp.

Kreisa, R. and Moila, R., 1986. Sigmoidal tidal bundles and other tide-generated sedimentary structures of the Curtis Formation, Utah. Geological Society of America Bulletin, 97: 381-387.

Krystinik, L.F. and DeJarnett, B.B., 1995. Lateral variability of sequence stratigraphic framework in the Campanian and Lower Maastrichtian of the Western Interior Seaway. In: J.C. Van Wagoner and G.T. Bertram (Editors), Sequence Stratigraphy of Foreland Basin Deposits:

Outcrop and Subsurface Examples from the Cretaceous of North America. Memoir 64. AAPG, Tulsa, Oklahoma, pp. 11–26.
Kurcinka, C., Dalrymple, R.W. and Gugliotta, M., 2018. Facies and architecture of river-dominated to tide-influenced mouth bars in the lower Lajas Formation (Jurassic), Argentina. AAPG Bulletin, 102: 885-912.
Kvale, E.P., 2006. The origin of neap–spring tidal cycles. Marine Geology, 235: 5-18.
Kvale, E.P., 2012. Tidal constituents of modern and ancient tidal rhythmites: criteria for recognition and analyses. In: R.A. Davis and R.W. Dalrymple (Editors), Principles of Tidal Sedimentology. Springer, New York, pp. 1-17.
Kvale, E.P., Archer, A.W. and Johnson, H.R., 1989. Daily, monthly, and yearly tidal cycles within laminated siltstones of the Mansfield Formation (Pennsylvanian) of Indiana. Geology, 17: 365-368.
Lamb, M.P., Myrow, P.M., Lukens, C., Houck, K. and Strauss, J., 2008. Deposits from Wave-Influenced Turbidity Currents: Pennsylvanian Minturn Formation, Colorado, U.S.A. Journal of Sedimentary Research, 78: 480-498.
Lambiase, J.J., Damit, A.R., Simmons, M.D., Abdoerrias, R. and Hussin, A., 2003. A depositional model and the stratigraphic development of modern and ancient tide-dominated deltas in NW Borneo. In: F.H. Sidi, D. Nummedal, P. Imbert, H. Darman and H.W. Posamentier (Editors), Tropical Deltas of Southeast Asia—Sedimentology, Stratigraphy, and Petroleum Geology SEPM Spec. Publ., pp. 109–123.
Leckie, D.A. and Rumpel, T., 2003. Tide-influenced sedimentation in a rift basin—Cretaceous Qishn Formation, Masila Block, Yemen: A billion barrel oil field. AAPG Bulletin, 87: 987-1013.
Lee, T.-Y. and Lawver, L.A., 1995. Cenozoic plate reconstruction of Southeast Asia. Tectonophysics, 251: 85-138.
Leeder, M.R., 2011. Sedimentology and sedimentary basins: from turbulence to tectonics. Wiley-Blackwell, Oxford, UK, 784 pp.
Legler, B., Hampson, G.J., Jackson, C.A.L., Johnson, H.D., Massart, B.Y.G., Sarginson, M. and Ravnås, R., 2014. Facies relationships and stratigraphic architecture of distal, mixed tide- and wave-influenced deltaic deposits: Lower Sego Sandstone, Western Colorado, U.S.A. Journal of Sedimentary Research, 84: 605–625.
Legler, B., Johnson, H.D., Hampson, G.J., Massart, B.Y.G., Jackson, C.A.L., Jackson, M.D., El-Barkooky, A. and Ravnås, R., 2013. Facies model of a fine-grained, tide-dominated delta: Lower Dir Abu Lifa Member (Eocene), Western Desert, Egypt. Sedimentology, 60: 1313–1356.
Leonardi, N., Sun, T. and Fagherazzi, S., 2014. Modeling tidal bedding in distributary-mouth bars. Journal of Sedimentary Research, 84: 499-512.
Levell, B.K., 1980. A late Precambrian tidal shelf deposit, the Lower Sandfjord Formation, Finnmark, north Norway. Sedimentology, 27: 539-557.
Levell, B.K., Johnson, H.D., Collins, D.S. and Van Cappelle, M., 2020. Deposition and preservation of fluvio-tidal shallow-marine sandstones: A re-evaluation of the Neoproterozoic Jura Quartzite (western Scotland). Sedimentology, 67: 173-206.
Li, W., Bhattacharya, J.P., Zhu, Y., Garza, D. and Blankenship, E., 2011. Evaluating delta asymmetry using three-dimensional facies architecture and ichnological analysis, Ferron 'Notom Delta', Capital Reef, Utah, USA. Sedimentology, 58: 478-507.
Li, Z., Bhattacharya, J.P. and Schieber, J., 2015. Evaluating along-strike variation using thin-bedded facies analysis, Upper Cretaceous Ferron Notom Delta, Utah. Sedimentology, 62: 2060–2089.
Lockhart, B.E., Chinoroje, O., Enomoto, C.B. and Hollomon, G.A., 1997. Early Tertiary deposition in the southern Pattani Trough, Gulf of Thailand. In: P. Dheeradilok, C. Hinthong, P. Chaodumrong, P. Putthaphiban, W. Tansathien, C. Utha-aroon, N. Sattyarak, T. Nuchanong and S. Techawan (Editors), The International Conference on Stratigraphy and Tectonic Evolution of Southeast Asia and the South Pacific, Bangkok, Thailand, pp. 476-489.
Longhitano, S.G., Mellere, D., Steel, R.J. and Ainsworth, R.B., 2012. Tidal depositional systems in the rock record: A review and new insights. Sedimentary Geology, 279: 2-22.

Longhitano, S.G., Sabato, L., Tropeano, M. and Gallicchio, S., 2010. A mixed bioclastic–siliciclastic flood-tidal delta in a micro tidal setting: depositional architectures and hierarchical internal organization (Pliocene, Southern Apennine, Italy). Journal of Sedimentary Research, 80: 36-53.

Longhitano, S.G. and Steel, R.J., 2017. Deflection of the progradational axis and asymmetry in tidal seaway and strait deltas: insights from two outcrop case studies. In: G.J. Hampson, A.D. Reynolds, B. Kostic and M.R. Wells (Editors), Sedimentology of Paralic Reservoirs: Recent Advances

Special Publication 444, Geological Society of London

pp. 141-172.

MacEachern, J.A. and Bann, K.L., 2008. The role of ichnology in refining shallow marine facies models. In: G.J. Hampson, R.J. Steel, P.M. Burgess and R.W. Dalrymple (Editors), Recent Advances in Models of Siliciclastic Shallow-Marine Stratigraphy. SEPM Spec. Publ., pp. 73–116.

MacEachern, J.A., Bann, K.L., Bhattacharya, J.P. and Howell, C.D., 2005. Ichnology of deltas: organism responses to the dynamic interplay of rivers, waves, storms, and tides. In: L. Giosan and J.P. Bhattacharya (Editors), River Deltas—Concepts, Models, and Examples. SEPM Special Publication. SEPM, pp. 45-85.

MacMillan, D.H., 1966. Tides. American Elsevier Publishing Company, New York, 240 pp.

Markwick, P.J. and Valdes, P.J., 2004. Palaeo-digital elevation models for use as boundary conditions in coupled ocean–atmosphere GCM experiments: a Maastrichtian (late Cretaceous) example. Palaeogeography Palaeoclimatology Palaeoecology, 213: 37-63.

Martel, A.T., Allen, P.A. and Slingerland, R., 1994. Use of tidal-circulation modeling in paleogeographical studies: an example from the Tertiary of the Alpine perimeter. Geology, 22: 925-928.

Martinius, A.W. and Gowland, S., 2011. Tide-influenced fluvial bedforms and tidal bore deposits (late Jurassic Lourinhã Formation, Lusitanian Basin, Western Portugal). Sedimentology, 58: 285–324.

Martinius, A.W., Jablonski, B.V.J., Fustic, M., Strobl, R. and van den Berg, J.H., 2015. Fluvial to tidal transition zone facies in the McMurray Formation (Christina River, Alberta, Canada), with emphasis on the reflection of flow intensity in bottomset architecture. In: P.J. Ashworth, J.L. Best and D.R. Parsons (Editors), Fluvial–Tidal Sedimentology. Developments in Sedimentology. Elsevier, pp. 445–480.

Martinius, A.W. and van den Berg, J.H., 2011. Atlas of sedimentary structures in estuarine and tidally-influenced river deposits of the Rhine-Meuse-Scheldt system. EAGE Publications BV, Houten, 298 pp.

Maselli, V., Normandeau, A., Nones, M., Tesi, T., Langone, L., Trincardi, F. and Bohacs, K.M., 2020. Tidal modulation of river-flood deposits: How low can you go? Geology, 48: 663–667.

McCabe, P.J. and Jones, C.M., 1977. Formation of reactivation surfaces within superimposed deltas and bedforms. Journal of Sedimentary Research, 47: 707-715.

McIlroy, D., 2006. Ichnology of a macrotidal tide-dominated deltaic depositional system: Lajas Formation, Neuquén Province, Argentina. In: R. Bromley, L.A. Buatois, J. Genise, M.G. Mángano and R. Melchor (Editors), Sediment–Organism Interactions: A Multifaceted Ichnology. Special Publication 88. SEPM, Tulsa, Oklahoma, pp. 195–211.

McIlroy, D., 2007. Lateral variability in shallow marine ichnofabrics: implications for the ichnofabric analysis method. Journal of the Geological Society, 164: 359-369.

Middleton, G.V., 1965. Primary sedimentary structures and their hydrodynamic interpretation, 12. SEPM Special Publication 265 pp.

Miller, K.G., Kominz, M.A., Browning, J.V., Wright, J.D., Mountain, G.S., Katz, M.E., Sugarman, P.J., Cramer, B.S., Christie-Blick, N. and Pekar, S.F., 2005. The Phanerozoic record of global sea-level change. Science, 310: 1293-1298.

Miller, K.G., Mountain, G.S., Wright, J.D. and Browning, J.V., 2011. A 180-Million-Year Record of Sea Level and Ice Volume Variations from Continental Margin and Deep-Sea Isotopic Records. Oceanography, 24: 40-53.

Milliman, J.D. and Farnsworth, K.L., 2011. River discharge to the coastal ocean: a global synthesis. Cambridge University Press, Cambridge, UK, 381 pp.

Milliman, J.D. and Syvitski, J.P., 1992. Geomorphic/tectonic control of sediment discharge to the ocean: the importance of small mountainous rivers. The Journal of Geology, 100: 525-544.

Mitchell, A.J., Allison, P.A., Gorman, G.J., Piggott, M.D. and Pain, C.C., 2011. Tidal circulation in an ancient epicontinental sea: The Early Jurassic Laurasian Seaway. Geology, 39: 207-210.

Mitchell, A.J., Uličný, D., Hampson, G.J., Allison, P.A., Gorman, G.J., Piggott, M.D., Wells, M.R. and Pain, C.C., 2010. Modelling tidal current-induced bed shear stress and palaeocirculation in an epicontinental seaway: the Bohemian Cretaceous Basin, Central Europe. Sedimentology, 57: 359-388.

Morley, C.K., 2016. Major unconformities/termination of extension events and associated surfaces in the South China Seas: Review and implications for tectonic development. Journal of Asian Earth Sciences, 120: 62-86.

Morley, R.J., Swiecicki, T. and Pham, D.T.T., 2011. A sequence stratigraphic framework for the Sunda region, based on integration of biostratigraphic, lithological and seismic data from Nam Con Son basin, Vietnam, Indonesian Petroleum Association 35th Annual Convention, Jakarta, Indonesia, pp. IPA11-G-002.

Mulhern, J.S., Johnson, C.L. and Martin, J.M., 2017. Is barrier island morphology a function of tidal and wave regime? Marine Geology, 387: 74-84.

Murtaza, M., Rahman, A.H.A., Sum, C.W. and Konjing, Z., 2018. Facies associations, depositional environments and stratigraphic framework of the Early Miocene–Pleistocene successions of the Mukah–Balingian Area, Sarawak, Malaysia. Journal of Asian Earth Sciences, 152: 23-38.

Muto, T. and Steel, R.J., 1997. Principles of regression and transgression: the nature of the interplay between accommodation and sediment supply. Journal of Sedimentary Research, 67: 994-1000.

Mutti, E., Allen, G. and Rosell, J., 1984. Sigmoidal cross stratification and sigmoidal bars: depositional features diagnostic of tidal sandstones, 5th IAS European Regional Meeting, Marsiglia, pp. 312-313.

Mutti, E., Rosell, J., Allen, G., Fonnesu, F. and Sgavetti, M., 1985. The Eocene Baronia tide dominated delta-shelf system in the Ager Basin. In: M.D. Mila and J. Rosell (Editors), Excursion guidebook: 6th International Association of Sedimentologists European Regional Meeting. International Association of Sedimentologists, Lleida, Spain, pp. 579-600.

Myrow, P.M., Fischer, W. and Goodge, J.W., 2002. Wave-modified turbidites: combined-flow shoreline and shelf deposits, Cambrian, Antarctica. Journal of Sedimentary Research, 72: 641-656.

Myrow, P.M. and Southard, J.B., 1996. Tempestite deposition. Journal of Sedimentary Research, 66: 992-1007.

Nahon, A., Bertin, X., Fortunato, A.B. and Oliveira, A., 2012. Process-based 2DH morphodynamic modeling of tidal inlets: A comparison with empirical classifications and theories. Marine Geology, 291: 1-11.

Nanson, R.A., Vakarelov, B.K., Ainsworth, R.B., Williams, F.M. and Price, D.M., 2013. Evolution of a Holocene, mixed-process, forced regressive shoreline: the Mitchell River delta, Queensland, Australia. Marine Geology, 339: 22-43.

Narayan, J., 1971. Sedimentary structures in the lower Greensand of the Weald, England, and Bas-Boulonnais, France. Sedimentary Geology, 6: 73-109.

Nguyen, V.L., Ta, T.K.O. and Tateishi, M., 2000. Late Holocene depositional environments and coastal evolution of the Mekong River Delta, Southern Vietnam. Journal of Asian Earth Sciences, 18: 427-439.

Nio, S.-D. and Yang, C.-S., 1991. Diagnostic attributes of clastic tidal deposits: a review. In: D. Smith, G.G.E. Reinson, B.A. Zaitlin and R.A. Rahmani (Editors), Clastic Tidal Sedimentology. Canadian Society of Petroleum Geologists, Memoir 16, pp. 3-27.

Nio, S., Siegenthaler, C. and Yang, C., 1983. Megaripple cross-bedding as a tool for the reconstruction of the paleo-hydraulics in a Holocene subtidal environment, SW Netherlands. Geologie en Mijnbouw, 62: 499-510.

Nyberg, B. and Howell, J.A., 2015. Is the present the key to the past? A global characterization of modern sedimentary basins. Geology, 43: 643-646.

Nyberg, B. and Howell, J.A., 2016. Global distribution of modern shallow marine shorelines. Implications for exploration and reservoir analogue studies. Marine and Petroleum Geology, 71: 83-104.

O'Reilly, C.T., Solvason, R. and Solomon, C., 2005. Where are the world's largest tides? In: J. Ryan (Editor), BIO Annual Report "2004 in Review", Washington, D. C., pp. 44–46.

Obradovich, J.D., 1993. A Cretaceous time scale. In: W.G.E. Caldwell and E.G. Kauffman (Editors), Evolution of the Western Interior Basin. Geological Association of Canada, Special Paper 39, St. John's, Newfoundland, pp. 379-396.

Off, T., 1963. Rhythmic linear sand bodies caused by tidal currents. AAPG Bulletin, 47: 324-341.

Ogg, J.G., Agterberg, F.P. and Gradstein, F.M., 2004. The Cretaceous period. In: G. F.M., O. J.G. and S. A.G (Editors), A Geologic Time Scale 2004. Cambridge University Press, Cambridge, pp. 344-383.

Olabarrieta, M., Geyer, W.R., Coco, G., Friedrichs, C.T. and Cao, Z., 2018. Effects of density-driven flows on the long-term morphodynamic evolution of funnel-shaped estuaries. Journal of Geophysical Research: Earth Surface, 123: 2901-2924.

Olson, W.S., 1972. Sedimentary Model for Determining Paleotidal Range: Discussion. Geological Society of America Bulletin, 83: 537-538.

Open University Course Team, 1999. Waves, Tides and Shallow-water Processes: Second Edition. Butterworth-Heinemann, Oxford, UK, 227 pp.

Orton, G.J. and Reading, H.G., 1993. Variability of deltaic processes in terms of sediment supply, with particular emphasis on grain size. Sedimentology, 40: 475-512.

Pain, C.C., Piggott, M.D., Goddard, A.J.H., Fang, F., Gorman, G.J., Marshall, D.P., Eaton, M.D., Power, P.W. and De Oliveira, C.R.E., 2005. Three-dimensional unstructured mesh ocean modelling. Ocean Modelling, 10: 5-33.

Partington, M., Copestake, P., Mitchener, B.a. and Underhill, J.R., 1993a. Biostratigraphic calibration of genetic stratigraphic sequences in the Jurassic–lowermost Cretaceous (Hettangian to Ryazanian) of the North Sea and adjacent areas, Geological Society, London, Petroleum Geology Conference Series. Geological Society of London, pp. 371-386.

Partington, M., Mitchener, B., Milton, N. and Fraser, A., 1993b. Genetic sequence stratigraphy for the North Sea Late Jurassic and Early Cretaceous: distribution and prediction of Kimmeridgian–Late Ryazanian reservoirs in the North Sea and adjacent areas, Geological Society, London, Petroleum Geology Conference series. Geological Society of London, pp. 347-370.

Peng, Y., Steel, R.J., Rossi, V.M. and Olariu, C., 2018. Mixed-energy process interactions read from a compound-clinoform delta (paleo–Orinoco Delta, Trinidad): preservation of river and tide signals by mud-induced wave damping. Journal of Sedimentary Research, 88: 75-90.

Perillo, M.M., Best, J.L. and Garcia, M.H., 2014. A new phase diagram for combined-flow bedforms. Journal of Sedimentary Research, 84: 301-313.

Piggott, M.D., Gorman, G.J., Pain, C.C., Allison, P.A., Candy, A.S., Martin, B.T. and Wells, M.R., 2008. A new computational framework for multi-scale ocean modelling based on adapting unstructured meshes. International Journal for Numerical Methods in Fluids, 56: 1003-1015.

Piper, D.J., Kontopoulos, N., Anagnostou, C., Chronis, G. and Panagos, A., 1990. Modern fan deltas in the western Gulf of Corinth, Greece. Geo-Marine Letters, 10: 5-12.

Posamentier, H.W. and Walker, R.G. (Editors), 2006. Facies models revisited. SEPM Special Publication 84.

Proudman, J., 1953. Dynamical Oceanography. Methuen-John Wiley, London, 409 pp.

Pugh, D. and Woodworth, P., 2014. Sea-level science: understanding tides, surges, tsunamis and mean sea-level changes. Cambridge University Press, Cambridge, UK, 407 pp.
Pugh, D.T., 1987. Tides, surges and mean sea-level: a handbook for engineers and scientists. John Wiley & Sons, Chichester, UK, 472 pp.
Rawson, P.F., 2006. Cretaceous: sea levels peak as the North Atlantic opens, The Geology of England and Wales, 2nd Edition. Geological Society, London, London, UK, pp. 365-393.
Reading, H.G., 1978. Sedimentary Environments and Facies, 60. Blackwell Scientific Publications, Oxford, 557 pp.
Reading, H.G., 1996. Sedimentary environments: processes, facies and stratigraphy. Blackwell Publishing Ltd, Oxford, U.K., 615 pp.
Reading, H.G. and Collinson, J.D., 1996. Clastic coasts. In: H.G. Reading (Editor), Sedimentary Environments; Processes, Facies and Stratigraphy. Blackwell Science Ltd, Oxford, UK, pp. 154–231.
Redfield, A.C., 1958. The influence of the continental shelf on the tides of the Atlantic coast of the United States. Journal of Marine Research, 17: 432-448.
Reineck, H.-E., 1963. Sedimentgefüge im Bereich der südlichen Nordsee. Senckenbergische Naturforschende Gesellschaft, Abhandlungen, 505: 1–138.
Reineck, H.-E. and Singh, I.B., 1980. Depositional Sedimentary Environments: With Reference to Terrigenous Clastics. Springer, Berlin, 549 pp.
Reineck, H.-E. and Wunderlich, F., 1968. Classification and Origin of Flaser and Lenticular Bedding. Sedimentology, 11: 99-104.
Reynaud, J.-Y. and Dalrymple, R.W., 2012. Shallow-marine tidal deposits. In: R.A. Davies Jr. and R.W. Dalrymple (Editors), Principles of Tidal Sedimentology. Springer, New York, pp. 335-369.
Ridd, M.F., Barber, A.J. and Crow, M.J., 2011. The Geology of Thailand. Geological Society of London, London, UK, 626 pp.
Robinson, A., 1966. Residual currents in relation to shoreline evolution of the East Anglian coast. Marine Geology, 4: 57-84.
Rodriguez, A.B., Hamilton, M.D. and Anderson, J.B., 2000. Facies and evolution of the modern Brazos Delta, Texas: wave versus flood influence. Journal of Sedimentary Research, 70: 283-295.
Rossi, V.M., Kim, W., Leva López, J., Edmonds, D., Geleynse, N., Olariu, C., Steel, R.J., Hiatt, M. and Passalacqua, P., 2016. Impact of tidal currents on delta-channel deepening, stratigraphic architecture, and sediment bypass beyond the shoreline. Geology, 44: 927-930.
Rossi, V.M., Longhitano, S.G., Mellere, D., Dalrymple, R.W., Steel, R.J., Chiarella, D. and Olariu, C., 2017a. Interplay of tidal and fluvial processes in an early Pleistocene, delta-fed, strait margin (Calabria, Southern Italy). Marine and Petroleum Geology, In Press, Accepted Article.
Rossi, V.M., Perillo, M.M., Steel, R.J. and Olariu, C., 2017b. Quantifying mixed-process variability in shallow-marine depositional systems: What are sedimentary structures really telling us? Journal of Sedimentary Research, 87: 1060-1074.
Rossi, V.M. and Steel, R.J., 2016. The role of tidal, wave and river currents in the evolution of mixed-energy deltas: Example from the Lajas Formation (Argentina). Sedimentology, 63: 824–864.
Roy, P., Thom, B. and Wright, L., 1980. Holocene sequences on an embayed high-energy coast: an evolutionary model. Sedimentary Geology, 26: 1-19.
Roy, P., Williams, R., Jones, A., Yassini, I., Gibbs, P., Coates, B., West, R., Scanes, P., Hudson, J. and Nichol, S., 2001. Structure and function of south-east Australian estuaries. Estuarine, Coastal and Shelf Science, 53: 351-384.
Rubin, D.M. and McCulloch, D.S., 1980. Single and superimposed bedforms: a synthesis of San Francisco Bay and flume observations. Sedimentary Geology, 26: 207-231.
Ruffell, A.H. and Wach, G.D., 1991. Sequence stratigraphic analysis of the Aptian-Albian Lower Greensand in southern England. Marine and Petroleum Geology, 8: 341-353.

Salahuddin and Lambiase, J.J., 2013. Sediment Dynamics and Depositional Systems of the Mahakam Delta, Indonesia: Ongoing Delta Abandonment On A Tide-Dominated Coast. Journal of Sedimentary Research, 83: 503–521.

Sames, B., Wagreich, M., Wendler, J., Haq, B., Conrad, C., Melinte-Dobrinescu, M., Hu, X., Wendler, I., Wolfgring, E. and Yilmaz, I., 2016. Short-term sea-level changes in a greenhouse world—A view from the Cretaceous. Palaeogeography, Palaeoclimatology, Palaeoecology, 441: 393-411.

Sandal, S.T., 1996. The Geology and Hydrocarbon Resources of Negara Brunei Darussalam. Brunei Shell Petroleum Company, Brunei Museum, Bandar Seri Begawan, Brunei Darussalam, 243 pp.

Shaw, D.P., 1964. Time in Stratigraphy. McGraw Hill, New York, 365 pp.

Shoup, R.C., Morley, R.J., Swiecicki, T. and Clark, S., 2013. Tectono-stratigraphic Framework and Tertiary Paleogeogeography of Southeast Asia; Gulf of Thailand to South Vietnam Shelf. Houston Geological Society Bulletin, 55: 27-39.

Shum, C., Woodworth, P., Andersen, O., Egbert, G.D., Francis, O., King, C., Klosko, S., Le Provost, C., Li, X. and Molines, J.M., 1997. Accuracy assessment of recent ocean tide models. Journal of geophysical research: oceans, 102: 25173-25194.

Sisulak, C.F. and Dashtgard, S.E., 2012. Seasonal Controls On the Development And Character of Inclined Heterolithic Stratification In A Tide-Influenced, Fluvially Dominated Channel: Fraser River, Canada. Journal of Sedimentary Research, 82: 244–257.

Sixsmith, P.J., Hampson, G.J., Gupta, S., Johnson, H.D. and Fontana, J.F., 2008. Facies architecture of a net transgressive sandstone reservoir analog: The Cretaceous Hosta Tongue, New Mexico. AAPG Bulletin, 92: 513-547.

Slater, R.D., 1985. A numerical model of tides in the Cretaceous Seaway of North America. The Journal of Geology, 93: 333-345.

Slingerland, R., 1986. Numerical computation of co-oscillating palaeotides in the Catskill epeiric Sea of eastern North America. Sedimentology, 33: 487-497.

Smith, D.G., 1988. Tidal bundles and mud couplets in the McMurray Formation, northeastern Alberta, Canada. Bulletin of Canadian Petroleum Geology, 36: 216-219.

Sømme, T.O., Helland-Hansen, W., Martinsen, O.J. and Thurmond, J.B., 2009. Relationships between morphological and sedimentological parameters in source-to-sink systems: a basis for predicting semi-quantitative characteristics in subsurface systems. Basin Research, 21: 361-387.

Sondi, I., Juračić, M. and Pravdić, V., 1995. Sedimentation in a disequilibrium river-dominated estuary: the Raša River Estuary (Adriatic Sea, Croatia). Sedimentology, 42: 769-782.

Southard, J.B. and Boguchwal, L.A., 1990. Bed configurations in steady unidirectional water flows. Part 2. Synthesis of flume data. Journal of Sedimentary Research, 60.

Stammer, D., Ray, R.D., Andersen, O.B., Arbic, B.K., Bosch, W., Carrère, L., Cheng, Y., Chinn, D.S., Dushaw, B.D., Egbert, G.D., Erofeeva, S.Y., Fok, H.S., Green, J.A.M., Griffiths, S., King, M.A., Lapin, V., Lemoine, F.G., Luthcke, S.B., Lyard, F., Morison, J., Müller, M., Padman, L., Richman, J.G., Shriver, J.F., Shum, C.K., Taguchi, E. and Yi, Y., 2014. Accuracy assessment of global barotropic ocean tide models. Reviews of Geophysics, 52: 243-282.

Stride, A.H., 1973. Sediment transport by the North Sea. In: E.D. Goldberg (Editor), North Sea Science. MIT Press, Cambridge, MA, pp. 101-130.

Stride, A.H., 1982. Offshore tidal sands: processes and deposits. Chapman & Hall, London, 222 pp.

Syvitski, J.P. and Milliman, J.D., 2007. Geology, geography, and humans battle for dominance over the delivery of fluvial sediment to the coastal ocean. The Journal of Geology, 115: 1-19.

Syvitski, J.P., Peckham, S.D., Hilberman, R. and Mulder, T., 2003. Predicting the terrestrial flux of sediment to the global ocean: a planetary perspective. Sedimentary Geology, 162: 5-24.

Ta, T.K.O., Nguyen, V.L., Tateishi, M., Kobayashi, I., Saito, Y. and Nakamura, T., 2002a. Sediment facies and Late Holocene progradation of the Mekong River Delta in Bentre Province,

southern Vietnam: an example of evolution from a tide-dominated to a tide- and wave-dominated delta. Sedimentary Geology, 152: 313-325.
Ta, T.K.O., Nguyen, V.L., Tateishi, M., Kobayashi, I., Tanabe, S. and Saito, Y., 2002b. Holocene delta evolution and sediment discharge of the Mekong River, southern Vietnam. Quaternary Science Reviews, 21: 1807-1819.
Terwindt, J. and Breusers, H., 1972. Experiments on the origin of flaser, lenticular and sand-clay alternating bedding. Sedimentology, 19: 85-98.
Terwindt, J.H., 1971. Litho-facies of inshore estuarine and tidal-inlet deposits. Geologie en Mijnbouw, 50: 515-526.
Thomas, R.G., Smith, D.G., Wood, J.M., Visser, J., Calverley-Range, E.A. and Koster, E.H., 1987. Inclined heterolithic stratification—terminology, description, interpretation and significance. Sedimentary Geology, 53: 123–179.
Tin, N.T. and Ty, N.D., 1995. Petroleum geology of the Nam Con Son Basin. Bulletin of the Geological Society of Malaysia, 37: 1-11.
Tinterri, R., 2011. Combined flow sedimentary structures and the genetic link between sigmoidal-and hummocky-cross stratification. GeoActa, 10: 1–43.
Togunwa, O.S., Abdullah, W.H., Hakimi, M.H. and Barbeito, P.J., 2018. Organic geochemical and petrographic characteristics of Neogene organic-rich sediments from the onshore West Baram Delta Province, Sarawak Basin: Implications for source rocks and hydrocarbon generation potential. Marine and Petroleum Geology, 63: 115-126.
Tomašových, A. and Kidwell, S.M., 2017. Nineteenth-century collapse of a benthic marine ecosystem on the open continental shelf. Proceedings of the Royal Society B: Biological Sciences, 284: 20170328.
Townend, I., 2012. The estimation of estuary dimensions using a simplified form model and the exogenous controls. Earth Surface Processes and Landforms, 37: 1573-1583.
Uehara, K., Scourse, J.D., Horsburgh, K.J., Lambeck, K. and Purcell, A.P., 2006. Tidal evolution of the northwest European shelf seas from the Last Glacial Maximum to the present. Journal of Geophysical Research: Oceans, 111: C09025.
Uličný, D., 2001. Depositional systems and sequence stratigraphy of coarse-grained deltas in a shallow-marine, strike-slip setting: the Bohemian Cretaceous Basin, Czech Republic. Sedimentology, 48: 599-628.
Uličný, D., Laurin, J. and Čech, S., 2009. Controls on clastic sequence geometries in a shallow-marine, transtensional basin: the Bohemian Cretaceous Basin, Czech Republic. Sedimentology, 56: 1077-1114.
Vakarelov, B.K. and Ainsworth, R.B., 2013. A hierarchical approach to architectural classification in marginal-marine systems: Bridging the gap between sedimentology and sequence stratigraphy. AAPG Bulletin, 97: 1121–1161.
Vakarelov, B.K., Ainsworth, R.B. and MacEachern, J.A., 2012. Recognition of wave-dominated, tide-influenced shoreline systems in the rock record: Variations from a microtidal shoreline model. Sedimentary Geology, 279: 23-41.
van Cappelle, M., Hampson, G.J. and Johnson, H.D., 2018. Spatial and Temporal Evolution of Coastal Depositional Systems and Regional Depositional Process Regimes: Campanian Western Interior Seaway, USA. Journal of Sedimentary Research, 88: 873-897.
van Cappelle, M., Stukins, S., Hampson, G.J. and Johnson, H.D., 2016. Fluvial to tidal transition in proximal, mixed tide-influenced and wave-influenced deltaic deposits: Cretaceous lower Sego Sandstone, Utah, USA. Sedimentology, 63: 1333–1361.
van den Berg, J.H., Boersma, J.R. and Gelder, A.v., 2007. Diagnostic sedimentary structures of the fluvial-tidal transition zone–Evidence from deposits of the Rhine and Meuse. Netherlands Journal of Geosciences/Geologie en Mijnbouw, 86: 287–306.
Van der Wegen, M. and Roelvink, J., 2008. Long-term morphodynamic evolution of a tidal embayment using a two-dimensional, process-based model. Journal of Geophysical Research: Oceans, 113.

van Hattum, M.W.A., Hall, R., Pickard, A.L. and Nichols, G.J., 2006. Southeast Asian sediments not from Asia: Provenance and geochronology of north Borneo sandstones. Geology, 34: 589.

Van Straaten, L., 1953. Megaripples in the Dutch Wadden Sea and in the basin of Arcachon (France). Geol. Mijnbouw, 15: 1-11.

van Vliet, A. and Schwander, M.M., 1987. Stratigraphic interpretation of a regional seismic section across the Labuan syncline and its flank structures, Sabah, North Borneo. In: A.W. Bailey (Editor), Atlas of Seismic Stratigraphy. AAPG Studies in Geology 27, pp. 163-167.

Van Wagoner, J.C., Mitchum, R.M., Campion, K.M. and Rahmanian, V.D., 1990. Siliciclastic Sequence Stratigraphy in Well Logs, Cores, and Outcrops: Concepts for High-Resolution Correlation of Time and Facies. Methods in Exploration, 7. AAPG, 55 pp.

Van Yperen, A.E., Poyatos-Moré, M., Holbrook, J.M. and Midtkandal, I., 2020. Internal mouth-bar variability and preservation of subordinate coastal processes in low-accommodation proximal deltaic settings (Cretaceous Dakota Group, New Mexico, USA). The Depositional Record.

Vaucher, R., Pittet, B., Hormière, H., Martin, E.L. and Lefebvre, B., 2016. A wave-dominated, tide-modulated model for the Lower Ordovician of the Anti-Atlas, Morocco. Sedimentology, 64: 777-807.

Visser, M.J., 1980. Neap-spring cycles reflected in Holocene subtidal large-scale bedform deposits: a preliminary note. Geology, 8: 543-546.

Voigt, T. and Tröger, K., 1996. Sea-level changes during Late Cenomanian and early Turonian in the Saxonian Cretaceous Basin. Mitteilungen aus dem Geologisch-Paläontologischen Institut der Universität Hamburg, 77: 275-290.

Walker, R.G. and James, N.P., 1992. Facies Models: Response to Sea Level Change. Geotext, 1. Geological Association of Canada, 409 pp.

Walker, R.G. and Plint, A.G., 1992. Wave-and storm-dominated shallow marine systems. In: R.G. Walker and N.P. James (Editors), Facies Models: Response to Sea-Level Change. Geological Association of Canada, St. John's, Newfoundland, pp. 219-238.

Wei, X., Steel, R.J., Ravnås, R., Jiang, Z., O'ariu, C. and Li, Z., 2016. Variability of tidal signals in the Brent Delta Front: New observations on the Rannoch Formation, northern North Sea. Sedimentary Geology, 335: 166-179.

Wells, M.R., 2008. Tidal modelling of modern and ancient seas and oceans, Imperial College London, 527 pp.

Wells, M.R., Allison, P.A., Hampson, G.J., Piggott, M.D. and Pain, C.C., 2005a. Modelling ancient tides: the Upper Carboniferous epi-continental seaway of Northwest Europe. Sedimentology, 52: 715-735.

Wells, M.R., Allison, P.A., Piggott, M.D., Gorman, G.J., Hampson, G.J., Pain, C.C. and Fang, F., 2007. Numerical Modeling of Tides in the Late Pennsylvanian Midcontinent Seaway of North America with Implications for Hydrography and Sedimentation. Journal of Sedimentary Research, 77: 843-865.

Wells, M.R., Allison, P.A., Piggott, M.D., Hampson, G.J., Pain, C.C. and Gorman, G.J., 2010a. Tidal Modeling of an Ancient Tide-Dominated Seaway, Part 1: Model Validation and Application to Global Early Cretaceous (Aptian) Tides. Journal of Sedimentary Research, 80: 393-410.

Wells, M.R., Allison, P.A., Piggott, M.D., Hampson, G.J., Pain, C.C. and Gorman, G.J., 2010b. Tidal Modeling of an Ancient Tide-Dominated Seaway, Part 2: The Aptian Lower Greensand Seaway of Northwest Europe. Journal of Sedimentary Research, 80: 411-439.

Wells, M.R., Allison, P.A., Piggott, M.D., Pain, C.C., Hampson, G.J. and De Oliveira, C.R., 2005b. Large sea, small tides: the Late Carboniferous seaway of NW Europe. Journal of the Geological Society, 162: 417-420.

Willis, B.J., 2005. Deposits of tide-influenced river deltas. In: L. Giosan and J.P. Bhattacharya (Editors), River Deltas—Concepts, Models, and Examples. SEPM Special Publication, pp. 87–129.

Willis, B.J. and Fitris, F., 2012. Sequence Stratigraphy of Miocene Tide-Influenced Sandstones In the Minas Field, Sumatra, Indonesia. Journal of Sedimentary Research, 82: 400-421.

Willis, B.J. and Gabel, S., 2001. Sharp-based, tide-dominated deltas of the Sego Sandstone, Book Cliffs, Utah, USA. Sedimentology, 48: 479–506.

Wilmes, S.-B. and Green, J.A.M., 2014. The evolution of tides and tidal dissipation over the past 21,000 years. Journal of Geophysical Research: Oceans, 119: 4083-4100.

Wolanski, E.E.J., Mazda, Y.Y. and Ridd, P.P.V., 1992. Mangrove hydrodynamics. In: A.I. Robertson and D.M. Alongi (Editors), Tropical Mangrove Ecosystems. Coastal and Estuarine Studies. American Geophysical Union, Washington, DC, pp. 43–62.

Wonham, J.P. and Elliott, T., 1996. High-resolution sequence stratigraphy of a mid-Cretaceous estuarine complex: the Woburn Sands of the Leighton Buzzard area, southern England. In: S.P. Hesselbo and D.N. Parkingson (Editors), Sequence Stratigraphy in the British Isles. Special Publications 103. Geological Society, London, pp. 41-62.

Woodroffe, C.D., Rogers, K., McKee, K.L., Lovelock, C.E., Mendelssohn, I.A. and Saintilan, N., 2016. Mangrove sedimentation and response to relative sea-level rise. Annual Review of Marine Science, 8: 243-66.

Yang, B., Gingras, M.K., Pemberton, S.G. and Dalrymple, R.W., 2008. Wave-generated tidal bundles as an indicator of wave-dominated tidal flats. Geology, 36: 39.

Yang, C.S. and Nio, S.D., 1985. The estimation of palaeohydrodynamic processes from subtidal deposits using time series analysis methods. Sedimentology, 32: 41-57.

Yoshida, S., Johnson, H.D., Pye, K. and Dixon, R.J., 2004. Transgressive changes from tidal estuarine to marine embayment depositional systems: The Lower Cretaceous Woburn Sands of southern England and comparison with Holocene analogs. AAPG Bulletin, 88: 1433-1460.

Yoshida, S., Steel, R.J. and Dalrymple, R.W., 2007. Changes in depositional processes—an ingredient in a new generation of sequence-stratigraphic models. Journal of Sedimentary Research, 77: 447-460.

Zheng, W. and Deng, H., 2012. The Tidal Sandstone Characteristic of the Zhuhai Formation, Huizhou Oil Field, Pearl River Mouth Basin, South China Sea. Petroleum Science and Technology, 30: 567-574.

Zhou, Z., Chen, L., Tao, J., Gong, Z., Guo, L., van der Wegen, M., Townend, I. and Zhang, C., 2020. The role of salinity in fluvio-deltaic morphodynamics: A long-term modelling study. Earth Surface Processes and Landforms, 45: 590-604.

Zhou, Z., Coco, G., Jiménez, M., Olabarrieta, M., Van der Wegen, M. and Townend, I., 2014. Morphodynamics of river-influenced back-barrier tidal basins: T he role of landscape and hydrodynamic settings. Water Resources Research, 50: 9514-9535.

Zhou, Z., Coco, G., Townend, I., Olabarrieta, M., Van Der Wegen, M., Gong, Z., D'alpaos, A., Gao, S., Jaffe, B.E. and Gelfenbaum, G., 2017. Is "morphodynamic equilibrium" an oxymoron? Earth-Science Reviews, 165: 257–67.

Zhou, Z., Coco, G., van der Wegen, M., Gong, Z., Zhang, C. and Townend, I., 2015. Modeling sorting dynamics of cohesive and non-cohesive sediments on intertidal flats under the effect of tides and wind waves. Continental Shelf Research, 104: 76-91.

Ziegler, P.A., 1990. Geological Atlas of Western and Central Europe. Maatschappij B.V., Shell Internationale Petroleum, The Hague, 239 pp.

Zuchuat, V., Sleveland, A.R., Pettigrew, R.P., Dodd, T.J., Clarke, S.M., Rabbel, O., Braathen, A. and Midtkandal, I., 2019. Overprinted allocyclic processes by tidal resonance in an epicontinental basin: The Upper Jurassic Curtis Formation, east-central Utah, USA. The Depositional Record, 5: 272-305.

$$F = \left(\frac{K_2 + O_1}{M_2 + S_2}\right)$$

Name		Description	Period (hr or day)	Equilibrium amplitude (m)
Semidiurnal				
M_2*†§	Principal Lunar	Rotation of Earth with respect to the Moon	12.42 hr	0.242334
S_2*†§	Principal Solar	Rotation of Earth with respect to the Sun	12.00 hr	0.112841
N_2*	Lunar elliptic	Eccentricity of Lunar orbit	12.66 hr	0.046398
K_2*	Luni-Solar declinational	Modulation of M_2 and S_2 due to Lunar and Solar declination changes	11.97 hr	0.030704
Diurnal				
K_1*†§	Luni-Solar declinational	Change in Lunar and Solar declination	23.94 hr	0.141565
O_1*†§	Principal Lunar	Change in Lunar declination	25.82 hr	0.100514
P_1*	Principal solar	Change in Solar declination	24.07 hr	0.046843
Q_1*	Lunar elliptic	Modulation of O_1 due to the elliptical orbit of the Moon	26.87 hr	0.019256
Long period				
M_f*	Lunar fortnightly	Non-sinusoidal Lunar declination changes	13.66 d	0.041742
M_m*	Lunar monthly	Irregularities in the rate of change of distance and speed of the Moon in orbit	27.55 d	0.022026
S_{sa}*	Solar semi-annual	Non-uniform changes in the Sun's declination and distance	182.6 d	0.019446

* tidal constituent used in Collins et al. (2017) and Collins et al. (2018) (Oligocene–Miocene South China Sea)

† tidal constituent used in Wells et al. (2010b) (Early Cretaceous Lower Greensand Seaway)

§ tidal constituent used in Mitchell et al. (2010) (Late Cretaceous Bohemian Cretaceous Basin)

Declaration of interests

☒ The authors declare that they have no known competing financial interests or personal relationships that could have appeared to influence the work reported in this paper.

☐The authors declare the following financial interests/personal relationships which may be considered as potential competing interests: